INFRARED EXCITATION OF CLUSTERS

JO GERAEDTS

INFRARED EXCITATION OF CLUSTERS

PROMOTOR:
PROF. DR. J. REUSS

CO-REFERENT:
DR. S. STOLTE

INFRARED EXCITATION OF CLUSTERS

PROEFSCHRIFT

TER VERKRIJGING VAN DE GRAAD VAN DOCTOR
IN DE WISKUNDE EN NATUURWETENSCHAPPEN
AAN DE KATHOLIEKE UNIVERSITEIT TE NIJMEGEN
OP GEZAG VAN DE RECTOR MAGNIFICUS
PROF DR J H G I GIESBERS
VOLGENS BESLUIT VAN HET COLLEGE VAN DEKANEN
IN HET OPENBAAR TE VERDEDIGEN
OP VRIJDAG 23 SEPTEMBER 1983
DES NAMIDDAGS TE 2 UUR PRECIES

door

JOHANNES MATHILDA PETER GERAEDTS

geboren te Swalmen

krips repro meppel
1983

Zoals ieder proefschrift is ook dit niet uitsluitend het werk van de auteur. Daarom wil ik iedereen die meegeholpen heeft aan de totstandkoming van dit proefschrift bedanken.

In het bijzonder:

de (oud) leden van de afdeling Atoom- en Molekuulfysika voor de prettige samenwerking;

de heren John Holtkamp en Frans van Rijn voor de bekwame adviezen en realisaties op digitaal en analoog gebied;

de heren Cor Sikkens en Eugène van Leeuwen voor de ondersteuning bij bouw en reparatie van de mechanische apparatuur;

de heer Sam Setiadi, de studenten Frans Lapoutre, Koo van der Sloot en Marcel Snels die aan dit onderzoek hebben meegewerkt;

de dienstverlenende afdelingen o.l.v. de heren J. van Langen, P. Walraven, H. Verschoor, J. Holten en J. van Bommel;

de heer Leo Hendriks, de afdeling illustratie o.l.v. de heer W. Verdijk en de afdeling fotografie o.l.v. de heer H. Spruyt;

de afdeling Experimentele Natuurkunde Algemeen voor de laser-technische adviezen;

Seeke Drost voor de tekening van Eveline en Tom;

Annette van der Heijden voor het typen van het manuscript;

en Riny van Hooft voor al het andere.

Het onderzoek dat in dit proefschrift beschreven staat is een gedeelte van het onderzoekprogramma van de "Stichting voor Fundamenteel Onderzoek der Materie" (FOM), welke financieel gesteund wordt door de "Nederlandse Organisatie voor Zuiver Wetenschappelijk Onderzoek" (ZWO).

TABLE OF CONTENTS PAGE

CHAPTER I THE SPECTROSCOPY OF CLUSTERS

I.1. What is a cluster

Clusters are defined as complexes of atoms and/or molecules bound by weak Van der Waals forces. When two molecules collide in a gas and there is a mechanism that can remove a part of their relative kinetic energy, they can be trapped by their own intermolecular forces. This new complex is commonly known as a Van der Waals molecule. The binding force between these two chemically non-binding molecules is at least one order of magnitude smaller than the ordinary chemical bond. The binding energy or dissociation energy is of the same order as kT at ordinary temperatures (kT = 2.5 $kJmol^{-1}$ or 200 cm^{-1}). Another feature of a Van der Waals molecule is the large intermolecular distance, which implies small rotational constants, low frequencies and large-amplitude vibrational motions. The structural and electronic properties, e.g. bond lengths and angles, dipole moments, polarizabilities, may also differ widely in different vibrational states.

The simplest Van der Waals molecules are dimers, but there are also trimers, tetramers and so on up to micro-crystals. Therefore we do not talk about molecules, but use the more neutral term cluster.

Clusters will always be present in a gas. Significant fractions are only found at low temperatures due to the low dissociation energy. Experimental studies of clusters in equilibrium in bulk are therefore often performed at the temperature of liquid nitrogen. This temperature, however, is still so high that a large number of states is populated and the interpretation of data is difficult.

Table 1. *Non-spectroscopic research on clusters. This table is a survey of the recent research; no attempt at completeness is made concerning the references.*

cluster property	investigation	technique	reference
production	concentration	mass-spectrometer	18,19
		bolometer	13,20
		raleigh-scattering	5,21
		electron diffraction	21,22
	velocity	mechanical velocity selector	18,23e
		time of flight	8,24
fragmentation	electron impact ionization	mass-spectrometer	8b,23b,25
		flux/density detector	26,27
		scattering chamber	18,28
size and structure	total cross section	scattering chamber	18
		electron diffraction	21,22
		crossed molecular beams	29,30,31
stability (magic numbers)	mass spectra		19
	theoretical		32
electric dipole moment	Stark effect		33
intermolecular potential energy surface	theoretical		34,35
	experimental		29,30,31

In the next two sections a survey is presented of recent experiments on clusters, which are mainly intended to acquire information about the properties of clusters. Once the relevant cluster properties are known it is possible to study for instance kinetics of chemical reactions, matrix spectroscopy in beams or the material properties in the transition regime between gas, liquid and solid phases.

I.2. Non-spectroscopic studies of clusters

Since the introduction of supersonic expansion this technique has been used to produce beams of extremely cold molecules [1]. The random internal energy, stored in the molecules before expansion, is converted into directed kinetic energy. The internal energy left in the molecules after expansion is reduced and the molecular velocity distribution becomes narrower. In 1956 Becker *et al* [2] observed a sudden discontinuity in the velocity distribution and an increase of the beam intensity at high pressures. This was the discovery of condensation, i.e. cluster production in beams, and a considerabel number of investigators started with cluster research. Their investigations are classified in table 1.

For our study most of their results are only a guide to produce well defined cluster beams. We shall show that it is possible to obtain additional information about production, size and structure by means of spectroscopic investigation of clusters.

I.3. Spectroscopic studies of clusters

At present cluster spectroscopy is mainly concerned with dimers, e.g. Ar-Ar, H_2-Ne, SF_6-SF_6, fluorene-Ar. The following chapter shall primarily deal

with the predissociation of dimers in a molecular beam which is irradiated by infrared lasers, viz. CO_2 or N_2O lasers. Predissociation may be defined as the transition of an excited molecule through a not totally unstable intermediate state before the dissociation continuum is reached. Predissociation spectra generally have broad lines which are almost without structure. With respect to the monomer band origins apparently random lineshifts occur to higher (blue) or lower (red) frequencies.

For the time being there are four methods of spectroscopy to investigate clusters, viz. the electronic excitation spectroscopy, the radio frequency (R.F.) and microwave spectroscopy, Raman scattering and the infrared spectroscopy. These methods produce a spectrum of clusters each.

Electronic excitation has been studied by laser induced fluorescence (LIF). An example is fluorene-Ar; this dimer shows a very structured spectrum [3] which can be measured with an exceptionally high resolution (35 MHz fwhm) in spite of the fact that the excited state is expected to dissociate. On the other hand, fluorene-Ar_2 does not show a sharp structure, presumably because here dissociation is a very fast process. It is from the rotational analysis that the structure of the dimer has been determined.

Radio frequency and microwave absorption leaves the dimer in the stable ground state, which implies that linewidths arise from conventional effects only. In a molecular beam the time of flight broadening dominates. For H_2-Ar the transition frequencies are determined with a resolution of 100 Hz [4].

Recently detection by means of Raman scattering has been reported of Ar-

dimers in a supersonic expansion [5].

Both the pure rotational and the much weaker vibrational Raman transitions were observed for the lowest two vibrational states of the dimer. The maximum resolution was about 3 GHz.

Infrared spectroscopy implies that an infrared photon is absorbed by the cluster. This leads to excitation of a vibrational mode of a cluster constituent. Normally the energy deposited in such a mode exceeds by far the dissociation energy of a cluster. Moreover, the vibrational motion is often strongly coupled to the Van der Waals stretch mode (or similar cluster modes). Contrary to the mentioned electronic excitation spectrum, lifetime effects of the intermediate state of the cluster strongly limit the resolution of the observed spectra. Infrared absorption measurements in bulk are often limited in resolution by pressure broadening. The already mentioned system H_2-Ar shows a linewidth of about 3 GHz [6], N_2-N_2 have linewidths of 150 GHz [7]. In a molecular beam SF_6-SF_6 excitation leads to a linewidth of $\pm$ 50 GHz (chapter III and IV) and C_2H_4-C_2H_4 excitation leads to a linewidth of $\pm$ 300 GHz ([8,9] and chapter VI). The resolution of these measurements is limited by lifetime effects.

The following general features emerge from the examples mentioned.

A. The Van der Waals stretch vibration and similar internal motions have absorption frequencies of about 10 - 50 cm^{-1}; they were resolved in Raman spectra [5] and in bulk i.r. absorption spectra, e.g. [7]. Almost free internal rotation of the molecular constituents of the dimer causes nearly equidistant rotational lines which have been resolved in i.r. bulk absorption measurements, e.g. for N_2-N_2 the rotational quantum numbers up to about J = 10 are resolved, see [7].

Table 2: *Spectroscopic research on clusters. This table is a survey of the recent research; no attempt at completeness is made concerning the references.*

cluster properties	technique used	references
rotational-vibrational behaviour	VUV photo-ionization mass spectroscopy	36
	laser induced fluorescence	3 37 38 39
	Raman scattering	5
	infrared absorption in bulk	6 7
	infrared predissociation in molecular beams	8 9 13 23 24 40
	microwave	11 41 42
	radiofrequency absorption/emission	4 10 11 12 43
size and structure	infrared predissociation in molecular beams	23 40

B. End over end rotations show typical spacings smaller than about 0.1 cm^{-1}. For hydrogen-rare gas complexes they are clearly resolved by i.r. bulk absorption measurements [6].

C. Hyperfine structure analysis of dimers has been developed by the Harvard group and others; it has become a major tool for the determination of structure of and molecular interactions within dimers [10,11,12].

In table 2 we list the present spectroscopic research on clusters.

I.4. Synopsis of the present investigations

Relatively new and unexploited so far are i.r. predissociation measurements in molecular beams, first attempted by the Waterloo group [13]. Due to beam cooling only a few states are occupied, limiting the amount of information. Neither do quasi-bound states (directly observed in bulk) contribute to these spectra. Normally broad single lines or scarcely structured lines have been observed. The main information in store consists of the linewidth - connected to the lifetime of the excited state - and the line shift with respect to the band origin of the monomer.

In figure 1. we have sketched a simplified version of our experimental set-up, with which i.r. predissociation spectra have been obtained. The molecular beam contains dimers and larger clusters which dissociate as a consequence of the absorption of a vibrational quantum from the CO_2 laser beam. The frequency of the laser can be tuned in little jumps of about 1.5 cm^{-1}. However, as mentioned above, normally the spectral structures are broader than the spacing between two CO_2 laser frequencies. The detection takes place on the mass spectrometer signal. An attenuation is observed on the axis of the beam

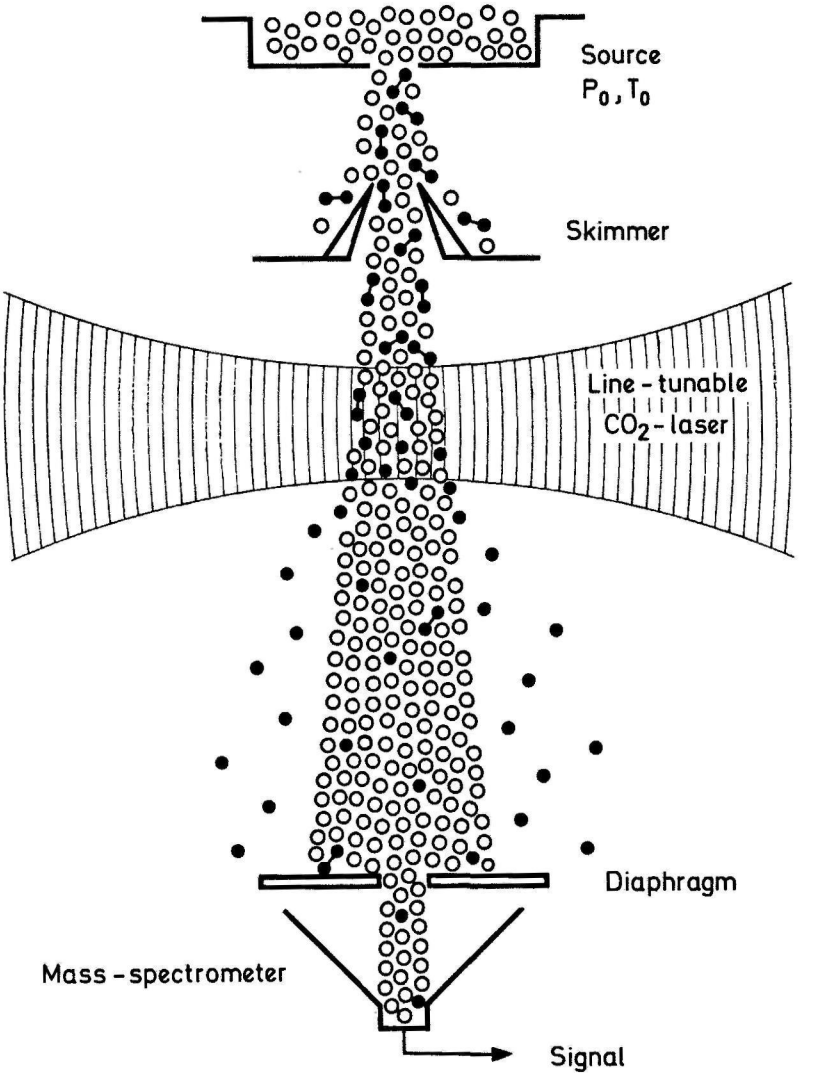

Fig. 1: Experimental arrangement. A nozzle beam containing dimers is crossed by a (line) tunable i.r. laser. The frequency dependence of the attenuation signal of the mass-spectrometer detector effects the predissociation spectrum of the dimers.

as a consequence of the cluster dissociation (chapter II).
In presenting the i.r. predissociation spectra from molecular beam experiments we distinguish between two groups: spectra with large splittings and spectra with unresolved structures.

Spectra of SF_6-SF_6, $(SF_6)_2$-Ar_n and SiF_4-SiF_4 belong to the first group. Due to the high symmetry of the molecules involved and the excitation of the threefold degenerate vibrational mode the transitional dipole moment has no preferential direction within the molecule. Consequently, the vibration can be considered as being decoupled from the rotation in good approximation. The excited dimer SF_6-SF_6 shows, thus, strong effects due to resonant dipole-dipole forces, with two i.r. active in-phase vibrations: one along the intermolecular axis and the other perpendicular to it. A negative energy shift (-2Δ) and a positive one (Δ) belong to these eigenstates respectively. The observed splitting between the two peaks has been quantitatively traced back to the resonant dipole-dipole interaction (chapter III, IV).

The differences between the spectra of the ν_3-mode of monomers, dimers or crystalline SF_6 are very well illustrated in figure 2. For the dimer spectrum the intensity equals the measured difference in beam intensity, with the laser on and off. This spectrum is obtained by a two-laser modulation technique (chapter IV). Clearly visible is the splitting between the two dimer peaks and the two shifts (-2Δ, Δ) with respect to the monomer absorption peak [14]. The absorption spectrum of the ν_3-mode in crystalline SF_6 possesses structure which indicates a loss of molecular symmetry and possibly a multi-occupied unit cell. The absorption intensities of the condensed and gaseous state are the same within the measuring uncertainty [15].

The natural abundance of SF_6 amounts to 95.0% of the sulphur isotope 32 and to 4.2% of the sulphur isotope 34. The dimers of SF_6 will therefore include

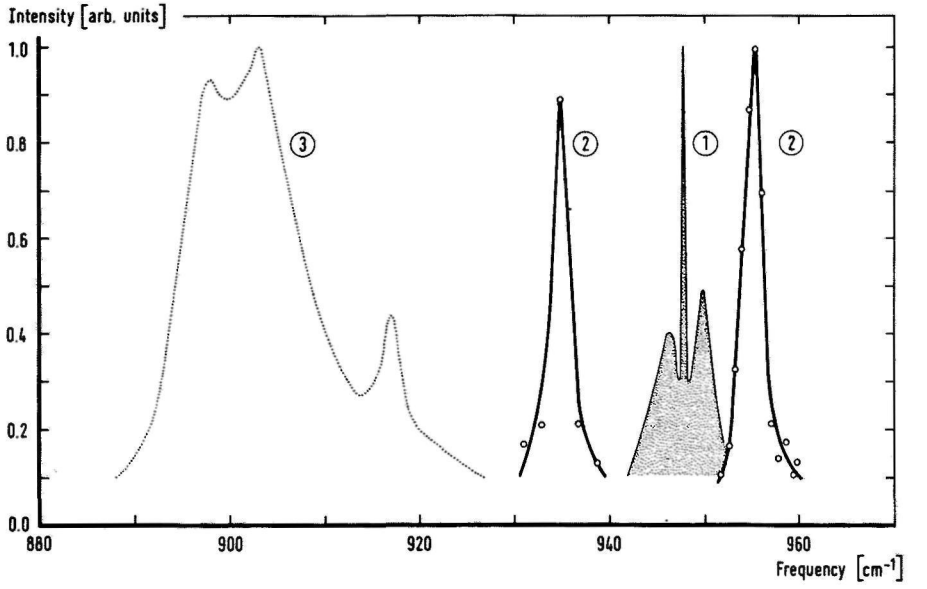

Fig. 2: *The SF_6-SF_6 predissociation spectrum (1) obtained by a two-laser modulation technique. Source conditions were, pressure P_o = 900 torr, temperature T_o = 233 K and nozzle diameter d_o = 30 µm. The probe laser fluence was fixed at 3 Jm^{-2}. For comparison, the shaded area (2) shows a grating spectrum of the ν_3 mode SF_6 at 150 K [14]; the dotted line (3) represents the infrared absorption spectrum of the ν_3 mode in crystalline SF_6 [15].*

8.4% $^{34}SF_6$-$^{32}SF_6$ complexes. With the two laser technique we were able to measure the spectrum of the isotope clusters. This spectrum can also be calculated qualitatively (chapter IV).

If the SF_6-SF_6 complex is loaded with Ar atoms, the double peak feature is preserved, although broadened and red-shifted. In this case really large clusters have been investigated. Spectra of a single SF_6-molecule packed in Ar atoms become similar to those found in matrix spectroscopy (chapter IV, [16,17]).

For SiF_4-SiF_4 the situation is similar to that of SF_6-SF_6. Unfortunately, the maximum of the red peak so far has escaped observation as no CO_2 laser lines were available below 1019 cm^{-1}. However, the expected blue-shifted line has been found leading to $\Delta \approx 6$ cm^{-1} (chapter V). The corresponding value for SF_6-SF_6 was about 7 cm^{-1}.

For CF_3Br the tetraeder structure is nearly perfect, but the excited mode is not threefold degenerate. Accordingly no big splitting due to decoupled resonant dipole-dipole forces has been observed for the CF_3Br dimer (chapter V).

The C_2H_4-C_2H_4 spectra also belong to the second group with nearly unstructured predissociation spectra. The free molecule C_2H_4 has two mode frequencies very near to each other, ν_7 = 948.8 cm^{-1} (i.r. active) and ν_8 = 940 cm^{-1} (Raman active). These two modes have a different symmetry. As one dimer partner perturbs the symmetry slightly with its molecular interaction it induces a Fermi resonance and subsequent blue shift of the ν_7 mode. This blue shift demonstrates mixing of eigenfunctions. Therefore, the ν_8 mode should become infrared active too, and show up at a frequency value of about 934 cm^{-1}, though significantly weaker than the blue shifted ν_7-peak. Accurate measurements using a two-laser modulation technique reveal this

feature.

We will analyze the recent C_2H_4 cluster experiments [8,9] together with our our own measurements (chapter VI).

We have had a look at the Fermi resonance effect in dimers. Qualitatively we can explain many observed line shifts from infrared predissociation spectra (chapter VII).

Finally all the relevant physical properties of the used molecules are given in an appendix.

Before engaging in a more detailed discussion of our investigations we would like to conclude this introduction with the following statement:

> Cluster spectroscopy is still in its infancy, but recent progress in understanding the dimer spectra strengthens our conviction that larger and more complicated complexes will be spectroscopically attacked and that their properties will be understood as well.

References

1. T.H. Johnson
   Nature 113 (1927) 745
2. E.W. Becker and W. Henkes
   Z. Phys. 146 (1956) 320
3. W.L. Meerts and W.A. Majewski
   "Laser Spectroscopy", vol. 6, Springer Verlag 1983 (in press)

4a. M. Waayer, M. Jacobs and J. Reuss
   Chem. Phys. 63 (1981) 247 and 257

4b. M. Waayer and J. Reuss
   Chem. Phys. 63 (1981) 263

5a. H.P. Godfried and I.F. Silvera
   Phys. Rev. Lett. 48 (1982) 1337

5b. H.P. Godfried and I.F. Silvera
   Phys. Rev. A27 (1983) 3008 and 3019

6. A.R.W. Kellar
   Faraday Disc. Chem. Soc. 73 (1982) 89
7. C.A. Long, G. Henderson and G.E. Ewing
   Chem. Phys. 2 (1973) 485

8a. M.A. Hoffbauer, W.R. Gentry and C.F. Giese, in "Laser Induced Processes in Molecules" eds. K. Kompa and S.D. Smith, Springer Series in Chem. Phys. 6, Springer Verlag, Heidelberg, 1978

8b. M.A. Hoffbauer, K. Liu, C.F. Giese and W.R. Gentry
   J. Chem. Phys. 78 (1983) 5567

9a. M.P. Casassa, D.S. Bomse, J.L. Beauchamp and K.C. Janda
   J. Chem. Phys. 72 (1980) 6805

9b. M.P. Casassa, D.S. Bomse and K.C. Janda
   J. Chem. Phys. 74 (1981) 5044

9c. M.P. Casassa, F.G. Celii and K.C. Janda
   J. Chem. Phys. 76 (1982) 5295

10. A.E. Barton and B.J. Howard
   Faraday Disc. Chem. Soc. 73 (1982) 45

11. J.S. Muenter, R.L. de Leon and A. Yokozeki
   Faraday Disc. Chem. Soc. 73 (1982) 63

12. W. Klemperer
   Faraday Disc. Chem. Soc. 73 (1982) 115

13. T.E. Gough, R.E. Miller and G. Scoles
J. Chem. Phys. 69 (1978) 1588
14. K.N. Rao
private communication
15. D.A. Dows and G.M. Wieder
Spectrochim. Acta 18 (1962) 1567
16. G. Delacrêtaz, J.-D. Ganière, P. Melion, R. Monot, R. Rechsteiner, L. Wöste, H. van den Bergh and J.M. Zellweger
Raf. Gas. Dynamics, Novosibirsk 1982 (in press)
17. T.E. Gough, D.G. Knight and G. Scoles
Chem. Phys. Lett. 97 (1983) 155
18. A.P.J. van Deursen
Thesis, University of Nijmegen, Nijmegen 1976
19. O. Echt, A.R. Flotte, M. Knapp, K. Sattler and E. Recknagel
Ber. Bunsenges. Physik. Chem. 86 (1982) 860
20. A.A. Vostrikov, S.G. Mironov, A.K. Rebrov and B.E. Semyachkin
Sov. Phys. Tech. Phys. 24 (1979) 1513
21. O. Abraham, S.S. Kim and G.D. Stein
J. Chem. Phys. 75 (1981) 402
22. J. Farges
J. of Crystal Growth 31 (1975) 79
23a. J. Geraedts, S. Setiadi, S. Stolte and J. Reuss
Chem. Phys. Lett. 78 (1981) 277
23b. J. Geraedts, S. Stolte and J. Reuss
Z. Phys. A 304 (1982) 167
23c. J. Geraedts, M. Waayer, S. Stolte and J. Reuss
Faraday Disc. Chem. Soc. 73 (1982) 375
23d. J. Geraedts, M. Snels, S. Stolte and J. Reuss
Submitted to Chem. Phys. 1983
24. P. Melinou, J.M. Zellweger, R. Monot and H. van den Bergh
1983, to be published
25. K. Stephan, J. Futrell, K. Peterson, A. Castleman Jr., H. Wagner, N. Djuric and T. Märk
Int. J. Mass Spectr. and Ion Phys. 44 (1982) 167
26. H. Tieu, S. Ryali, P. Gale and J. Fenn
Chem. Phys. Lett. 93 (1982) 213

27. J. Geraedts, S. Setiadi, S. Stolte and J. Reuss
Internal Report, 1980
28. A. van Lumig
Thesis, University of Nijmegen, Nijmegen 1978
29. U. Buck
Faraday Disc. Chem. Soc. 73 (1983) 187
30. M. Faubel, K.-H. Kohl and J.P. Toennies
Faraday Disc. Chem. Soc. 73 (1983) 205
31. R.T. Pack, J.J. Valentini and J.B. Cross
J. Chem. Phys. 77 (1982) 5486
32. E.E. Polymeropoulos and J. Brickmann
Chem. Phys. Lett. 96 (1983) 860
33. F.A. Baiocchi and W. Klemperer
J. Chem. Phys. 78 (1983) 3509
34. A. v.d. Avoird, P. Wormer, F. Mulder and R. Berns
in 'Topics in Current Chemistry' 93 (1980) 1
35. W. Meyer, P.C. Hariharan and W. Kutzelnigg
J. Chem. Phys. 73 (1980) 1880
36. P.M. Dehmer and S.T. Pratt
J. Chem. Phys. 76 (1982) 843
37. D.V. Brambaugh, J.E. Kenny and D.H. Levy
J. Chem. Phys. 78 (1983) 3415
38. J.J.F. Ramaekers, H.K. van Dijk, J. Langelaar and R.P.H. Rettschnick
Faraday Disc. Chem. Soc. 75 (1983) in press
39. U. Even and J. Jortner
J. Chem. Phys. 78 (1983) 3445
40. M.F. Vernon, J.M. Lisy, D.J. Krajnovich, A. Tramer, H.S. Kwok,
Y.R. Shen and Y.T. Lee
Faraday Disc. Chem. Soc. 73 (1982) 387
41. A.C. Legon and D.J. Millen
Faraday Disc. Chem. Soc. 73 (1982) 71
42. E.J. Campbell, A.C. Legon and W.H. Flygare
J. Chem. Phys. 78 (1983) 3494
43. J. Verberne
Thesis, University of Nijmegen, Nijmegen 1979

II.1. Introduction

The use of the molecular beam technique enables us to study clusters which don't interact with each other or with a support medium such as a solvent, a matrix or a substrate. This isolation is achieved at the cost of low cluster density in the beam. A problem is the impossibility to form clusters of one specific size in the beam. In the case of a carrier gas it is also possible that mixed clusters of carrier and seed are formed. The mixed cluster on the contrary can be a good alternative for matrix spectroscopy.

To investigate cluster formation and cluster properties in a molecular beam the disposal of a more specialized source is necessary. The design of the cluster source is based on higher reservoir pressures P_o, lower temperatures T_o, and a higher expansion rate than in the case of a monomer source.

To characterize the cluster beam we use a mass spectrometer for the density and the size distribution and a slotted-disc velocity selector for the speed distribution. The calibration of the mass spectrometer is a difficult problem because the relation between the mass-to-charge ratio of the cluster ions - produced by electron impact - and the neutral cluster size depends on the ionization cross section and the degree of fragmentation induced by electron impact. A second possibility to analyze the cluster beam is the spectroscopic method. We selected the dissociation of clusters by means of infrared laser photons. This directly narrows the selection of molecules that can be considered for cluster research. Only those molecules with an i.r. active mode in the range of the laser frequencies at our disposal can be investigated.

In the next section we describe in a bird's eye view the formation of clusters

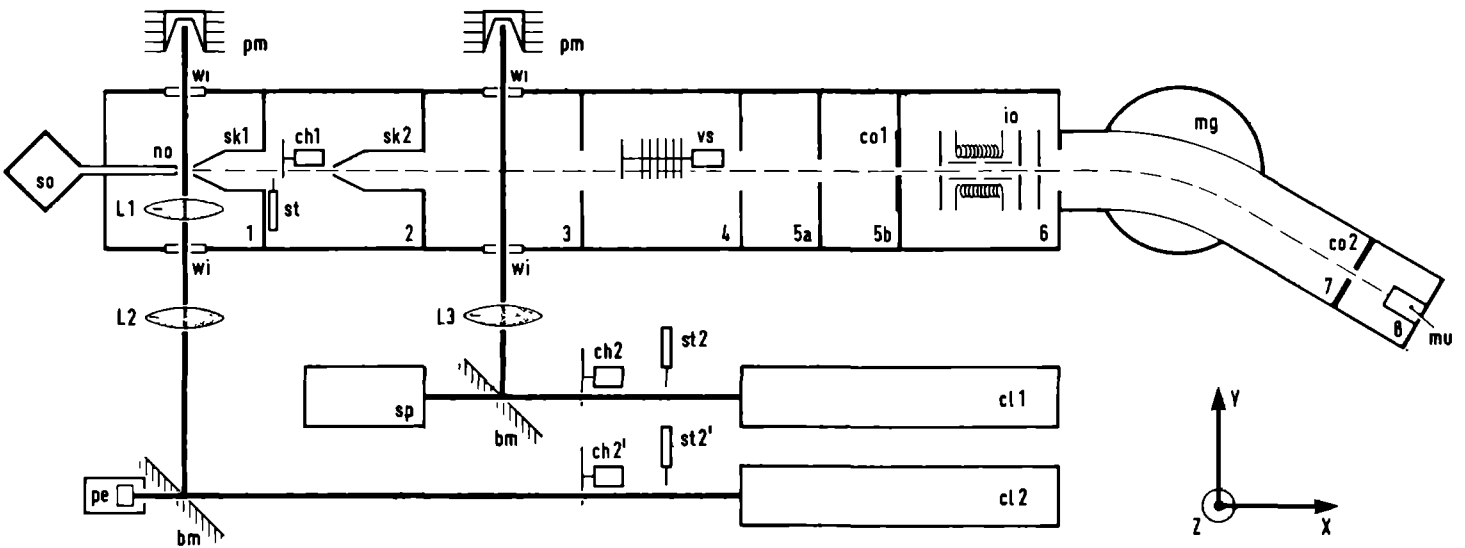

Fig. 1: Schematic view of the experimental set-up.

Components and specifications of Fig. 1

1. The molecular beam machine

so	source	pressure P_o : 50 -5000 torr temperature T_o : 100 - 300 K movability : x, y and z-direction
no	nozzle	hole diameter d_o : 20 - 200 µm channel length : 50/2000 µm
sk 1	conical skimmer	top diameter : 0.5 - 1.1 mm Ø movability : x-direction
st	molecular beam stop	
ch 1	chopper	frequency : 5 - 100 Hz
sk 2	conical skimmer	top diameter : 3.0 mm Ø
wi	window	material : ZnSe, AR-coated
vs	velocity selector	frequency : 50 - 300 Hz
co 1	collimator	rectangular : y * z = 1.2 x 8 mm
io	ionizer and ion lenses	electron energy : 25 - 100 eV
mg	deflection magnet	field : 0 - 8 kGauss pole diameter : 140 mm
co 2	collimator	rectangular : y * z = (0.8 - 1.3) x 8 mm
mu	multiplier	18 stages

2. The laser system:

cl 1	CO_2/N_2O laser	cw line tunable, power 0 - 45/20 Watt
cl 2	CO_2 laser	cw line tunable, power 0 - 45 Watt
st 2	laser beam stop	
ch 2	chopper	frequency : 5 - 100 Hz
bm	beam splitter or gold coated mirror	
L 1	lens	focal length : 100 mm movability : x, y and z-direction
L 2 L 3)	lenses	focal length : 1000 - 3000 mm
sp	spectrum analyzer	resolution : 0.3 nm range : 9 - 11 µm
pe	pyro electric detector	
pm	power meter	range : 0 - 100 Watt

3. The maximum pressures under working conditions are:

	high gasload	low gasload
chamber 1	2.10^{-1} torr	1.10^{-3} torr
chamber 2	2.10^{-5} torr	5.10^{-6} torr
chamber 3, 4, 5a	5.10^{-7} torr	5.10^{-7} torr
chamber 5b, 6	1.10^{-8} torr	1.10^{-8} torr
chamber 7, 8	5.10^{-7} torr	5.10^{-7} torr

in a supersonic nozzle beam. In the last section the most important details of the cluster apparatus are discussed. A schematic view of the experimental set-up, as used for our experiments, is given in fig 1.

II.2. Theoretical background

II.2.1. Supersonic expansion

A supersonic expansion requires a reservoir with gas at constant pressure P_o and temperature T_o, an exit hole or nozzle with diameter d_o, an expansion volume at lower background pressure P_b and a pump system to maintain P_b constant in the presence of the flow through the nozzle. If the pressure P_o is high enough the mean free path of the molecules is smaller than the nozzle diameter d_o and the velocity distribution of the flow can be narrowed drastically [1]. By collimating the flow with an aperture or skimmer downstream of the nozzle, a supersonic molecular beam is produced.

In the first stage of the expansion many collisions occur and the state of the expanding gas can be completely described by thermodynamics. In this stage the cold translational bath acts as an ideal refrigerant for all degrees of freedom. As the expansion proceeds, the density of the molecules drops and thermal equilibrium will no longer be present. In the absence of collisions no energy can flow from the internal degrees of freedom to the translational bath; the state of the system is frozen.

For an ideal gas the expansion will be isentropic and the temperature, the pressure, the density and the Mach number are related by the requirements of thermodynamics [1]

$$\frac{T}{T_o} = \left(\frac{P}{P_o}\right)^{\frac{\gamma-1}{\gamma}} = \left(\frac{n}{n_o}\right)^{\gamma-1} = \left[1 + \left(\frac{\gamma-1}{2}\right)M^2\right]^{-1} \qquad (2.1)$$

where T_o, P_o and n_o are the temperature, pressure and density in the reservoir; T, P and n are the same quantities in the isentropic part of the expansion; γ is the heat capacity ratio C_p/C_v and M is the Mach number, which is the ratio of the final flow velocity v_∞ to the local speed of sound.

Under appropriate conditions the nozzle acts like a particle point source and the density for the region close to the beam axis is given by [2]

$$n(z) \sim z^{-2} \tag{2.2}$$

where z is the distance to the nozzle. For an adiabatic expansion the relation between the local density n(z) and the local temperature T(z) in the beam is given by [2]

$$n(z)^{-(\gamma-1)} \cdot T(z) = \text{constant} \tag{2.3a}$$

and hence, from (2.2)

$$T(z) \sim z^{-2(\gamma-1)} \tag{2.3b}$$

The temperature drop in an expansion of a monatomic gas ($\gamma = 5/3$) will be faster than in a polyatomic molecule ($\gamma \to 1$). For $\gamma = \gamma(T)$ see Appendix B.

The final flow velocity can be obtained from the conservation of enthalpy in an adiabatic expansion

$$h_o = \frac{1}{2} m v_\infty^2 \tag{2.4}$$

where h_o is the enthalpy per particle with mass m in the reservoir. For an ideal gas h_o can be expressed as

$$h_o = \frac{\gamma}{\gamma-1} \cdot kT_o \tag{2.5}$$

and

$$v_\infty = \left(\frac{\gamma}{\gamma-1}\right)^{\frac{1}{2}} \cdot \alpha_o \tag{2.6}$$

where α_o is the characteristic velocity in the reservoir

$$\alpha_o = \left(\frac{2kT_o}{m}\right)^{\frac{1}{2}} \tag{2.7}$$

and k is the Boltzmann factor.

Measurements of the thermal relaxation in nozzle beams can be done by measuring the velocity distribution of the beam [3]

$$n(v) \sim v^2 \cdot \exp\left[-S^2\left(\frac{v}{v_s} - 1\right)^2\right] \tag{2.8}$$

where v_s is the flow velocity and S the speed ratio defined as the ratio between v_s and α_o. The Mach number M and the speed ratio S are related as follows

$$M = \sqrt{\tfrac{1}{2}\gamma} \cdot S \tag{2.9}$$

In a nozzle beam we can distinguish two temperatures inherent to the velocity parallel and perpendicular to the expansion axis. The parallel beam temperature, $T_{//}$, describing the mean kinetic energy of the molecular motion in the flow moving with velocity v_s is given by

$$T_{//} = \frac{1}{2}\frac{m}{k}\left(\frac{v_s}{S}\right)^2 \tag{2.10}$$

With increasing distance from the nozzle exit the collisional cooling decreases and $T_{//}$ will be frozen. The temperature of the perpendicular velocity distribution, $T_\perp$, behaves in first approximation as a collisionless expansion and cool geometrically, $T_\perp \sim z^{-1}$. In the frozen region of the beam $T_\perp$ will be more than a factor ten smaller than $T_{//}$ [2].

For a monatomic gas the final flow velocity, v_∞, and the flow velocity, v_s, are related by the energy balance

$$h_o = \frac{1}{2}mv_s^2 + \frac{3}{2}kT_{//} + kT_\perp$$

Hence, for $T_\perp = 0$

$$v_\infty = (1 + \frac{3}{2} \cdot \frac{1}{S^2})^{\frac{1}{2}} \cdot v_s \qquad (2.11)$$

The energy balance for a polyatomic gas is given by

$$h_o = \frac{1}{2} m v_s^2 + \frac{3}{2} kT_{//} + \frac{2}{2} kT_{\perp} + \int_o^{T_{rot}} C_{rot} dT + \int_o^{T_{vib}} C_{vib} dT \qquad (2.12)$$

where C_{rot} amd C_{vib} are the rotational and vibrational specific heats. With h_o known, v_s and $T_{//}$ measured, the internal energy remaining in the molecules in the beam can be calculated.

The energy balance is useful to estimate the terminal parallel temperature $T_{//}$ as a function of the source conditions P_o, T_o and d_o. According to equation (2.5) and (2.12) one obtains

$$v_s^2 = 2\frac{1}{m} \left[\frac{\gamma}{\gamma-1} kT_o - \frac{3}{2} kT_{//} - E_{int} \right] \qquad (2.13)$$

where $E_{int} = \int_o^{T_{rot}} C_{rot} dT + \int_o^{T_{vib}} C_{vib} dT$ and $T_{\perp}$ is supposed to be negligible. The parallel beam temperature $T_{//}$ can be obtained from (2.10) and (2.13)

$$T_{//} = (\frac{\gamma}{\gamma-1} T_o - \frac{1}{k} E_{int})(S^2 + \frac{3}{2})^{-1} \approx \frac{\gamma}{\gamma-1} \frac{T_o}{S^2} \qquad (2.14)$$

if $E_{int} << \frac{\gamma}{\gamma-1} kT_o$ and $S >> 1$.

The speed ratio S is related to the product of the number of collisions Z and the average viscosity collision cross section σ [4]

$$S = a(Z\sigma)^b \qquad (2.15)$$

where a and b depend on the gas used. Z is proportional to $P_o d_o T_o^{-1}$ and σ is proportional to $(\varepsilon R_m^6 T_o^{-1})^{\frac{1}{3}}$ in the case of a Lennard-Jones (12,6) potential with R_m the intermolecular distance at which the potential has its minimum energy ε.

The optimum value for b is given in table I in the case of atoms, diatoms, hydrocarbons, CO_2, NH_3 and SF_6. For the hydrocarbons and SF_6 it is

Table 1 *Experimental results for the speed ratio S in comparison with the calculated results.* $S \sim (Z \cdot \sigma)^b$.

method	gas	b	reference
experiment	He, Ne, Ar	0.48 ± 0.03	5
	Ar	0.50 ± 0.01	6
	CO, N_2	0.36 ± 0.03	5
	CO_2, NH_3	0.36 ± ?	7
	CH_4, C_2H_2, C_2H_4	0.29 ± 0.05	5
	C_2H_2, SF_6	0.29 ± ?	7
theory	He, Ne, Ar	0.530	4
	He, Ne, Ar	0.545	6

clear that the internal energy transferred into translational energy is larger than in the case of a diatom. The gases used mostly in our experiments are rare gases, SF_6 and C_2H_4. From equation (2.15) and the experimental results for b (table 1) we derive simple scaling laws

$$\text{He, Ne, Ar} \qquad T_{//} \sim T_o^{1.3} \cdot (P_o d_o)^{-1.0} \tag{2.16a}$$

$$SF_6,\ C_2H_4 \qquad T_{//} \sim T_o^{0.8} \cdot (P_o d_o)^{-0.6} \tag{2.16b}$$

II.2.2. Clusterformation

During the expansion the isentrope – starting from the reservoir conditions (P_o, T_o) – will intersect the saturated-vapour line of the gas used (Appendix C). In case of equilibrium between the phases, the expansion would depart from the isentrope and continue along the saturated-vapour line. In reality the expansion will continue along the isentrope without any condensation into the region where the gas is supersaturated.

The start of condensation is the formation of dimers. The expansion will deviate from the isentropic behaviour at the beam temperature where potential dimers are stabilized by the impact of a third molecule. The onset of dimerization is determined by the binding energy of the molecules, i.e. the well depth ϵ in the case of a Lennard-Jones potential.

H. Godfried [8] has investigated the formation of dimers in an Ar-beam using Raman diagnostics. His conclusion is that the optimum of the $(Ar)_2$ signal is located at $z/d_o \approx 2$. Slightly downstream of this optimum the dimer signal disappeared completely. (Source conditions P_o = 4560 torr, T_o = 293 K and d_o = 140 μm.)

Cluster formation of a polyatomic gas differs from the clustering of a monatomic gas because the internal degrees of freedom are also important here.

In general supersonic cooling requires two processes: expansion to provide the geometric cooling and collisions to provide equilibrium between $T_{\perp}$ and the other degrees of freedom [4].

For SF_6 at T_o = 293 K only 30% of the molecules are in the vibrational ground state. In the expansion the "hot" molecules escape from the region near axis, thereby lowering $T_{\perp}$ for two translational degrees of freedom. All the other 19 degrees of freedom have to release their thermal energy in the $T_{\perp}$ reservoir by collisions; one degree comes from the remaining translational degree, $T_{//}$, three from the rotational degrees, T_{rot}, and fifteen from the vibrational degrees, T_{vib}. Evidently in a pure SF_6 expansion lowering of T_{vib} is a slow process, even if one assumes high vibrational relaxation rates; too much energy (19 kT_o) must flow into the geometrical cooled tiny reservoir ($kT_{\perp}$). The specific heat ratio value γ is close to unity, its high temperature value being 19/18. If the reservoir temperature T_o decreases, γ increases (see Appendix B), due to partial freezing of the vibrational degrees of freedom. This effect is suppressed by decreasing relaxation rates for vibrational cooling at decreasing temperatures, due to energy mismatch. Cooling of the SF_6 nozzle expansion has been observed by Raman diagnostics in our laboratory [10].

The cluster formation in an SF_6 beam has been recently investigated by Melion et al [9] using the infrared predissociation technique. Their conclusion is that the optimum of the cluster dissociation signal is located at $z/d_o \approx 10$. The collisional zone corresponds to $z/d_o \leq 20$. (Measurement conditions P_o = 1050 torr, T_o = 222 K, d_o = 100 μm and the used laserfrequency ν = 938.7 cm^{-1}.)

The "seeded beam" technique has been utilized succesfully to cool the rotational and vibrational degrees of freedom of a polyatomic molecule in the translational cold bath provided by the expanding monatomic gas, the carrier.

For an effective equilibration of the internal degrees of freedom the seed molecules must be accelerated to the forward velocity of the carrier gas, in order to achieve the lowest relative collision energy. The release of the large internal energy stored in the polyatomic seed molecules will heat and also disturb the expansion behaviour of the carrier gas.

Cooling the rotational and vibrational degrees of freedom depends on their relaxation cross sections for collisions with the carrier gas atoms. For the rotational degrees of freedom the cross sections are known to be roughly equal to the gas kinetic. The rotational temperature T_{rot} will closely follow the translational temperature $T_{//}$ of the carrier gas. The cross sections for vibrational relaxation are known to be smaller than the gas kinetic. However, experiments show that the vibrational relaxation is sufficiently effective to cool the vibrational temperature T_{vib} much faster in a carrier gas than in a pure expansion [10].

In practice a small amount of seeding gas will perceptibly heat the carrier gas. In fig. 2 we show the mass spectra of a pure Ar expansion and a 0.5% SF_6 in Ar expansion. The reservoir conditions are in both cases P_o = 2250 torr, T_o = 233 K and d_o = 30 μm. The electron impact energy of the ionizer for the mass spectrometric detection was set on 32 eV. The mass spectrum of the pure Ar beam shows the condensation present in the beam. This condensation behaviour is disturbed in the case of the seeded beam. The Ar_2^+ signal decreases by 20%, the Ar_3^+ signal by 70% and the Ar_4^+ signal by 80%. As function of the reservoir pressure P_o (500 torr $\leq P_o \leq$ 2250 torr) this behaviour is almost constant. The Ar^+ signal increased by 10% with respect to the pure beam.

Finally we want to discuss briefly which is the best carrier molecule for cluster beams. From equation (2.6) follows that the "velocity slip" between

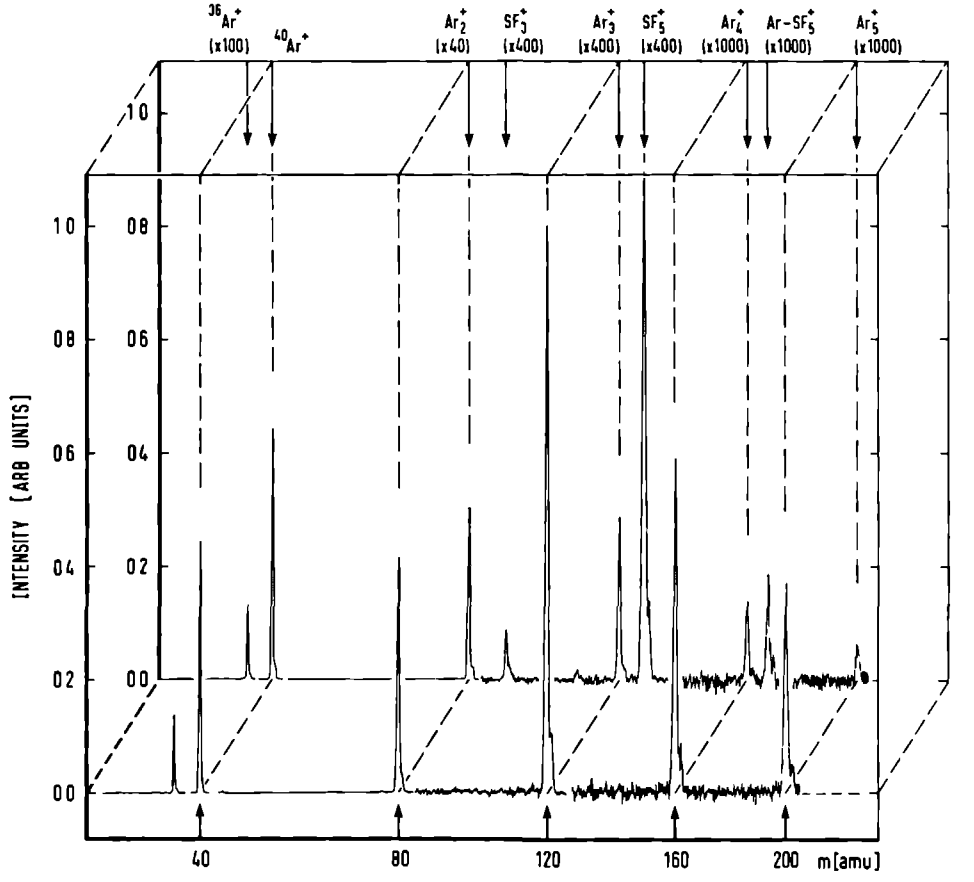

Fig. 2: Mass spectra of a pure Ar beam (foreground) and a 0.5% SF_6 seeded in Ar (background). The reservoir conditions are P_o = 2250 torr, T_o = 233 K and d_o = 30 µm. Note the disturbance of the Ar condensation in the case of the seeded beam.

the seed and the carrier molecules will depend primarily on the seed-carrier mass ratio. For an effective equilibrium of the internal energies the mass ratio must be nearly unity. Molecules which satisfy this condition are Ar, Kr or Xe. However, condensation behaviour of these molecules and carrier-seed complex formation limits the final translational (and rotational) cooling. The best choice for low beam temperatures still remains He, if the pumping capacity of the cluster beam apparatus is large.

II.3. The experimental apparatus

II.3.1. The source system

The major tool to get an intense supersonic beam is an adequate pumping capacity to handle the gas flow through the nozzle. In the past the only solution available was the brute force approach of large pumps to handle a great flow. Recently two other techniques have been developed. The first technique is the use of a pulsed nozzle [11]. In this case the gas flows for only a small fraction of the time; the pump need only be large enough to evacuate the source chamber before the next pulse is generated. The second technique developed by Campargue [12], is based on pumping at relatively high background pressures P_B, $0.1 \leq P_B \leq 1$ torr.

To maintain the low temperature produced by supersonic expansion, the cold jet must not collide with the background gas at room temperature. This scattering is traditionally avoided by evacuating the source chamber to low pressures (10^{-3} - 10^{-4} torr); the mean free path between background collisions is larger than the dimensions of the source chamber. At increasing background pressure shock waves are formed around the cold isentropic core of the expansion and shield the cold jet from the "warm" background gas. To form a well defined molecular beam the isentropic core of the expansion has to be

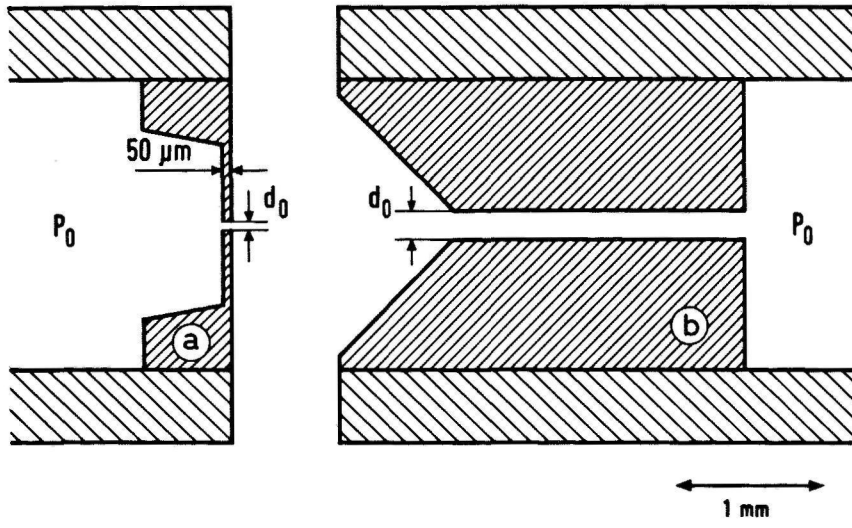

Fig. 3: The nozzles. Nozzle a is a circular diaphragm; nozzle b is a cylindrical pipe. P_o indicates the reservoir (pressure) and d_o the nozzle diameter.

extracted into a low density region by means of a skimmer. Skimming high density beams, however, is technically difficult. High flow rates and high background pressures in the source chamber result in a relatively high gas flow through the skimmer into the second (buffer) chamber.

The pump system of the source chamber consists of a baffled oil diffusion pump (Leybojet 1000/4), a mechanical booster pump (Edwards EH 500) and a mechanical two stage rotary pump (Edwards E2H80). The efficient range of pumping speed of a booster pump fills the gap left between standard speed curves of oil diffusion pumps and rotary pumps. The peak gas flow from our oil diffusion pump ranges from about 0.5 torrls^{-1} at 10^{-4}torr to 2 torrls^{-1} at 10^{-2}torr; the peak gas flow of the mechanical booster pump ranges from about 1 torrls^{-1} at 10^{-2}torr to 100 torrls^{-1} at 1 torr. The pump speed of the rotary pump is 22 ls^{-1}. At low flow rates (< 1 torrls^{-1}) the source chamber is pumped by the oil diffusion pump backed by the booster pump in series with the rotary pump. At high flow rates (> 1 torrls^{-1}) the booster pump evacuates directly the source chamber.

The pump system of the buffer chamber consists of a baffled oil diffusion pump (Leybold DI 3000 6B) backed by a mechanical two stage rotary pump (Alcatel 2030 H). The peak gas flow of this oil diffusion pump ranges from about 0.02 torrls^{-1} at 10^{-6}torr to 0.2 torrls^{-1} at 10^{-4} torr. The pump speed of the rotary pump is 10 ls^{-1}.

The nozzle, mounted in a stainless steel pipe, consists of a platinum-iridium electron-microscope diaphragm (Siemens). The nozzle diameters d_o used were 20 µm, 30 µm, 50 µm and 100 µm (see fig. 3a). For strong clustering a special channel nozzle of stainless steel was used with a diameter d_o = 200 µm (see fig. 3b). The flow rate $\dot{N}$ through the nozzle can be expressed as [2]

$$\dot{N} = P_o \cdot \frac{\pi}{4} d_o^2 \cdot \alpha_o \cdot f(\gamma) \qquad f(\gamma) = \left(\frac{\gamma}{\gamma+1}\right)^{0.5} \left(\frac{2}{\gamma+1}\right)^{\frac{1}{\gamma-1}} \qquad (2.17)$$

where P_o is the reservoir pressure, d_o the nozzle diameter, α_o the characteristic velocity and γ the heat capacity ratio. The numerical value of $f(\gamma)$ equals 0.50 ± 0.03 for $\frac{19}{18} \leq \gamma \leq \frac{5}{3}$.

A boundary layer will be formed in the nozzle due to the viscosity of the gas and the real flow rate is smaller than predicted by equation (2.17). For noble gases the thickness of the boundary layer will be smaller than 5% of the nozzle diameter if the reservoir pressure exceeds 200 torr.

The pump speed S_p is related to the flow rate by [13]

$$S_p = \dot{N}/P_B \tag{2.18}$$

The shock wave forming the side walls of the isentropic core is called the barrel shock and the shock wave transverse to the beam axis is called the Mach disk. The position of the Mach disk does not depend on whether or not the flow is partly condensed [14].

The experimental results for the position of the Mach disk can be approximated by [14]

$$z_m = 0.67\, d_o \sqrt{P_o/P_B} \quad \text{for} \quad 15 < P_o/P_B < 15.000 \tag{2.19}$$

From the last three formulae it follows that

$$z_m \approx 1.1 \sqrt{S_p/\alpha_o} \tag{2.20}$$

The skimmer top has to be positioned at a distance $z < z_m$; a shock free flow into the skimmer can be obtained by placing the skimmer at $z < \frac{1}{2} z_m$ [15]. However, the gas flow through the skimmer has to be minimized to avoid high pressures in the buffer chamber. The skimmer also has to be positioned as far as possible from the nozzle. At working conditions this means that the optimum nozzle-skimmer distance has to be determined for each reservoir pressure.

Another important component of the source is the control system for the reservoir pressure P_o and temperature T_o. Since the condensation process is very sensitive to changes in both P_o and T_o, a careful control of these variables is necessary. The pressure P_o is set with the help of a pressure reducer (L'air liquide, DIRS no. 7). The temperature T_o is at or below room temperature. A two stage feedback control system has been built for the temperature control. The first stage consists of a copper reservoir cooled by a regulated liquid nitrogen flow system. The reservoir is connected to a copper enclosure around the nozzle pipe by plaited copper-wire. The temperature of the reservoir and the nozzle enclosure are measured by two P(ositive)-T(emperature)-resistors (temperature range: 77 K to 300 K). The second stage of the control system regulates the energy dissipation of a transistor, which is mounted at the nozzle exclosure. The long time stability of this two stage temperature control system is better than 0.25 K per 12 hours.

II.3.2. The mass spectrometer

The mass spectrometer consists of an ionizer, a deflection magnet and a particle multiplier (see fig. 1). Before entering the ionizing volume the incoming beam of neutrals is collimated by a rectangular slit with an aperture of 1.2 x 8.0 mm^2. The ionizer has been developed and built in our molecular group. Continuous improvements over the years have led to a stable ionizer with an efficiency of about 1:500 yielding an enhancement of the SNR as compared to commercial models [16]. The one used was installed five years ago and has worked well continuously. In the ionizer volume electrons with an energy of 25 to 100 eV (adjustable) traverse the neutral beam path. The ionizer is set by the ion lenses to work without any detectable ion space charge in the ionizer volume. The pressure in the ionizer is lower than

10^{-8} torr under working conditions.

After acceleration the ions are deflected by a switching magnet (Spectromagnetic Industries, model 1038) which selects the ion-masses. The ion energy can reach 900 eV; the mass range belonging to it is 1 - 2500 with a resolution $M/\Delta M \simeq 75$.

In fig. 4 the stabilization system of the magnet is shown. It consists of a Hall probe (Siemens, type FC 34) inside the polar pieces of the deflection magnet, an amplifier for the Hall voltage (A1) and a feedback system for the current (I_B) of the magnetic coils. The Hall voltage V_H is directly proportional to the (reference) current I_H and the magnetic field generated by the two magnetic coils. By setting a voltage V_o to amplifier A_2 the whole system tunes the magnet to the desired field which is directly proportional to V_o. The control unit consists of a manual part and an interface for a microcomputer which can be connected by a peripheral interface adapter (VIA). The

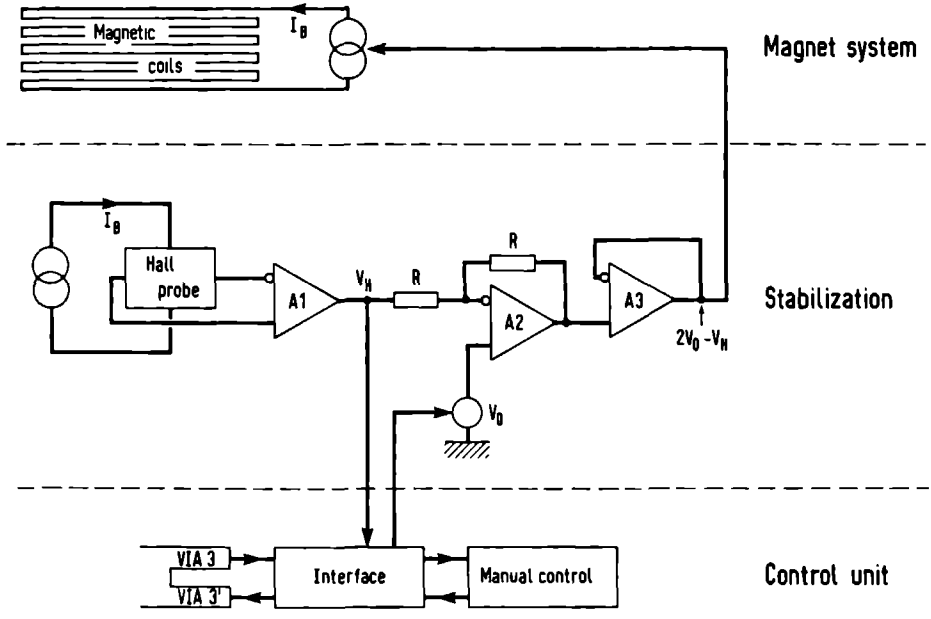

Fig. 4: Diagram of the stabilization of the deflection magnet.

stabilization system has a short time (< 1 hour) stability better than $1x10^{-4}$ and an absolute stability better than $5x10^{-4}$.

II.3.3. The laser system

The lasers c1 1 and c1 2 (designed and constructed by H. Bluyssen and A.F. van Etteger) have a 10 mm inner diameter plasma tube, which is vacuum sealed by a ZnSe Brewster window and a ZnSe outcoupling mirror with a 10 m radius or curvature. The plasma tube has a central anode and two cathodes at each side; the total discharge length (1.4 m) is divided in two equal parts to reduce the high voltage under working conditions (10 kV and 25 mA at maximum output power). The electrical system consists of an unstabilized high voltage power supply and a current stabilizer. Stabilization of the laser current occurs by regulating the conductance of a pass tube between the laser cathode and the ground. Through the plasma tube a gas mixture of CO_2 (N_2O), N_2 and He is flown continuously by a rotary pump which is fitted with an oil dust filter.

The optical resonator consists of the outcoupling mirror and a flat grating (135 lines per mm, relative efficiency 97% between 9 μm and 11 μm). The resonator length is passively stabilized with three super invar rods or with three quartz rods clasped in aluminium tubes.

The grating is mounted on a piezoelectric transducer which enables us to stabilize the resonator length. Within the linewidth of an emission line the frequency is determined by the resonator length, for the 2 m cavities this means a bandwidth of 75 MHz. The maximum output power is 45 Watt single line.

The spacing between the emission lines of $^{12}C^{16}O_2$ is about 2 cm^{-1}. To get more emission lines available we have the possibility to use also N_2O and the isotope $^{13}C^{16}O_2$.

In table 2 we show the frequency domain and the average frequency spacing between two emission lines for the gases used.

Table 2 *Comparison of the vibrational transitions, the wavelength range and the average frequency spacing between the rotational transitions of vibrational band for $^{12}C^{16}O_2$, $^{13}C^{16}O_2$ and $^{28}N_2{}^{16}O$.*

gas	transitions		wavelength range (cm^{-1})	average frequency spacing (cm^{-1})
$^{12}C^{16}O_2$ a)	001-020	R(48)-R(02)	1093.9-1066.0	1.2
	001-020	P(02)-P(50)	1062.2-1016.7	1.8
	001-100	R(50)-R(02)	992.5- 963.3	1.2
	001-100	P(02)-P(54)	959.4- 910.0	1.9
$^{13}C^{16}O_2$ a)	001-020	R(30)-R(12)	1038.3-1027.2	0.8
	001-020	P(10)-P(36)	1009.5- 985.0	1.9
	001-100	R(44)-R(04)	943.3- 917.2	1.3
	001-100	P(06)-P(48)	908.7- 870.5	1.8
$^{28}N_2{}^{16}O$ b)	001-100	R(40)-R(1)	970.1- 940.5	0.7
	001-100	P(03)-P(35)	936.3- 907.7	0.9

a) ref. [17] b) ref. [18]

During the experiments we used two outcoupling mirrors, one with a transmission of 30% to maximize the power output, the other with a transmission of 10% to get the maximum number of emission lines.

When we used the two lasers simultaneously the modulation laser was tuned to a high power output. To avoid power fluctuations during the measurement (4 - 12 hours) the resonator length was actively stabilized.

II.3.4. The microcomputer

The measurements on the cluster apparatus can be controlled by a "home" computer, an instrument that takes up far less space and costs far less than a full scale computer. With some additional hardware the computer can control

external devices. A microprocessor with an easy link with the "outside world" is the 8 bit R6502 with a memory-mapped input/output device. Memory mapped means that input and output devices are assigned to specific adresses in the memory to be read from (input) or written to (output). We have selected the Rockwell AIM 65, with 20K-byte read only memory (ROM) and 32K-byte random access memory (RAM). The useful units of processing equipment external to the central processing unit are a keyboard/printer (in our case a teletype KSR 43A), an interface for input/output to two tape recorders and the R6522 versatile interface adaptors (VIA). We have extended the number of VIA's to five. A schematic of the connections between the microcomputer and the cluster machine is shown in fig. 5.

To control the beamstops and other on/off devices VIA 1 is used. VIA 1 also starts the counter and for the reading of their memories, after the measurement, VIA 2 is used. To tune and control the mass spectrometer stabilization we employ VIA 3. The last two, VIA 4 and VIA 5, are to handle the data flow between the microprocessor and the control unit of the mechanical velocity selector. After each measurement the microcomputer carries out a data reduction and stores all the relevant data on tape.

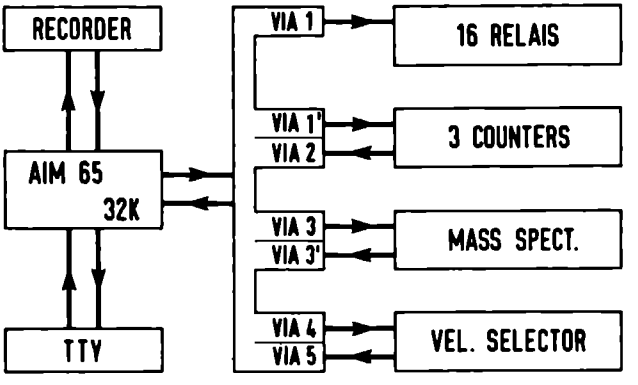

Fig. 5. Schematic of the microcomputer and important external devices. Several parts are explained in the text.

References

1. J.B. Anderson, in "Molecular Beam and Low Density Gasdynamics" vol IV, ed. P.P. Wegner, Macel Dekker Inc., New York 1974
2. H. Beyerinck and N.F. Verster
   Physica 111C (1981) 327
3. J.B. Anderson and J.B. Fenn
   Phys. Fluids 8 (1965) 780
4. J.P. Toennies and K. Winkelmann
   J. Chem. Phys. 66 (1977) 3965
5. G. Brusdeylins and D.H. Meyers, in "Rarefied Gas Dynamics" proc. XI Symp., vol. II, ed. R. Campargue, Comm. á l'Energie Atomique, Paris 1979, p. 919
6. A.H.M. Habets
   Thesis, Eindhoven University of Technology, Eindhoven
7. N. Takahashi, K. Teshima and I. Kusunoki
   Jpn. J. Appl. Phys. 20 (1981) 1981
8. H. Godfried
   Thesis, University of Amsterdam, Amsterdam 1982
9. P. Melinon, J.-M. Zellweger, R. Monot and H. van den Berg, preprint
10. G. Luijks, J. Timmerman, S. Stolte and J. Reuss
    Chem. Phys. 77 (1983) 169
11. W.R. Gentry and C.F. Giese
    Rev. Sci. Instr. 49 (1978) 595
12. R. Campargue
    Rev. Sci. Instr. 35 (1964) 111
13. O.F. Hagena and P. Schüller
    Z. Angew. Phys. 17 (1964) 524
14. S. Christ, P.M. Shermann and D.R. Glas
    AIAA 4 (1966) 68
15. K. Bier and O.F. Hagena
    Z. Angew. Phys. 14 (1962) 658
16. J.F.C. Verberne
    Thesis, University of Nijmegen, Nijmegen 1979
17. Ch. Freed, L.C, Bradley and R.G. O'Donell
    IEEE J. Quantum Electr. QE-16 (1980) 1195
18. B.G. Whitford, K.J. Siemens, H.D. Riccus and G.R. Hanes
    Opt. Comm. 14 (1975) 70

III.1. Introduction

The last few years many publications deal with the dissociation of polyatomic molecules by high power infrared lasers. Demonstration of isotope separation [1] and selective destruction of impurities in mixtures [2] have stimulated an extensive research on multiphoton dissociation. One of the benchmark molecules for infrared multiphoton excitation experiments is SF_6. It exhibits isotopically selective decomposition and strongly absorbs the radiation of the 10.6 μm band of the CO_2 laser. The large transition dipole moment (0.39 D) of the ν_3 fundamental vibration of the SF_6 molecule ($\nu_3 = 10.549$ μm) explains this strong absorption. Experiments of Lyman [3] have shown that the SF_6 molecule can be photolized

$$SF_6 + nh\nu \rightarrow SF_5 + F \qquad \Delta H = 385 \text{ kJmol}^{-1}$$

where n is the number of absorbed photons ($n \geq 34$) and ΔH the necessary energy for photolizing. The photolysis treshold is about 1.2×10^{-4} Jm^{-2} for $\nu = 10.591$ μm radiation.

The infrared spectroscopy of the ν_3 band of SF_6 has achieved a high resolution (1 kHz). Recently J. Bordé and C. Bordé [4] have presented a detailed theoretical approach that reproduces the hyperfine and superhyperfine structure of the rovibronic spectrum of the ν_3 band.

Our aim is to dissociate SF_6 clusters. In chapter II we have already explained the production of clusters in a molecular beam. The first step in cluster investigations is the analysis of the mass spectrum of a cluster beam. The mass spectrum of SF_6 is shown in figure 1. Clearly visible is the

violent fragmentation of the SF_6 molecule. The SF_6^+ ion, the primary product of electron bombardment in the ionizer, is unstable and decays immediately into SF_n^+ ($1 \leq n \leq 5$), S^+ and F^+. The maximum value of the ionization cross section, yielding SF_5^+, appears to be $3.4 \cdot 10^{-20} m^2$, at an electron impact energy of 145 eV [5]. In practice our electron impact energy is varied between 25 and 100 eV. At 25 eV the SF_5^+ ion signal amounts to 88% of the total ion signal; at 100 eV this percentage is 66%. Fragmentation decreases for lower electron impact energy. The hope that this would occur for SF_6 clusters as well, turned out to be idle. In chapter IV, section 2, a detailed treatment of the fragmentation process of SF_6 clusters is given.

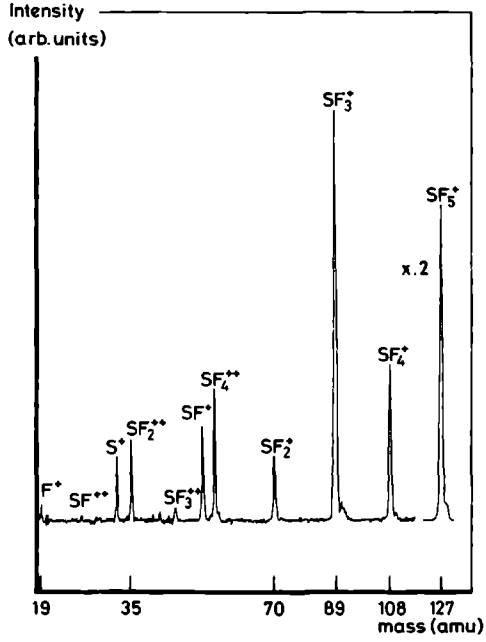

Fig. 1: Mass spectrum of a molecular beam of 5% SF_6 seeded in He at P_o = 3000 torr and T_o = 295 K. Note the change in intensity for the ion mass SF_5^+.

The predissociation measurements of SF_6 clusters are performed by crossing the molecular beam - containing the clusters - with a line tunable CO_2 laser of moderate power. The dissociation of the clusters is observed on the mass spectrometer signal. Schematically this experiment is displayed in figure 1, chapter I. The dissociation process starts by vibrational excitation of the infrared active ν_3 mode of the SF_6 molecules in the cluster. Since the Van der Waals binding energy of the cluster is by far smaller than one infrared quantum, the cluster dissociates. Vibrational excitation of SF_6 molecules will not affect the ionization cross section significantly. Brunner et al [6] have shown that the decay of SF_6^+ into lighter fragments SF_n^+ ($1 \leq n \leq 5$) depends on the fluence used for excitation of the SF_6 molecule before ionization. In our fluence range, $0 \leq F \leq 10\ Jm^{-2}$, no measurable effect is present.

One of our first results is shown in figure 2. Simultaneously two signals are recorded, the total beam signal from a miniature manometer gauge and the mass specific signal (the ion mass SF_5^+) from the mass spectrometer. The ratio $\Delta I/I$ is the difference in beam signal, caused by the laser, divided by the total beam signal. The spectrum, measured on ion mass SF_5^+, shows more structure than the spectrum derived from the manometer gauge. (The reason for measuring the cluster spectrum on the monomer ion mass SF_5^+ will be explained in the next section). The spectrum, taken with the mass spectrometer, shows three clearly resolved absorption peaks, near 935, 944 and 955 cm^{-1}, respectively. The spectrum will be explained in chapter IV, section 7.

The attenuation on the miniature manometer gauge demonstrated that clusters dissociate as a consequence of the CO_2 radiation. Part of the vibrational energy is transferred to translational energy directed perpendicularly to the flow direction. The mass spectrometer attenuation signal is about 50%

stronger and the spectrum appears more structured (figure 2). The plausible cause for this difference is the smaller acceptance angle of the mass spectrometer ($\approx 5 \cdot 10^{-4}$ sterrad) with respect to the miniature manometer gauge ($\approx 3 \cdot 10^{-3}$ sterrad).

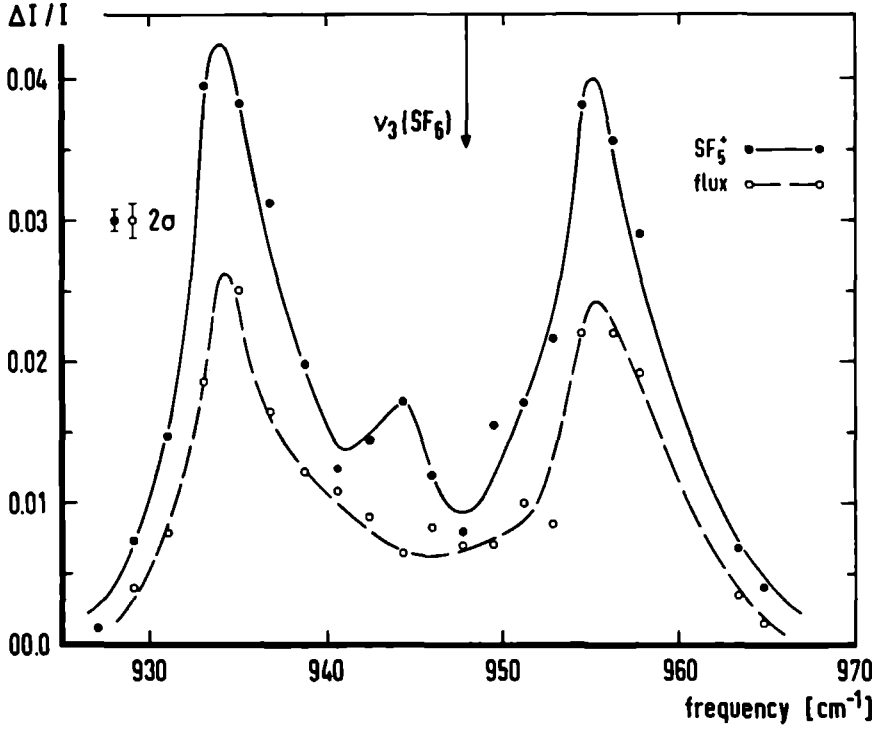

Fig. 2: The molecular beam attenuation spectra as a function of the frequency. The beam consists of pure SF_6 expanded at the source conditions P_o = 1000 torr and T_o = 228 K. The ratio $\Delta I/I$ is the difference in beam signal, caused by the laser, divided by the total beam signal. The solid curve corresponds to the mass-specific attenuation on ion mass SF_5^+; the dashed curve to the total beam attenuation from a manometer gauge. The arrow indicates the ν_3 mode frequency of the SF_6 molecule.

The dissociation of clusters depends on the fluence used, which is equal to the laser intensity times the irradiation time t. The dependence of the irradiation time is shown in figure 3, where the velocity distribution I_m and the velocity dependence of $\Delta I/I_m$ are displayed. The velocity distribution I_m is determined by a slotted disk velocity selector. (The beam consists of 5% SF_6 seeded in Ar at room temperature. The mass-spectrometer is tuned to the ion mass SF_5^+.)

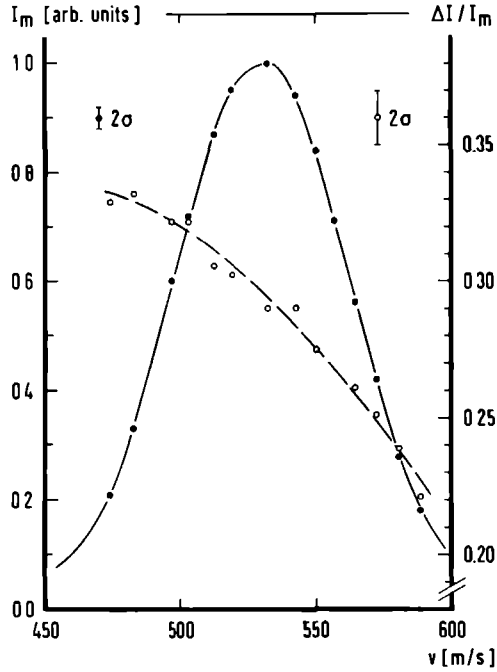

Fig. 3: Experimentally determined velocity distribution I_m(•) for 5% SF_6 seeded in Ar. The source conditions are P_o = 3400 torr and T_o = 294 K; the spectrometer is tuned to ion mass SF_5^+. The solid curve corresponds with the fit: v_s = 536 ms^{-1} and $T_{//}$ = 18 K. The second curve represents the velocity dependence of the predissociation signal $\Delta I/I_m$(○); ΔI is the measured difference in beam signal with laser on and off. The laser frequency is 934.9 cm^{-1}, the laser power is 475 Wcm^{-2} at the point of laser and molecular beam intersection.

The CO_2 laser is set on the frequency of 934.9 cm^{-1} with 475 W/cm^2 laser intensity at the point of laser and molecular beam intersection. The dissociation signal clearly decreases with increasing velocity v; the irradiation time t is proportional to 1/v. In the next section we will also consider the power dependence of the cluster predissociation signals.

Our first investigations of SF_6 clusters were performed with pure SF_6 beams. By varying the source conditions (P_o, T_o) it was possible to change the line shape and the number of peaks in the predissociation spectra. The dependence of clustering on seeding gases (He, Ar) is also studied in more detail. This early work on SF_6 clusters has been published in Chemical Physics Letters [7] and is reprinted in the next section.
Finally, conclusions and arising questions will be discussed in the last section of this chapter.

CHEMICAL PHYSICS LETTERS

Volume 78, number 2

1 March 1981

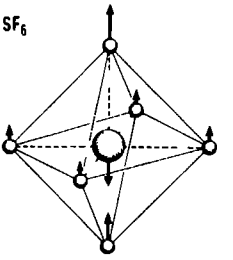

LASER INDUCED PREDISSOCIATION OF SF_6 CLUSTERS

J. GERAEDTS, S. STOLTE and J. REUSS

Fysisch Laboratorium, Katholieke Universiteit, 6525 ED Nijmegen, The Netherlands

Received 27 October 1980, in final form 2 December 1980

Dimer predissociation is sensitively detected as attenuation of the SF_5^+ ion signal from a SF_6 molecular beam crossed by a line tunable cw CO_2 laser. The dimer spectra show a double peak structure which is assigned to the symmetric and antisymmetric combination of the ν_3 vibration. The minimum observed linewidth is 3 cm^{-1} fwhm.

1 Introduction

Recently, N_2O dimers were observed to dissociate under exposure of a continuously tunable diode laser; the dissociation probability as a function of the laser frequency showed a double peak structure, with a separation of $\approx$13 cm^{-1} [1]. The peak at the blue side had about half the maximum height of the red one, it was suggested that this peak originates from a combination tone of the ν_3 asymmetric stretch and a N_2O libration motion of one constituent with respect to the other.

From the linewidth of $\approx$10 cm^{-1} the lower limit of the lifetime of the vibrationally excited complex was suggested to amount to 10^{-12} s. In a theoretical study [2] this lower limit was increased to 10^{-7} s taking into account the internal degrees of freedom of the dimer and the corresponding number of states which are populated in the seeded N_2O beam.

Similar measurements on C_2H_4 dimers were reported [3] where in the limit of low CO_2 laser power a single peak with a width of 16 cm^{-1} and a lower limit of 3×10^{-12} s for the lifetime from the vibrating complex was given.

At Berkeley, predissociation of H_2O, HF, NH_3, CH_3OH, C_6H_6 and C_6H_{12} dimers was measured, very recently [4], with a line resolution of $\approx$3.5 cm^{-1}.

We have measured the effects of a cw CO_2 laser beam on a SF_6 molecular beam, the molecular beam is detected by a very efficient space charge free electron bombardment ionizer followed by a magnetic mass spectrometer. Unlike the goal of Coulter et al. [5] in a similar experiment, our interest was focused on the destruction of clusters by the CO_2 laser and not on recoil effects of vibrationally excited monomers in the expansion zone immediately behind the nozzle, where collisions still occur. Whereas the beam attenuation spectrum of ref. [5] – measured on mass SF_5^+ – resembles those obtained by photoacoustical cells [6], our spectra look quite different and show – at low source pressures – two sharp peaks of roughly equal height which we suggest to represent the symmetric and asymmetric combination of single ν_3 excitations of the dimer constituents

There are some interesting and partially novel features in our method

(A) The best spectra were obtained tuning the mass spectrometer to the monomer mass SF_5^+ (127 amu). The reason is that due to massive fragmentation in the ionizer, the effect of small clusters appears on the monomer SF_5^+ mass before e.g. a signal on $SF_5^+ \cdot SF_6$ (273 amu) becomes detectable.

(B) Simultaneously, the total beam signal can be taken using a miniature manometer gauge which is partially transmitting the beam to the ionizer.

(C) A velocity selector permits the determination of the beam temperature $T_{\parallel}$ and the stream velocity v_s under experimental conditions [7].

(D) Although not being put into practice our experimental arrangement is such as to permit a scattering chamber attenuation measurement to assist the identification of the light cluster masses [8].

(E) The cw CO_2 laser is powerful enough and the transition matrix element of SF_6 is large enough to drive the observed dissociation into saturation.
(F) The observed spectra are simple and yield immediately information about the dipole–dipole term of the molecular potential which depends on the vibrational coordinate ξ_3 of the ν_3 mode.

The basic apparatus with its main features was described in ref. [8]. The added cw CO_2 laser can be used at a maximum power level of 35 W where the laser intersects the molecular beam. Its adjustment to properly cross the molecular beam was facilitated by the large attenuation observed already on the monomer mass, e.g. ≈5% for a pure SF_6 beam and 20% for an Ar-seeded beam at ≈210 K source temperature and at ≈1000 Torr source pressure with a nozzle of 20 μm diameter. The laser molecular beam crossing point is 45 cm downstream of the nozzle.

2. Results

In fig. 1 we show two attenuation spectra of a pure SF_6 beam. In fig. 1 ΔI is the measured difference in the beam intensity, in arbitrary units, with the laser on and off. These spectra are not corrected for saturation effects. The laser beam intersected the molecular beam at a right angle, where the optical beam diameter was 3 mm. The laser beam intensity was ≈140 W/cm^2 for all lines. The sharpest spectrum belongs to the attenuation measured at mass SF_5^+ in a SF_6–He mixture, P_0 = 1900 Torr stagnation pressure and T_0 = 295 K source temperature. The maximum attenuation at the P(30) (the red peak) and P(8) (the blue peak) line amounts to 0.8% in this case. The attenuation spectrum – measured on mass $SF_6 \cdot SF_5^+$ in a pure SF_6 beam, T_0 = 250 K and P_0 = 920 Torr – is broader and shows ≈50% attenuation at the P(24) and P(2) lines.

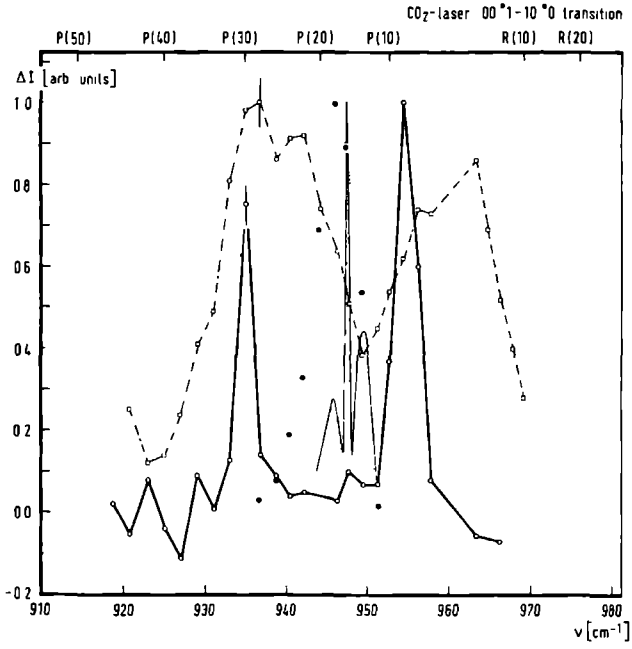

Fig. 1. The uncorrected molecular beam attenuation spectra as function of the frequency. The solid line corresponds to the attenuation at mass SF_5^+ and the dot and dash line to the attenuation at mass $SF_5^+ \cdot SF_6$. The beam and laser conditions of these two curves are summarized in table 1. The dotted curve is the recoil attenuation spectrum at mass SF_5^+ obtained by Coulter et al. [5]. The shaded area shows a grating spectrum of SF_6 at 150 K, measured by Rao [6].

In fig. 1 we also show the monomer recoil attenuation spectrum obtained by Coulter et al. [5] to demonstrate that in our experiment we really investigate an entirely different phenomenon. Also the linear absorption spectrum is shown [6].

The occurrence of two distinguished peaks at mass SF_5^+, which at our laser power, cannot be attributed to absorption of the monomer, leads to the conclusion that a substantial portion of the signal at mass SF_5^+ originates from $(SF_6)_2$ or heavier clusters present in the beam.

In fig. 2 we reproduce spectra, each taken at fixed

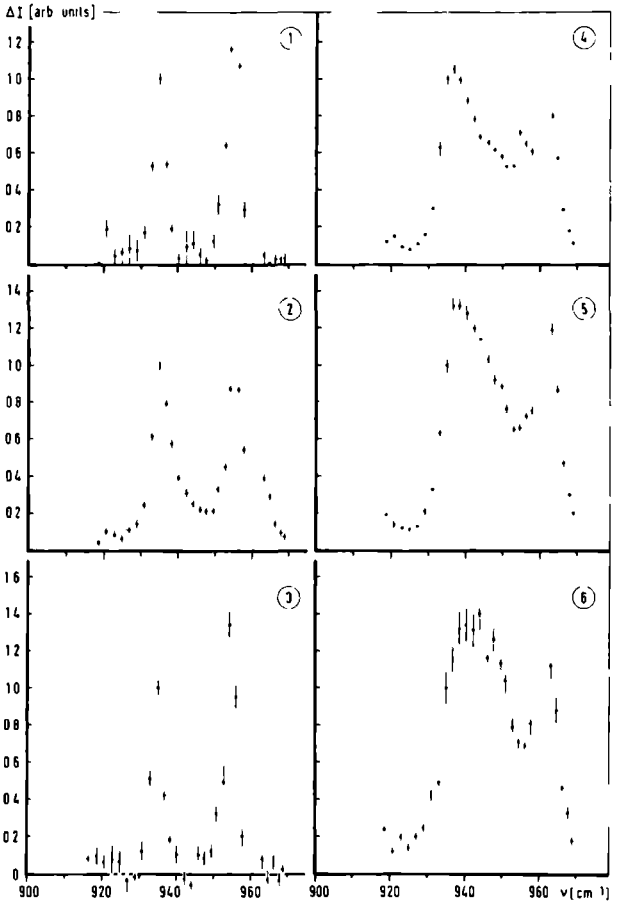

Fig. 2 Survey of molecular beam attenuation spectra as function of the frequency at several beam conditions. The attenuation in curves 1 and 3 are attributed solely to dimers, in curves 2 and 4, however, we estimate a significant contribution of heavier clusters. Curves 4, 5 and 6 give the difference between tuning of the mass spectrometer to mass SF_5^+, $SF_5^+ \cdot SF_6$ and $SF_5^+ \cdot (SF_6)_2$, respectively, at the same laser and beam conditions The experimental conditions are summarized in table 1, see last column. Curves 3–6 are measured at low laser power thus avoiding saturation effects.

Table 1
Compilation of results for pure SF_6 and SF_6–He and SF_6–Ar mixtures. P_0 is the stagnation pressure, T_0 is the source temperature, $T_\parallel$ is the beam temperature, v_s the stream velocity, both derived from the velocity distribution and L is the laser intensity at the point of beam intersection. The beam is detected at the mass spectrometer setting given in the column "mass". The two peak positions correspond to the red and blue peak, in case of the SF_6–Ar mixture two blue peaks can be distinguished The "peak height" is the attenuation taken at the P(30) transition of the CO_2 laser. The peak height given in parentheses gives the attenuation detected on the dimer mass $SF_5^+ \cdot SF_6$ relative to the monomer mass signal

Gas composition	P_0 (Torr)	T_0 (K)	$T_\parallel$ (K)	v_s (m/s)	L (W/cm^2)	Mass	Peak position (cm^{-1})		Peak height (%)	Figure
100% SF_6	350	210	28 2	294	140	SF_5^+	935	956	0.8 ± 0.3	2.1
	500	210	25.2	300	140	SF_5^+	935	956	0.9 ± 0.3	
	760	210	24.2	305	140	SF_5^+	935	956	3.2 + 1.0	–
	920	210	23.2	310	140	SF_5^+	935	956	3 7 ± 1.0	3/2.2
	920	210		–	140	$SF_5^+ \cdot SF_6$	938	960	53 ± 5(0.03)	1
5% SF_6 in He	1900	295	21.1	978	140	SF_5^+	935	955	0.7 ± 0.1	1
	780	200	–	–	140	$SF_5^+ \cdot SF_6$	938	960	–	–
5% SF_6 in Ar	1210	295	7.6	526	43	SF_5^+	935	955	0.5 ± 0.1	2.3
	760	200	–		43	SF_5^+	935	954/963	16 ± 2	–
	1500	200	8.95	445	43	SF_5^+	937	954/963	21 ± 2	2.4
	1500	200	–	–	43	$SF_5^+ \cdot SF_6$	938	963	24 ± 2(1.4)	2 5
	1500	200	9 35	439	43	$SF_5^+ \cdot (SF_6)_2$	943	963	7 + 1(0.2)	2.6

laser intensity and source conditions specified in table 1. Here, curves 1 and 3 correspond to a source condition where we expect only monomers and dimers to be present in the beam, curves 2 and 4 are measured under conditions where heavier clusters are present. These curves were obtained on mass SF_5^+. Clearly visible is the line broadening and the shoulder forming by increasing stagnation pressure. The two peaks have a separation which is rather independent of P_0 and amounts to ≈20 cm^{-1}. The minimum observed linewidth is ≈3 cm^{-1} fwhm. A line broadening is observed at the red peak for higher P_0 values. The saturation behaviour on both attenuation peaks (see fig 3) agrees with what is expected from $B_{12} F W \tau \approx 1$, where B_{12} stands for the Einstein absorption coefficient, F for a line shape function (e.g. a lorentzian with $\hbar\Delta\omega$ = 3 cm^{-1} fwhm), W for the energy density of the laser field (e.g. 20 W laser output and a spot diameter of 3 mm) and τ for the interaction time (≈10^{-5} s). The blue peak does not show a significant broadening with increasing P_0, however, at 963 cm^{-1} a new sharp line appears (see fig. 2, curve 4)

In fig. 2, curves 4, 5 and 6 show attenuation spectra each taken under the same source conditions but with the mass spectrometer tuned to mass SF_5^+, $SF_5^+ \cdot SF_6$ and $SF_5^+ \cdot (SF_6)_2$, respectively. We see that the sharp blue peak at ≈955 cm^{-1} disappears in curves 5 and 6 suggesting its origin as due to a pure dimer absorption (the dimers being most efficiently detected on mass SF_5^+). The red peak is asymmetrically broadened if measured on larger masses suggesting that trimers and tetramers absorb around 945 cm^{-1}. The line at 963 cm^{-1} which was also observed on mass $SF_5^+ \cdot (SF_6)_3$, remains sharp and cannot be attributed to absorption by a trimer $(SF_6)_3$, solely.

In fig. 3, the beam attenuation for increasing laser power L is depicted at P_0 = 920 Torr, for P(8), P(12), P(28) and P(30) A clear saturation is found (similar to results reported in ref. [5]), with an asymptotic L dependence as $\Delta I(L) = \Delta I(L = \infty) - CL^{-1/2}$ (where C is a constant) which permits the determination of $\Delta I(L = \infty)$.

At the source condition P_0 = 920 Torr and T_0 = 210 K (see fig. 2, curve 2) we find $\Delta I(L = \infty) \approx 6\%$, on mass SF_5^+ for P(30) and P(8) CO_2 laser transition. In the ionizer fragmentation of clusters to SF_5^+ yields a much larger signal than that found on the different cluster masses, for instance the ratio of the laser at-

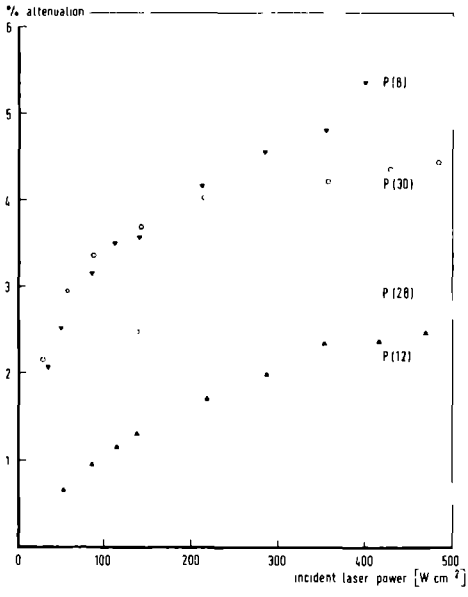

Fig. 3. The molecular beam attenuation ΔI versus the laser power L, obtained at 934.9, 936.8, 951.2 and 954.6 cm^{-1}, i.e. the $P(30)$, $P(28)$, $P(12)$ and $P(8)$ CO_2 laser transitions. The experimental conditions can be found in table 1, see last column.

tenuated signals at $SF_5^+ \cdot SF_6$ and SF_5^+ was ≈0.01 (see table 1).

An increase by a factor 2 in attenuation has been observed for the signal on mass SF_5^+ when L is increased from 150 W/cm^2 to very high values, the same ratio has been found on mass $SF_5^+ \cdot SF_6$, where practically 100% of the dimer-ion signal can be burnt out of the beam for large L, whereas at 140 W/cm^2 53% of the beam is attenuated (see table 1).

3. Discussion

The clear feature emerging from our results is the double peak structure with a spacing of 20 cm^{-1}. We interprete this feature as the splitting of the ν_3 excitation of a dimer constituent with symmetric and antisymmetric combinations of localized degenerate vibrations. This splitting must equal twice the interaction energy between the dimer constituents sandwiched between the symmetrized excited wave functions. In good approximation, the three-fold degenerate ν_3 vibration leads to two-fold degeneracy splitting of similar origin as that calculated for the H(2p)–H(1s) interaction [9]. Only two of the four calculated levels lead to a resultant non-vanishing transition dipole moment and can be excited. This yields a splitting of $S = 3\mu_{01}^2\langle R^{-3}\rangle$. Because of the large transition dipole moment μ_{01} of SF_6 the experimental splitting of 20 cm^{-1} should be regarded as reasonable; under the plausible assumption of a rather soft repulsion between two SF_6 molecules with $\langle R^{-3}\rangle \approx 1.4\, R_m^{-3}$ (R_m = 5.3 Å) perfect agreement with the observed splitting is found. With respect to the monomer Q head, the center of the doublet should appear redshifted by $\frac{1}{6}S$; this is in agreement with our observations.

The shoulder (at 945 cm^{-1}) in curve 4, fig. 2, becomes more pronounced and produces a significant shift if the mass spectrometer is tuned to mass $SF_5^+ \cdot SF_6$ (curve 5) and $SF_5^+ \cdot (SF_6)_2$ (curve 6) under unchanged source conditions. Interestingly, a new sharp blue peak appears, shifted to higher frequencies again by ≈10 cm^{-1} and to be attributed to larger clusters, see fig. 2 curves 4–6; simultaneously, the height of the red peak is significantly enlarged.

The peak height entry in table 1 shows that dimers must be expected to break up in the ionizer yielding monomer ions with a much higher probability than to show up as dimer ions (e.g. the $SF_5^+ \cdot SF_6$ signal at 920 Torr is ≈100 times weaker than the laser fragmented monomer signal).

At high source pressure P_0, a significant fraction of the monomer signal can be fragmented out of the Ar-seeded beam (more than 50%) leading one to speculate on the suitability of the laser-cluster-fragmentation process to obtain an efficient isotope separation method. For very dilute mixtures with clusters of one SF_6 surrounded by Ar atoms very efficient isotopic enrichment may be obtained. Probably, due to the large velocity differences between Ar and SF_6 molecules in that part of the nozzle expansion where cluster formation takes place, we could not detect $SF_5^+ \cdot (Ar)_n$, n = 1, 2, ..., as principal effect of the Ar seeding we observed only a considerable cooling ($T_\parallel \approx$ 8 K, see table 1). This effect, too, could be of great importance if isotope separation is achieved by mul-

tiple photon dissociation and if a small isotope shift necessitates line narrowing by lowering the beam temperature.

The fragmentation process saturates for high laser powers in agreement with a transition dipole moment of 0.4 debye.

There is the possibility that the relatively broad spectral features reported in refs. [1,3,4] are partially due to the poor detection efficiency of the dimer ions. If we would have detected the laser-fragmentation process on the dimer mass $SF_5^+ \cdot SF_6$, also for our very efficient space charge free ionizer [8] this would have meant measurements at 920 Torr with a linewidth at least 3X the minimum observed one. In case of a low efficiency ionizer the observed strong cluster fragmentation effects would require higher stagnation pressures yielding even broader lines.

Further work is in progress.

Acknowledgement

The help of Dr. H. Bluyssen and A. van Etteger who provided us with their well functioning tunable CO_2 laser and many advices are gratefully acknowledged. This work is part of the research program of the "Stichting voor Fundamenteel Onderzoek der Materie (F.O.M.)" and has been made possible by financial support from the "Nederlandse Stichting voor Zuiver-Wetenschappelijk Onderzoek (Z.W.O)".

References

[1] T.E. Gough, R.F. Miller and G. Scoles, J. Chem. Phys. 69 (1978) 1588.

[2] L.S. Bernstein and C.L. Kolb, J. Chem. Phys. 71 (1979) 2818.

[3] M.P Cassasa, D.S. Bomse, J.L. Beauchamp and K.C. Janda, J. Chem. Phys. 72 (1980) 6805, M.A. Hofbauer, W.R. Gentry and C.F. Giese, in Laser induced processes in molecules, eds. K.L. Kompa and S.D. Smith (Springer, Berlin, 1979).

[4] Y.T. Lee and Y. Ron Shen, Phys Today, submitted for publication.

[5] D.R. Coulter, F R. Grabiner, L M. Casson, G.W. Flynn and R.B. Bernstein, J. Chem. Phys. 73 (1980) 281.

[6] K.N. Rao, private communication

[7] D. van den Ende and S. Stolte, Chem. Phys. 45 (1980) 55.

[8] L. van Deursen and J. Reuss, Intern. J. Mass Spectrom. Ion Phys 23 (1977) 109.

[9] H. Margenau and N Kestner, Theory of intermolecular forces (Pergamon Press, Oxford, 1969) pp. 267, 268.

After the succesful theoretical approach to explain the observed splitting of the ν_3 vibration for SF_6 dimers the next step should be the calculation of the spectra for larger clusters.

Neither the linewidths nor the ratio of the peak heights at 935 cm^{-1} and 955 cm^{-1} of the attenuation peaks are constant in the measured spectra at dimer conditions (page fig. 1, and page fig. 2.1 and 2.3). Is it possible to develop a dissociation model for SF_6 clusters which depends on the rate of excitation of clusters to a predissociative state and the interaction time of the clusters with the radiation ?
Can there be anything concluded from the line shape and linewidth of the predissociation spectra of the various clusters ?

The best resolved and most intense spectra are obtained tuning the mass spectrometer to the monomer ion mass SF_5^+ (127 amu.). Is it possible to estimate the fragmentation probability of SF_6 clusters upon ionization ?

To produce clusters we have used beams of pure SF_6, 5% SF_6 in He and 5% SF_6 in Ar mixtures. Do we produce only $(SF_6)_n$, $n \geq 2$, or the clusters $(SF_6)_n$-He_m and $(SF_6)_n$-Ar_m, $n \geq 1$, $m \geq 1$, too ?

In the next chapter we will try to give an answer to some of the questions above.

References

1. J.L. Lyman, R.J. Jensen, J. Rink, C.P. Robinson and S.D. Rockwood
   Appl. Phys. Lett. 27 (1975) 87
2. J.H. Clark and R.G. Anderson
   Appl. Phys. Lett. 32 (1978) 46
3. J.L. Lyman
   J. Chem. Phys. 67 (1977) 1868
4. J. Bordé and C. Bordé
   Chem. Phys. 71 (1982) 417
5. T. Stanski and B. Adamczyk
   Int. J. Mass Spectr. and Ion Phys. 46 (1983) 31
6. F. Brunner, T.P. Cotter, K.L. Kompa and D. Proch
   J. Chem. Phys. 67 (1977) 1547
7. J. Geraedts, S. Setiadi, S. Stolte and J. Reuss
   Chem. Phys. Lett. 78 (1981) 277

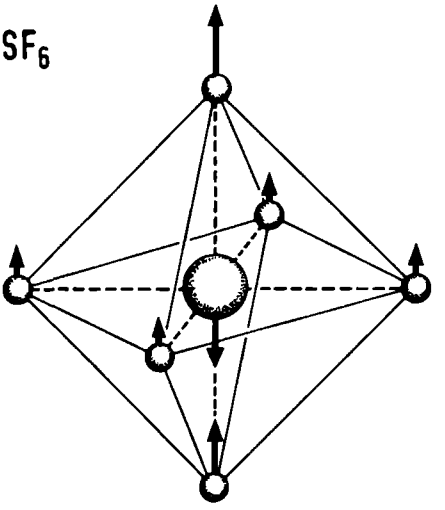

IV.1. Introduction

In this chapter $^{32}SF_6$ bound to $^{32}SF_6$, $^{34}SF_6$ and Ar will be discussed. The experimental results will be compared with a theoretical model. The results have been published in Zeitschrift für Physik A [1] which is reprinted in section 2.

In section 3 special attention is given to the line shape and saturation behaviour as influenced by orientational averaging effects. This section is a reprint of a contribution to the Faraday Discussion of the Chemical Society on Van der Waals molecules [2]. In section 4 an extension of the theory developed in section 3 is given and the results are confronted with some experimental data.

To isolate specific clusters we developed a two-laser modulation technique. A brief description of the method and some results are given in section 5.

In an SF_6 cluster isotopic substitution is also possible as natural SF_6 consists of 4.2% $^{34}SF_6$ molecules; dimers will therefore include 8.0% $^{34}SF_6$-$^{32}SF_6$ complexes. These isotopic clusters will be considered in section 6. In this section we will also discuss the aspects of isotope selective infrared cluster predissociation.

In the last section we describe the first results of the extension of the predissociation technique to the study of SF_6 in rare gas solid produced in a molecular beam. We have reported some of these measurements in the Faraday Discussion of the Chemical Society on Van der Waals Molecules [3].

Zeitschrift für Physik A Atoms and Nuclei

Z Phys A Atoms and Nuclei 304 167–175 (1982)

Vibrational Predissociation of SF_6 Dimers and Trimers

J Geraedts S Stolte and J Reuss
Fysisch Laboratorium Katholicke Universiteit Nijmegen The Netherlands

Received September 8 1981

IR photo-dissociation spectra of SF_6 clusters have been studied A He-seeded molecular beam has been attenuated by crossing it with a line tunable cw CO_2 laser of moderate power – In the electron bombardment beam ionizer ($E_{el} = 100$ eV) small neutral clusters are found to fragment predominantly to the main monomer mass (SF_5^+) – Predissociation spectra have been calculated for clusters containing up to six SF_6-molecules invoking the dipole-dipole resonance force to lift the degeneracy of the molecule – excited molecule interaction On the basis of these spectra dimer and trimer concentrations have been determined quantitatively for different molecular beam conditions

1. Introduction

Recently we have shown [1] that predissociation of $(SF_6)_2$ leads to a simple double-peaked absorption spectrum with a spacing of 20 cm^{-1} and a linewidth of about 3 cm^{-1} fwhm By measuring the attenuation of an SF_6 molecular beam on axis caused by a line tunable cw CO_2 laser of moderate power, one obtains the absorption-spectrum The typical attenuation peaks – at 935 cm^{-1} and 955 cm^{-1} – allowed us to single out the neutral parent-dimers in the molecular beam and to observe their fragmentation in the mass-spectrometer ionizer

For higher stagnation pressures larger cluster fragment ions become detectable, we have also analyzed the attenuation spectra under these conditions Although no unambiguous correspondence has been found between the sharp spectral features and the single parent clusters, a fit of a theoretical cluster spectrum to the measured attenuation curves yields the neutral cluster concentrations All present measurements have utilized an electron bombardment ionizer for mass spectrometric detection with an electron energy of 100 eV leading to high fragmentation probabilities of the clusters upon ionization Correspondingly we detect the attenuation of the SF_5^+-ion signal as consequence of the interaction of the CO_2 laser photons with the molecular beam because the strong fragmentation of small clusters results in highest detectibility of these clusters on mass SF_5^+

In the analysis a simple interaction potential of the electric dipole-dipole type (R^{-3}) suffices to describe the observations This dominant resonant force has been discussed by many authors at great lengths e g Mullikan [2] Hirschfelder [3] and Margenau [4] To our knowledge the two sharp dimer-peaks of the attenuation spectrum are the first direct measurements of resonant dipole-dipole forces between molecules Of the two interacting molecules one is in the vibrational ground state and the other one is excited in the ν_3-mode The molecule SF_6 is especially suitable to reveal this interaction because in the threefold degenerate ν_3-mode the molecule behaves like an isotropic harmonic oscillator in good approximation Perturbations e g Coriolis forces cause effects which are much smaller than the observed splitting of 20 cm^{-1} The large dipole transition matrix element μ_{01} of the ν_3-mode of SF_6 (0.388D [5]) is responsible for the large splitting observed

To produce clusters we have used beams of pure SF_6 and of 5% SF_6–He and 5% SF_6–Ar mixtures On the masses of He^+ and Ar^+ we also have detected a weak laser-induced attenuation signal This indicates that there are neutral $(SF_6)_n$–$(He)_m$ and $(SF_6)_n$–$(Ar)_m$ complexes present in the beam

Their concentration is too weak to influence the present spectra.

In this paper we restrict ourselves to the observations made with the 5% SF_6 – He mixture. The source conditions are characterized by a stagnation temperature $T_0 = 233$ K, a stagnation pressure P_0 between 1.000 and 1.850 torr and a nozzle diameter of 30 μm; only casual remarks will be found based on observations at other source conditions.

The SF_6-component consist of 4.2% $^{34}SF_6$-molecules [8]. The dimers will therefore include 8% $^{34}SF_6 \cdot {}^{32}SF_6$-complexes. The measured spectra contain one distinct attenuation peak of this mixed dimer at 921 cm^{-1}. Other peaks were not yet observed.

Recently, the predissociation lifetime of the vibrationally excited N_2O dimer was calculated [6] and compared with the limiting values of 10^{-4}–10^{-7} s, obtained experimentally [7]. In order to find agreement Morales and Ewing had to invoke a resonant dipole-dipole force. The results of the present paper on $(SF_6)_n$ may be regarded as strong backing of their argumentation.

2. The Experiment

The apparatus is shown schematically in Fig. 1. The molecular-beam machine consists of five separate vacuum chambers, each with its own pumping system. In the source chamber the beam is produced by gas expansion through a nozzle of 30 µm [9]. After a distance of 10–15 mm the beam passes through a skimmer (sk 1) into the buffer chamber. In the next chamber the chopper (ch 1) and the velocity selector

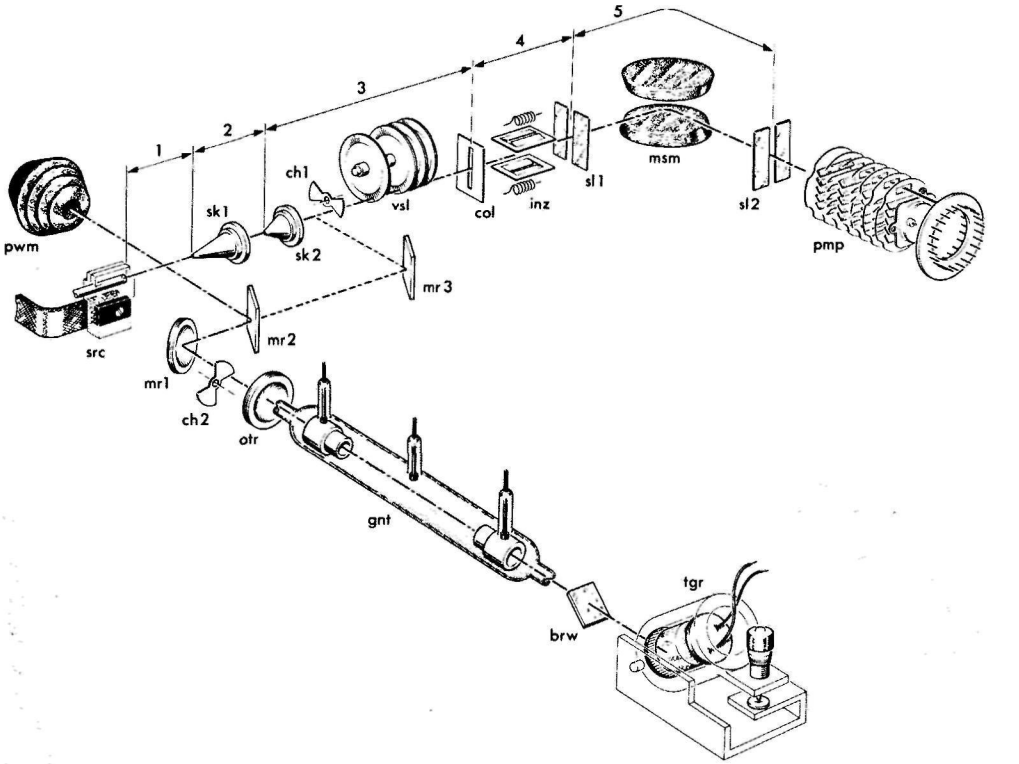

Fig. 1. The experimental set up. The molecular beam apparatus consists of the source (src, 0.03 mm ∅), skimmer 1 (sk 1, 1.1 mm ∅), skimmer 2 (sk 2, 3 mm ∅), the chopper (ch 1), the velocity selector (vsl), the collimator (col, 1.3 * 1.8 mm^2), the ionizer (inz), slit 1 (sl 1, 1.3 mm), the mass spectrometer magnet (msm), slit 2 (sl 2, 1.3 mm) and the particle multiplier (pmp). The laser system consists of the tunable grating (tgr), the brewster angle window (brw), the gain tube (gnt), the plano concave output reflector (otr), the chopper (ch 2), the concave mirror (mr 1), and one flat mirror (mr 2 or mr 3), and the power meter (pwm). The distances are 10 mm (1), 300 mm (2), 1500 mm (3), 900 mm (4) and 1500 mm (5)

(vs I) - slotted disk type - are mounted. In the fourth chamber the molecular beam is ionized by means of a high efficiency ionizer (inz) and, in the fifth chamber, focussed by ion lenses into the mass spectrometer magnet (msm) - 14 mm pole diameter, 0-9 kGauss - to be detected by a particle multiplier (pmp) at the end of the machine. The maximum pressures - under working conditions - are: 10^{-3} torr (1), $5\ 10^{-6}$ torr (2), $5\ 10^{-7}$ torr (3), $<10^{-8}$ torr (4) and $5\ 10^{-7}$ torr (5).

The lasersystem consist of a line tunable cw CO_2 laser [10], a chopper (ch 2), a power meter (pwm) and a spectrum analyzer The laser has a flow system and operates typically at a total pressure of 30 torr The gas flows through a longitudinally excited gain tube (gnt) The maximum single-line power ranges from 5 W to 45 W and is found to be stable within 2% over several hours

Two choppers - one in the molecular-beam (ch 1) machine and one in the laser-system (ch 2) - permit phase - sensitive detection, either of the molecular beam or of the effect of the laser radiation on the molecular beam.

The experimental data, the molecular beam signal and the laser power, are directly transferred to an AIM-65 microcomputer (Rockwell Corp) for storage and data reduction The microcomputer also monitors the temperature of the source and the flux in the m s. magnet

The laser beam crosses the molecular beam at a right angle, between nozzle (30 μm ∅) and skimmer (1 1 mm ∅), about 7 mm downstream the nozzle. The position of this intersection has been changed with respect to [1] Another change is that for the present results the laser has been focussed to a two times smaller waist. The spectra discussed in Sect. 4 are measured at 1 Watt laser power Changing the laser frequency the power level was adjusted by changing the discharge current in the gain tube of the laser. Power reduction was achieved by utilizing a wire mesh (stainless steel, 0.2 mm ∅, 0 5 * 0 5 mm^2 opening). With a molecular beam velocity of about 870 m/s and the assumption of a Gaussian laser beam profile with a wast of 0.7 mm, 1 W corresponds with a laser fluency of 1.3 J/m^2

The molecular beam collimation is effected by the skimmer (sk 1) and a collimator (col) Fragments with a transverse recoil velocity $\geqq 30$ m/s do not pass through this slit (col). No effect of monomer recoil (i.e beam attenuation) is detectable [1].

3. Theoretical Spectrum

We assume that the geometry of a SF_6-cluster agrees with the equilibrium-geometry of clusters as calculated by Bonisent and Mutaftschiev [11]. In Table 1 we give the positions $\mathbf{R}_i$ for $1 \leqq i \leqq 6$ of the SF_6-molecules in a hexamer which is fixed in x, y, z-space. The oligomers up to and including the hexamer, $n=6$, are built up by adding each time one SF_6-molecule to the previous structure, starting from the monomer, $n=1$ The length of the distance vector $\mathbf{R}_{ij}=\mathbf{R}_i-\mathbf{R}_j$ between two nearest neighbour molecules i and j for $1 \leqq i \neq j \leqq n$ in a cluster is determined by the isotropic SF_6-SF_6-interaction. In Table 1 this distance is taken unity An SF_6 molecule behaves as a three-dimensional oscillator and has three orthogonal equivalent vibrational axes, $\mathbf{x}_i$, $\mathbf{y}_i$ and $\mathbf{z}_i$ what concerns the ν_3-mode.

Table 1. The components of the position vectors $\mathbf{R}_i=(x_i, y_i, z_i)$ for clusters containing up to six SF_6-molecules Nearest neighbours distances are unity

i	1	2	3	4	5	6
x_i	$-\sqrt{3}\,3$	$\sqrt{3}\,6$	$\sqrt{3}\,6$	0	0	$5\sqrt{3}\,9$
y_i	0	1 2	−1 2	0	0	0
z_i	0	0	0	$\sqrt{6}\,3$	$-\sqrt{6}\,3$	$2\sqrt{6}\,9$

In good approximation the observed spectral features correspond to the eigen values of an interaction hamiltonian which contains as operator solely dipole-dipole terms

$$H_{DD}=\frac{1}{4\pi\varepsilon_0}\sum_{i<j} R_{ij}^{-3}\ [\boldsymbol{\mu}_i\ \boldsymbol{\mu}_j-3(\boldsymbol{\mu}_i\ \hat{\mathbf{R}}_{ij})(\boldsymbol{\mu}_j\ \hat{\mathbf{R}}_{ij})] \qquad (3.1)$$

where $R_{ij}=|\mathbf{R}_{ij}|$, $\hat{\mathbf{R}}_{ij}=\mathbf{R}_{ij}/R_{ij}$ and where $\boldsymbol{\mu}_i$ represents the dipole operator.

The total wave functions of a simply excited cluster can be written as, e.g

$$|x_1, y_1, z_1, \cdots, x_i, y_i, z_i^{\dagger}, \cdots, x_n, y_n, z_n\rangle = |z_i^{\dagger}\rangle \qquad (3.2)$$

indicating that only one molecule i is excited and *the excitation is along the z-axis* The $3n$ wave functions form a subset of degenerate states if H_{DD} is neglected

Only the matrix elements between different singly excited eigen functions are non-vanishing, e g.

$$\langle z_i^{\dagger}\,|H_{DD}|\,y_j^{\dagger}\rangle \neq 0. \quad \text{if } i \neq j \qquad (3.3)$$

Diagonalization of the energy-matrix for a n-cluster yields the eigen values, i.e. the energy shifts $\Delta_{n,m}$ with respect to the fundamental frequency. The eigen functions $|u_{n\,m}\rangle$ are used to calculate the transition strengths

$$S_{n\,m} \propto |\langle u_{n\,m}|\boldsymbol{\mu}|0\rangle|^2 \qquad (3.4)$$

where $|0\rangle$ indicates the groundstate $|x_1, y_1, \cdots, z_n\rangle$ and $\boldsymbol{\mu}=\sum_{i=1}^{n}\boldsymbol{\mu}_i$.

Table 2 The theoretical spectrum The energy shift $\Delta_{n\,m}$ is in units of $(4\pi\varepsilon_0)^{-1}\,\mu_{01}^2\,\langle R^{-3}\rangle$ where R describes the nearest neighbour distance and $\mu_{01}=0.388D$ The column $g_{n\,m}$ describes the degeneracy and $g_{n\,m}\,S_{n\,m}$ the total transition strength - from the ground state to a individual excited level m - of an n cluster

m	$\Delta_{n\,m}$	$g_{n\,m}$	$g_{n\,m}\,S_{n\,m}$
monomer $n=1$			
1	+0.00	3	3.00
dimer $n=2$			
1	−2.00	1	2.00
2	−1.00	2	0
3	+1.00	2	4.00
4	+2.00	1	0
trimer $n=3$			
1	−2.50	1	0
2	−1.93	2	4.34
3	−1.00	2	0
4	+1.43	2	1.66
5	+2.00	1	3.00
6	+3.50	1	0
tetramer $n=4$			
1	−2.50	3	0
2	−1.89	3	6.70
3	+0.50	2	0
4	+2.39	3	5.30
5	+5.00	1	0
pentamer $n=5$			
1	−3.09	2	0
2	−2.50	1	0
3	−2.04	2	2.66
4	−1.97	1	4.46
5	−1.80	1	0
6	−0.86	2	1.99
7	+1.86	2	0
8	+2.63	2	5.35
9	+3.51	1	0.54
10	+5.76	1	0
hexamer $n=6$			
1	−3.34	1	0
2	−3.32	1	0.0015
3	−2.88	1	0.011
4	−2.56	1	0.38
5	−2.21	1	4.13
6	−2.12	1	1.07
7	−1.90	1	0.44
8	−1.57	1	0.94
9	−1.47	1	0
10	−1.36	1	2.70
11	+0.54	1	1.06
12	+0.59	1	1.60
13	+2.54	1	0.10
14	+2.61	1	0
15	+2.63	1	3.31
16	+3.36	1	1.87
17	+4.24	1	0.38
18	+6.25	1	0.00014

Table 3 Energy shifts and transition probabilities for the mixed dimer $^{34}SF_6$, $^{32}SF_6$ The index m describes a particular transition $\Delta_{2\,m}$ the energy shift in cm^{-1} $S_{2\,m}$ the strength of the correspond ing transition and $g_{2\,m}$ the degeneracy of the excited level

m	$\Delta_{2\,m}$ [cm^{-1}]	$g_{2\,m}$	$g_{2\,m}\,S_{2\,m}$
mixed dimer $n=2$			
1	−2.47±0.5	1	1.84
2	7.5±0.3	1	0.16
3	−1.96+0.3	2	0.76
4	2.4±0.1	2	3.24

Following the assumption that the SF_6-molecule behaves like an isotropic oscillator the influence of the rotational states is entirely neglected

In Table 2 the energy shifts $\Delta_{n\,m}$ in units of $(4\pi\varepsilon_0)^{-1}\,\mu_{01}^2\,\langle R^{-3}\rangle$ are shown In our case the fundamental frequency of the ν_3-mode is 948 cm^{-1} [8] and the transition dipole moment $\mu_{01}=0.388D$ [5] One has to take as unit the value of (6.8 ±0.2) cm^{-1} in order to be consistent with the experimental data for the dimer and the trimer as will be discussed below In Table 2 also is shown the transition strength $S_{n\,m}$ for a vibrational transition of a cluster relative to the transition strength of a monomer $S_{1\,1}$ The sum over all the products of transition strengths $S_{n\,m}$ and degeneracy $g_{n\,m}$ of an n-cluster is $3n$ in accordance with the sum rule

In the SF_6-beam there is a natural abundance of 4% of the $^{34}SF_6$-isotope, its ν_3-frequency is red shifted by 17 cm^{-1} [8] with respect to the main $^{32}SF_6$-component Therefore we expect also to find an attenuation signal caused by predissociation of the mixed-dimer $^{34}SF_6$ $^{32}SF_6$ on mass $^{34}SF_5^+$ as well as on mass $^{32}SF_5^+$ if the correct laser lines are chosen The mixed dimer possesses three times two nearly degenerate states (1.7 cm^{-1} apart) which have off-diagonal elements due to the dipole dipole interaction of +6.8 cm^{-1} and −13.6 cm^{-1} depending on whether the dipole moments are perpendicular or parallel to the intermolecular axis In Table 3 the energy shifts $\Delta_{n\,m}$ and the transition strengths $S_{n\,m}$ for the mixed-dimer are displayed In Fig 2 the stick-spectra for $(^{32}SF_6)_n$ $n=1$ -- 6 and for the mixed-dimer $^{34}SF_6$ $^{32}SF_6$ are shown

4. The Fit Procedure

Above we have calculated the theoretical spectrum for a dominant dipole-dipole interaction In order to compare these results to our measurements we must assume a certain line form and line width for the different cluster-transitions A Lorentz-profile has been chosen without, however, implying that the line

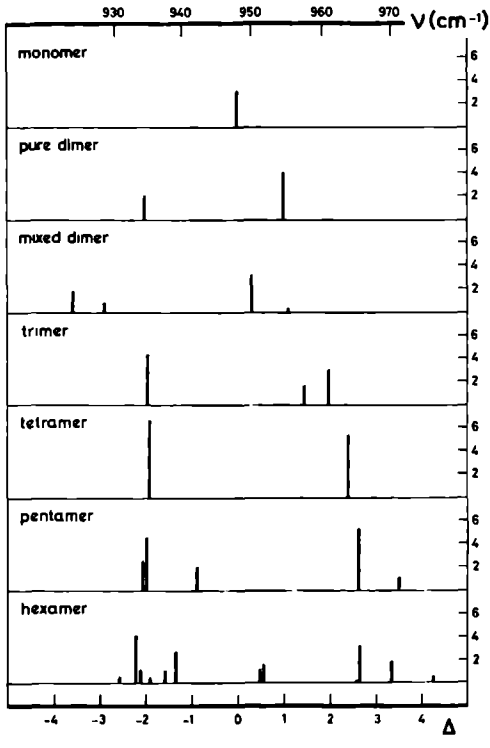

Fig. 2. The stick spectrum The energy shift Δ is given below in units of $(4\pi\varepsilon_0)^{-1}\,\mu_{01}^2\,\langle R^{-3}\rangle$ On the upper scale use is made of the fit to the experimental dimer results The relative intensity corresponds to g S, see Tables 2 and 3

width is necessarily caused by predissociation lifetime.

We propose a very simple model to explain the dissociation of the clusters; rapid predissociation of the excited cluster supersedes stimulated emission. The probability of dissociation d_n of N_n n-clusters is

$$d_n = N_n \exp(-r_n t) \tag{4.1}$$

where t is the laser interaction time and r_n is the rate of excitation of a n-cluster. The difference of the mass spectrometer signal without and with laser action contains the factor $(1-\exp(-r_n\cdot t))$. Normally, the mass spectrometer signal is determined not only by the concentration of n-clusters, but also by their relative ionization and fragmentation probability upon electron bombardment. We take the ionization probability proportional to n; the monomer ionization probability equals α_1. The fragmentation probability of a cluster of size n to an ion of size k – i.e. SF_k^+ $(SF_6)_{k-1}$ – is denoted by f_{kn}. The observed difference of the ion signal, without and with laser, amounts to

$$\Delta I_k = \alpha_1 \cdot \sum_{n\geqq k} n f_{kn} N_n (1-\exp(-r_n\cdot t)) \tag{4.2}$$

The product of the rate r_n and the interaction time t can be written as

$$r_n\cdot t = \sum_m \frac{\mu_{01}^2}{\hbar^2\varepsilon_0}\cdot\frac{F}{c}\cdot\frac{2}{\Gamma_{n\,m}}\cdot\frac{g_{n\,m}\cdot S_{n\,m}}{3} \cdot\frac{(\Gamma_{n,m}/2)^2}{(\omega-\omega_{n,m})^2+(\Gamma_{n,m}/2)^2} \tag{4.3}$$

where F represents the laser fluency and μ_{01} the transition dipole moment, $\omega_{m,n}$, $\Gamma_{m\,n}$, $g_{n\,m}$ and $S_{n,m}$ stand for the (angular) transition frequency, the line width, the degeneracy and the strength of a particular transition m of an n-cluster The degeneracy and strength of a transition are shown in Table 2. The transition frequency can be taken from the same table, $\hbar\omega_{m,n} = 948\,\mathrm{cm}^{-1} + \Delta_{m\,n}$, where a scaling was already applied by fitting the experimental results – one unit corresponds with $(6.8\pm0.2)\,\mathrm{cm}^{-1}$ –, the line width has to be fitted, too, from the experimental results. Writing down (4.3) a Lorentz-profile was assumed to describe the experiments.

Our He-seeded SF_6 beams allowed the observations of dimers and trimers, only, i.e $n\leqq 3$, in accordance with the absence of any trace of SF_5^+ $(SF_6)_3$ in our mass spectra, see Fig. 3 In Figs 4–7 the experimental results – obtained on the ion-mass SF_5^+ with 1 W laser power – are displayed together with the fit using (4.2). The calculated rate r_2 has been tested at a frequency of $935\,\mathrm{cm}^{-1}$ and a stagnation pressure $P_0 = 1{,}000$ torr where only monomers and dimers are present in the beam in a measurable amount. The product $r_2\cdot t \doteq 0.36$ is calculated for a molecular beam velocity of 870 m/s, a laser waist of 0.7 mm at the point of intersection, $\Gamma_2 = \Gamma_{2,1} = \Gamma_{2\,3} = 1.5\,\mathrm{cm}^{-1}$ and for 1 W laser power. The power dependence of the attenuation signal at $P_0 = 1{,}000$ torr does not allow a very precise determination of $r_2\cdot t$; $r_2(1\,\mathrm{W})\cdot t = 0.36$ describes the observation very well (Fig. 8). An uncertainty of 30% in the rate r_2 yields a 10% variation of ΔI_∞, the attenuation at high laser fluency. – In parenthesis, $r_2(1\,\mathrm{W})\cdot t = 0.36$ corresponds to a photodissociation cross section of $0.5\cdot10^{-20}\,\mathrm{m}^2$, for the red dimer peak at $935\,\mathrm{cm}^{-1}$.

5. The Fragmentation Probabilities

From our measurements quantitative conclusions can be drawn with respect to the fragmentation

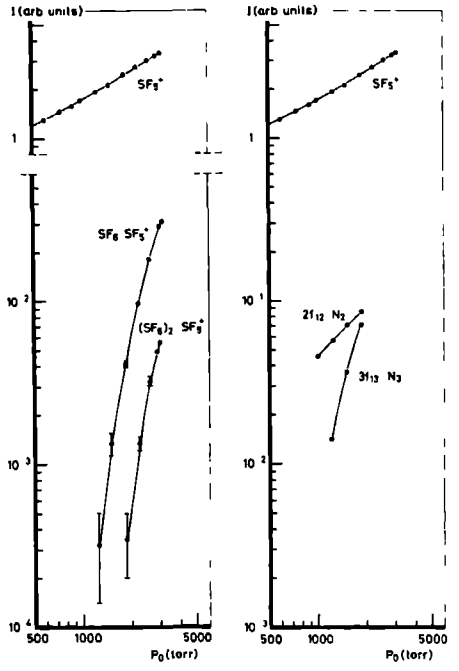

Fig 3 Mass spectrometric (left) and spectropic (right) intensities vs the stagnation pressure P_0 The SF_5 signal corresponds to the mass spectrometric signal of the SF_6 beam at higher stagnation pressures this signal contains cluster-admixtures to a maximum of 4% The SF_6 SF_5^+ [$(SF_6)_2$ SF_5^+] signal normally is taken as a measure of dimer [trimer]-concentrations The $2f_{12}$ $N_2[3f_{13}N_3]$ signal is more than ten times stronger and correspond to the actual cluster intensity $f_{12} \geqq 0.99$ [$f_{13} \geqq 0.93$] at $P_0 = 1850$ torr (see Sect 5) The spectroscopic signals are the saturated values (e g $2f_{12}N_2$) for high laser power

probabilities f_{kn} First the reminder that $k=1(2)$ stands for the probability that an n-cluster fragments to SF_5^+ (SF_5^+ SF_6), a fragmentation to masses like SF_3^+ or SF_3^+ SF_6 was not systematically studied in the present work though roughly speaking a repetition of the relative monomer-fragment-intensities SF_x^+ for $1 \leqq x \leqq 5$ was observed amongst the SF_6 SF_x^+ fragments

The value of $nf_{1n}N_n$ can be obtained from the fit displayed in Figs 4–7 In the corresponding captions the ratios $nf_{1n}N_n/(\sum_{\nu=1} \nu f_{1\nu}N_\nu)$ are given which multiplied by the strength of the SF_5^+-signal yield $2f_{12}N_2$ and $3f_{13}N_3$

From Fig 3 one learns that $f_{12}/f_{22} \geqq 100$ at $P_0 = 1250$ torr, this follows directly from the ratio R of the $2f_{12}N_2$-signal to the SF_5^+ SF_6 signal the latter one being ideally equal to $2\alpha_1 f_{22} N_2$ This ratio assumes the value 100 if admixture from larger clusters is neglected to the SF_5^+ SF_6-signal For higher P_0-values the ratio R assumes smaller values, yet the highest masured value $f_{12}/f_{22} - 100$ should hold for f_{12}/f_{22} also at these higher pressures, as lower limit, e g $R = 20$ at $P_0 = 1850$ torr evidently points to the influence of trimers contributing to the SF_5^+ SF_6-signal

Next we use the plausible assumption that the total ionization probability that an n-cluster yields an ion cluster containing SF_5^+ equals the monomer frag-

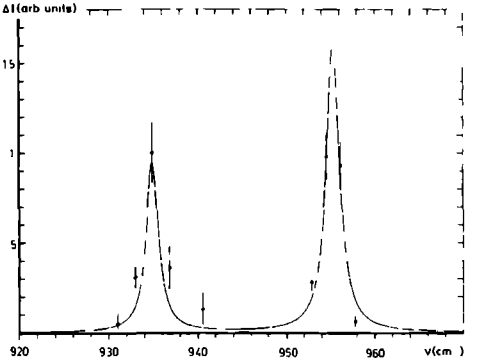

Fig 4 The cluster spectrum at $P_0 = 1000$ torr $T_0 = 233$ K and 1 W laser power The fit (solid curve) yields $\Gamma_2 = 1.5 \pm 0.4$ cm^{-1} $2f_{12}N_2/(f_{11}N_1 + 2f_{12}N_2 + 3f_{13}N_3) = (2.7 \pm 0.5)$ and $3f_{13}N_3/(f_{11}N_1 + 2f_{12}N_2 + 3f_{13}N_3) = \text{zero}$ Optimum agreement was found for $(4\pi r_0)^{-1}\mu_{01}^2\langle R^{-3}\rangle = 6.8$ cm^{-1} The unshifted frequency was taken equal to 948.5 cm^{-1} The spectrum is normalized (see *NF* Table 4)

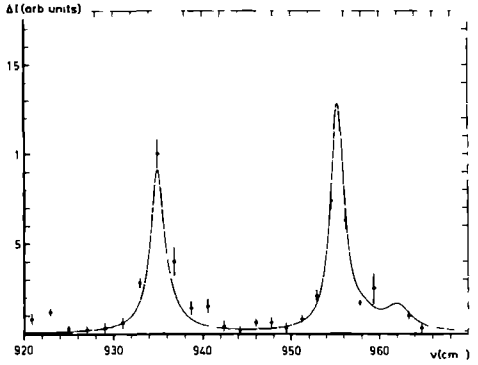

Fig 5 The cluster spectrum at $P_0 = 1250$ torr The fit (solid curve) with fixed $\Gamma_2 = 1.5$ cm^{-1} (see Fig 4) and with fixed $\Gamma_3 = 3.3$ cm^{-1} (see Fig 6) yields $2f_{12}N_2/(f_{11}N_1 + 2f_{12}N_2 + 3f_{13}N_3) = (3.0 \pm 0.4)\%$ and $3f_{13}N_3/(f_{11}N_1 + 2f_{12}N_2 + 3f_{13}N_3) = (0.8 \pm 0.2)\%$ Further details in caption of Fig 4

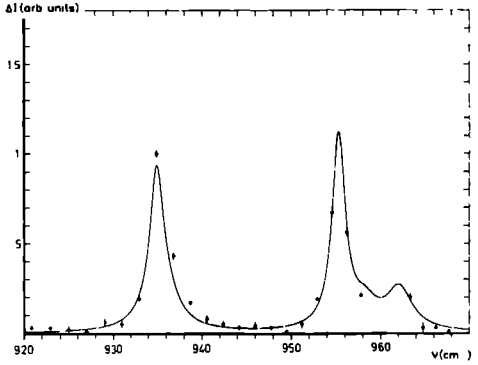

Fig. 6. The cluster spectrum at $P_0 = 1\,500$ torr With fixed $\Gamma_2 = 1.5\,cm^{-1}$ the fit yields $2N_2 f_{12}/(f_{11}N_1 + 2f_{12}N_2 + 3f_{13}N_3) = (3.5 \pm 0.5)\%$ and $3N_3 f_{13}/(f_{11}N_1 + 2f_{12}N_2 + 3f_{13}N_3) = (1.8 \pm 0.3)\%$ The line width for this P_0-value was determined to $\Gamma_3 = (3.3 \pm 0.4)\,cm^{-1}$ considering too measurements at 0.5 W and 2.5 W Further details in the caption of Fig 4

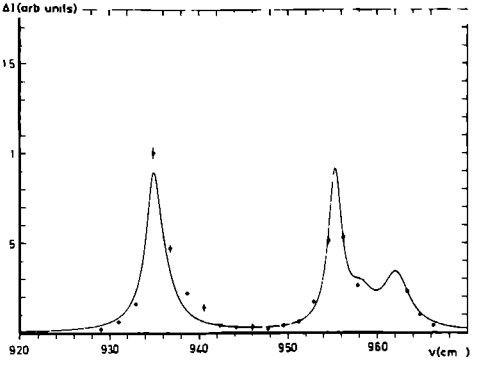

Fig 7 The cluster spectrum at 1 850 torr With fixed $\Gamma_2 = 1.5\,cm^{-1}$ and $\Gamma_3 = 3.3\,cm^{-1}$ the fit yields $2f_{12}N_2/(f_{11}N_1 + 2f_{12}N_2 + 3f_{13}N_3 + 4f_{14}N_4) = (3.6 \pm 0.6)\%$ and $3f_{13}N_3/(f_{11}N_1 + 2f_{12}N_2 + 3f_{13}N_3 + 4f_{14}N_4) = (3.0 \pm 0.5)\%$ and $4f_{14}N_4/(f_{11}N_1 + 2f_{12}N_2 + 3f_{13}N_3 + 4f_{14}N_4) =$ zero The trimer shoulder at 962 cm^{-1} is clearly visible Further details in the caption of Fig 4

mentation probability f_{11} to SF_5^+, i e

$$f_{11} = \sum_{k=1}^{n} f_{kn} \qquad (5.1)$$

The violent eruption of SF_6^+ emitting an uncharged F-atom is not measurably influenced by the presence of loosely bound SF_6-partners, an assumption plausible at least for small n-values

Then, $f_{12}/f_{22} \geqq 100$ yields $0.99 \leqq f_{12}/f_{11} \leqq 1$ Hence, one can simplify the fit-parameter of caption 4, $2f_{12}N_2/(f_{11}N_1 + 2f_{12}N_2) \approx 2N_2/(N_1 + 2N_2)$ within 1 % (see Table 4)

For $P_0 = 1\,850$ torr, the ratio of the $3f_{13}N_3$ - to the SF_5^+ $(SF_6)_2$ - signal yields $f_{13}/f_{33} \geqq 150$, the inequality again because of possible contributions of larger clusters to the latter signal. Similarly the ratio of the $3f_{13}N_3$ - to the SF_5^+ SF_6-signal yields $f_{13}/f_{23} \geqq 15$, here the inequality stems from possible contributions of larger and smaller (i e dimer) clus-

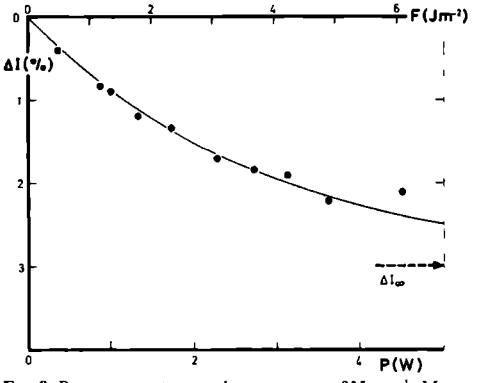

Fig. 8. Beam attenuation vs laser power, at 915 cm^{-1} Measurements were performed at $P_0 = 1\,000$ torr (see Fig 4) The upper scale F indicates the laser fluency seen by the dimers The experimental results (•) have been compared to a $(1 - \exp(-r_2 \cdot t))$ dependence with $r_2(1\,W)\ t = 0.36$ (solid curve) $\Delta I_\infty = (3.0 \pm 0.1)\%$ means that 1.5 % dimers are present in the beam

Table 4 Cluster concentrations for different stagnation pressures P_0 The second column (NF) yields the normalization factor leading from the normalized spectra in Figs 4–7 to the observed beam attenuations The third and fourth column describe the dimer and trimer concentrations N_2/N_1 and N_3/N_1 obtained from the fits to the spectra in Figs 4–7 The uncertainty corresponds to one standard deviation The fifth column yields the relative number of SF_6 molecules bound in dimers and trimers (the sum of column 3 and 4) This can be compared to the last column obtained from the saturation behaviour, e g displayed in Fig 8

P_0 [torr]	$10^{-2}\ NF$	$2N_2/N_1$ %	$3N_3/N_1$ %	$(2N_2 + 3N_3)/N_1$ %	$(2N_2 + 3N_3)/N_1$ %
1 000	0.86 ± 0.09	2.7 ± 0.5	–	2.7 ± 0.5	1.0 ± 0.1
1 250	1.23 ± 0.12	3.0 ± 0.5	0.8 ± 0.2	1.8 ± 0.7	–
1 500	1.65 ± 0.17	3.5 ± 0.5	1.8 ± 0.3	5.3 ± 0.8	4.8 ± 0.2
1 850	2.16 ± 0.22	1.6 ± 0.6	1.0 ± 0.5	6.6 ± 1.1	6.7 ± 0.2

ters to the SF_5^+ SF_6-signal Assumption (5 1) then gives $0\,93 \leq f_{13}/f_{11} \leq 1$ Again one can simplify the fit parameter of Fig 5

$$3f_{13}N_3/(f_{11}N_1 + 2f_{12}N_2 + 3f_{13}N_3)$$
$$\approx 3N_3/(N_1 + 2N_2 + 3N_3)$$

within 8% (see Table 4)

6. Discussion

It should be clear from the foregoing that we do not pretend to have achieved high resolution spectroscopy of SF_6-clusters, neither experimentally nor what concerns the theoretical treatment On the other hand spectra have been obtained at probing frequencies spaced by about $2\,cm^{-1}$ which show a remarkable structure, a very simple theoretical model seems to explain very well this observed structure with a single parameter i e $(4\pi\varepsilon_0)^{-1}\ \mu_{01}^2\ \langle R^{-3}\rangle = 6\,8\,cm^{-1}$

The Lorentzian line widths $\Gamma_{n\,m}$ introduced to reproduce the line shape perhaps suggests that the lifetime of the vibrationally excited clusters is of dominant influence on the line widths In our opinion however, there is no evidence for such interpretation, it is equally possible that the width reflects the internal state distribution of the excited cluster

We have assumed in our fits displayed in Figs 4–7 that $\Gamma_{n\,m}$ is independent of the level index m (see Table 2) Inspection of Fig 4 demonstrates that this assumption can be questioned, the $(n\ m)=(2\ 1)$ peak seems clearly broader than the (2 3) peak In view of the coarse nature of our results we felt an introduction of different width $\Gamma_{n\,m}$ for the different transitions m of one n-cluster unwarranted

The fact that for the trimer we had to apply a two times larger $\Gamma_3(3\,3 \pm 0\,4\,cm^{-1})$ as compared to $\Gamma_2(1\,5 \pm 0\,4)$ may point to a shorter lifetime as well as to the lifting of the degeneracy of the more numerous internal states (e g van der Waals stretching modi) This energy splitting can be influenced by hexadecapole forces or angle dependent dispersion forces

The mixed dimer $^{32}SF_6$ $^{34}SF_6$ shows experimentally a transition at $921 \pm 2\,cm^{-1}$ compatible with the theoretical value $923\,cm^{-1}$ One deduces $\mu_{01}(^{32}S)\ \langle R^{-3}(^{32}S - ^{32}S)\rangle/\mu_{01}(^{34}S)\ \ \langle R^{-3}(^{34}S - ^{32}S)\rangle = 0\,9 \pm 1$ Due to the natural abundance, the mixed dimer peak is expected to be about a factor 25 weaker than the pure dimer peak ($935\,cm^{-1}$), a ratio born out by the experiment (Fig 9)

Table 4 displays absolute concentrations of clusters in the SF_6 beam determined by our fit procedure

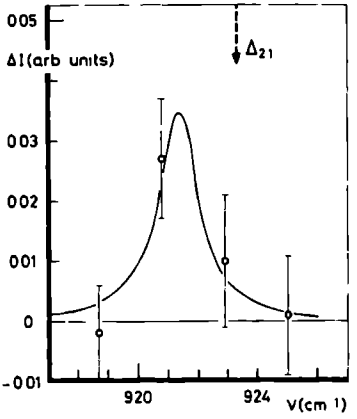

Fig 9 A $^{32}SF_6$ $^{34}SF_6$ dimer line Detail study of Fig 6 around $923\,cm^{-1}$ (dashed arrow) where the stick spectrum predicts a mixed dimer transition The contribution of pure $^{32}SF_6$-clusters has been subtracted utilizing the fitted spectrum of Fig 6 The solid line corresponds to a fitted Lorentzian (with $\Gamma_2 = 1\,5\,cm^{-1}$) centered at $\Delta_{2\,1} = (-26\,5 \pm 1\,5\,cm^{-1})$

(For a consistency check the concentrations were too determined from the saturation behaviour of the attenuation at a fixed frequency ($935\,cm^{-1}$) and found in good agreement) Compared to the large uncertainties of purely mass spectrometric cluster detection due to fragmentation processes in the ionizer our rather precise spectroscopic determination contrasts satisfactorily Figure 3 allows to compare directly the spectroscopic determination of the dimer and trimer concentration (at right) to the conventional mass spectrometer signals (at left) The two determinations differ by more than a factor ten

In addition the fragmentation can be directly measured by measuring the attenuation signal at fixed laser frequency for different masses [1]

Preliminary experiments at an electron energy of 25 eV indicate that fragmentation may be significantly reduced, we shall investigate this suggestion [11] in the future – A second extension of the current investigation will employ two lasers, a chopped one to mark a cluster signal setting the frequency to a clear spectral peak the other to scan the entire spectrum Thereby we expect to resolve the spectrum of larger clusters for fixed sizes

After completion of this work we became acquainted with two recent important papers on similar objects Casassa et al [13] have thoroughly investigated the system C_2H_4 Van der Waals bonded to C_2H_4 C_2F_4 Ne Ar and Kr Lisy et al [14] have found the ring structure of $(HF)_n$ $n=3$ to 6 from the predissociation spectra

This work is part of the research program of the "Stichting Fundamenteel Onderzoek der Materie (F O M)" and has been made possible by financial support from the "Nederlandse Stichting voor Zuiver-Wetenschappelijk Onderzoek (Z W O)"
We thank F Lapoutre for his valuable assistance

References

1 Geraedts, J., Setiadi, S., Stolte S Reuss J Chem Phys Lett **78** 277 (1981)
2 Mulliken R S Phys Rev **120**, 1674 (1960)
3 Hirschfelder J., Curtis, C Bird, R Molecular Theory of gases and liquids p 992 New York Wiley & Sons 1965
4 Margenau H Kestner, N Theory of intermolecular forces 2nd ed., p 291 Oxford Pergamon Press 1971
5 Fox, K Person, W J Chem Phys **64** 5218 (1976)
6 Morales, D Ewing G Chem Phys **53** 141 (1980)
7 Gough, T., Miller, K Scoles G J Chem Phys **69**, 1588 (1978)
8 Brodbeck, C., Rossi, I., Strapelias H., Bouanic J P Chem Phys **54**, 1 (1980)
9 The nozzle is a cheap Pt–Ir lens fabricated for an electronmicroscope (Siemens or Philips) It is soft-soldered to a stainless-steel pipe (3 mm ∅) This pipe is enclosed by a copper block, cooled by contact with a liquid nitrogen reservoir and stabilized by the energy dissipation of a transistor The temperature of the block can be controlled from 100 to 300 K
10 The help of Dr H Bluyssen and A van Etteger who provided us with their well fuctioning CO_2 laser and many advices is gratefully acknowledged
11 Bonissent, A Mutaftschiev, B J Chem Phys **58**, 1727 (1973)
12 Echt O., Sattler K Private communication (1981)
13 Casassa, M P Bomse, D S Janda K C J Chem Phys **74** 5044 (1981)
14 Lisy, J M., Tramer A Vernon M F Lee, Y T J Chem Phys (to be published)

J Geraedts
S Stolte
J Reuss
Fysisch Laboratorium
Katholieke Universiteit
NL-6525 ED Nijmegen
The Netherlands

Faraday Discuss Chem Soc, 1982, **73**, 375–386

Dimer Spectroscopy

BY JO GERAEDTS, MARTIN WAAYER, STEPHEN STOLTE AND JORG REUSS

Fysisch Laboratorium, Katholieke Universiteit, Toernooiveld,
6525 ED Nijmegen, The Netherlands

Received 2nd December, 1981

Measurements of vibrational predissociation of SF_6 clusters are discussed and compared with theoretical spectra. Attention is given to the line-shape and saturation behaviour as influenced by spatial averaging effects. Also isotopic dimers are considered. Hyperfine-structure measurements of H_2–H_2, H_2–Ne, H_2–Ar and H_2–Kr dimers are dealt with, and information from these results concerning the intermolecular potentials is discussed.

1. INTRODUCTION

Properties of vibrationally excited Van der Waals complexes will be discussed in section 2, whereas H_2 complexes will be considered in their ground state in section 3. Both investigations have in common only the method of production of clusters, *i.e.* by supersonic expansion in a molecular beam, the method of probing their properties, however, is rather different in both cases. As described in section 2, dimers of SF_6 are predissociated by laser vibrational excitation of their constituents, the ν_3 mode of SF_6 being conveniently accessible through the nearly coincident line spectrum emitted by a CO_2 laser. The predissociation spectrum is then observed as molecular-beam attenuation. In section 3 the magnetic-beam resonance (m.b.r.) method is employed to observe the hyperfine spectrum (h.f.s.) of H_2–H_2, H_2–Ne, H_2–Ar and H_2–Kr, *i.e.* the change of magnetic deflection due to the h.f.s. transition renders these complexes observable.

The information obtained from the two experiments is very different. As far as we are aware the vibrational predissociation spectrum of $(SF_6)_2$ is the first leading to sharp spectral features which permits a straightforward interpretation. In this the high symmetry of SF_6 and the threefold degeneracy of its ν_3-mode vibration along three orthogonal axes are important. Consequently the SF_6 molecule behaves like a three-dimensional harmonic oscillator, to a sufficient approximation. The influence of the possible rotation of the SF_6 molecules becomes negligible. The dominant interaction lifting the high degree of degeneracy of the singly excited SF_6 clusters turns out to be the electric dipole interaction determined by the quantity $\mu_{01}^2 \langle R^{-3} \rangle$, where μ_{01} stands for the dipole transition matrix element and R for the intermolecular distance between nearest-neighbour molecules in a cluster.

On the other hand, the information from the ground state of H_2 dimers resides in the shift that the h.f.s. lines experience due to the (angle-dependent) forces between the constituents. These forces slightly perturb, in a first approximation, the free rotation of the *ortho*-hydrogen ($j = 1$) within the complex. Although admixture of higher j states (*e.g.* $j = 3$) can still be neglected due to the large rotational constant of H_2 (60 cm^{-1}), the orientational coupling (determined by the quantum number m_j) causes deviations from straightforward vector-model expectations. These deviations lead to h.f.s. shifts of *ca.* 1 kHz for $(H_2)_2$ to *ca.* 100 kHz for H_2–Kr. A theoretical model allows one then to translate these observed shifts into a single-potential para-

meter for each system probing especially the $V_2(R)P_2(\hat{R}\cdot\hat{r})$ contribution to the intermolecular potential; $\hat{R}\cdot\hat{r}$ stands for the cosine of the angle between the molecular axis, r, and the intermolecular distance vector, R.

2. PREDISSOCIATION OF VIBRATIONALLY EXCITED SF_6 CLUSTERS

2.1. CALCULATION OF THE SPECTRUM

In fig. 1 an illustration by Leonardo da Vinci [1] demonstrates the geometry of an octomer; each corner might be thought of as the position of an SF_6 molecule in the

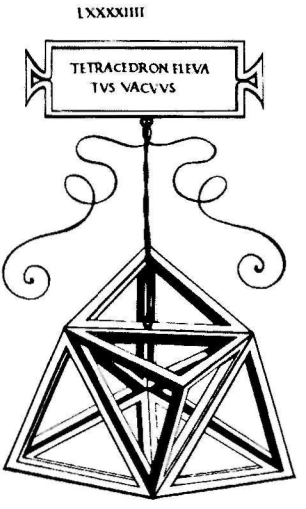

FIG. 1.– Leonardo da Vinci's illustration of an octomer, from ref. (1).

case of $(SF_6)_8$. The special feature of this geometry is that it can be stripped down one by one leading through heptamer, hexamer *etc.*, finally to the dimer and the monomer, each in its supposed equilibrium geometry.[2]

We treat vibrationally excited $(SF_6)_n$ clusters in the approximation that the $3n$ degenerate states with one ν_3 quantum absorbed are diagonalized, taking as off-diagonal coupling elements the terms derived from the electric dipole–dipole interaction. Responsible for the strong coupling is the dipole transition element of SF_6 for the ν_3 mode, 0.39 D.* Each SF_6 molecule is treated as a three-dimensional harmonic oscillator, neglecting Coriolis effects.

The positions of the SF_6 molecules constituting the octomer are given in table 1. The off-diagonal elements are shown in table 2, together with the energy eigenvalues and the corresponding transition strength. The procedure is discussed in ref. (3), here extended up to octomers. In fig. 2 the results are displayed in a stick spectrum, where the height corresponds to the transition strength times the degeneracy. It is

* $1\ \mathrm{D} \approx 3.3356 \times 10^{-30}\ \mathrm{C\,m}$.

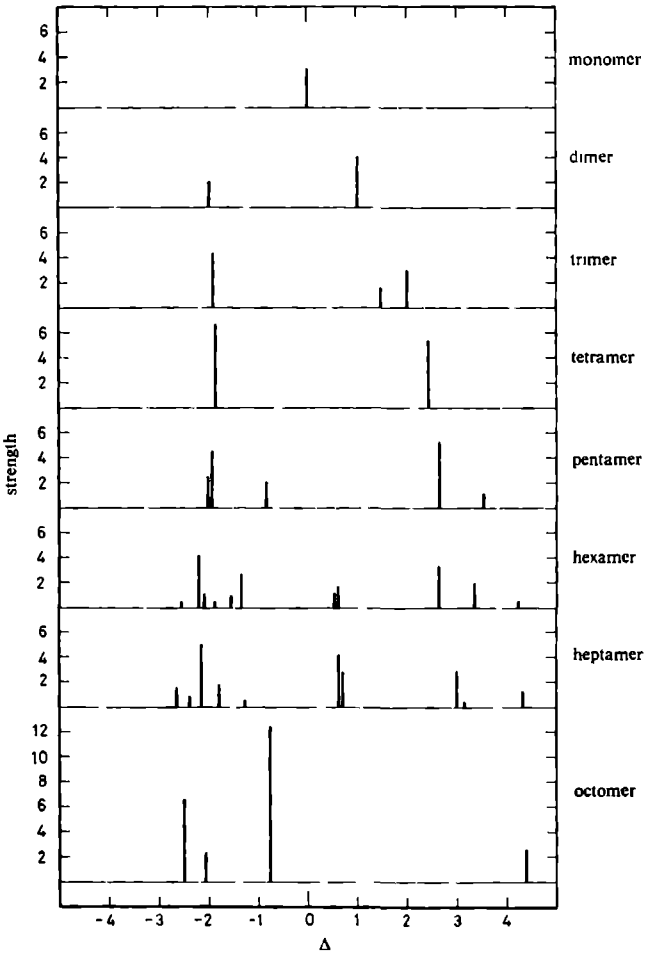

FIG 2 — Stick spectrum of $(SF_6)_n$, $n = 1,$,8 The height of each bar corresponds to the transition strength times degeneracy The energy shift Δ is given units of $\mu_{01}^2\langle R^{-3}\rangle$ Note how the high symmetry of the tetramer and the octomer is reflected by high degeneracy The three largest clusters contribute lines near $\Delta - 0$

assumed that the nearest-neighbour distance remains unchanged for clusters growing from dimers to octomers. The absolute calibration is then taken from the precisely measured distance of the two sharp dimer lines 20 cm^{-1},[3] corresponding to $\mu_{01}^2\langle R^{-3}\rangle$ 6 8 cm $^{-1}$ and $\langle R^{-3}\rangle^{-1/3}$ = 4 8 Å.

TABLE 1.—EQUILIBRIUM POSITIONS OF THE CLUSTER CONSTITUENTS, ACCORDING TO REF. (2), IN UNITS OF NEAREST-NEIGHBOUR DISTANCES

	1	2	3	4	5	6	7	8
x_i	$\frac{-\sqrt{3}}{3}$	$\frac{\sqrt{3}}{6}$	$\frac{\sqrt{3}}{6}$	0	0	$\frac{5\sqrt{3}}{9}$	$\frac{-5\sqrt{3}}{18}$	$\frac{-5\sqrt{3}}{18}$
y_i	0	$\frac{1}{2}$	$-\frac{1}{2}$	0	0	0	$\frac{5}{6}$	$-\frac{5}{6}$
z_i	0	0	0	$\frac{\sqrt{6}}{3}$	$\frac{-\sqrt{6}}{3}$	$\frac{2\sqrt{6}}{9}$	$\frac{2\sqrt{6}}{9}$	$\frac{2\sqrt{6}}{9}$

In ref. (3) experiments were reported with fits up to the trimers, the latter especially contributing a significant absorption around 962 cm^{-1}. Under conditions of heavy clustering some gross features were communicated in ref (4) which are not contradictory to the stick spectrum (fig. 2). However, further and precise experimental confirmation is still needed. The above treatment resembles the theory of the Davydov effect [*e g* ref (4)], where the vibration spectrum of solids with more than one molecule of the same sort per unit cell yields splittings owing to electric-dipole forces similar to those found by us

2.2 THE EXPERIMENT

To measure the predissociation of clusters by vibrational excitation a molecular beam (containing clusters at concentrations determined by the choice of the source conditions) is crossed by a line-tunable CO_2 laser of moderate power After excitation the clusters leave the collimated beam owing to the recoil upon dissociation. Thus a beam attenuation is measured which reflects the absorption spectrum of the clusters.

Beam detection takes place using an efficient electron-bombardment ionizer, followed by a magnetic mass spectrometer. As violent fragmentation of the cluster ions takes place in the ionizer we have generally measured the attenuation spectra on mass SF_5^+. Quantitative conclusions about this fragmentation and details of the experimental arrangement are discussed in ref (3). So far we have not been successful in utilizing the selective properties of the mass spectrometer to disentangle the congested spectrum in the case of heavy clustering. Normally, the beam is ionized by 100 eV electrons Reducing the electron energy to 25 eV was of no avail; the monomer fragmentation appeared markedly diminished whereas the clusters unvaryingly kept their propensity to show up at the mass of the SF_5^+ ion

2 3. POWER DEPENDENCE AND LINE-SHAPE

In ref. (3) we have described a simple model, which, owing to dissociation, yields $[1 - \exp(-r_2 t)]$ for the relative attenuation of dimers in the beam, where r_2 describes the rate of excitation of dimers to a predissociative state and t the time of interaction. As common practice we had written [see eqn (4.3) of ref. (3)]

Table I *Energy matrix, eigenvalues and transition strengths of ν_3-excited $(SF_6)_n$, n=1,....,8.*

The energy matrix (upper right) is symmetric and has to be complemented by values reflected with respect to the diagonal; the diagonal elements are all equal (948 cm^{-1}), near diagonal elements of the type $(nx|\text{operator}|n'y)$ with $n=n'$ being zero. For the operator the dipole-dipole interaction is chosen, $[(\bar{\mu}_i\cdot\bar{\mu}_j) - 3(\bar{\mu}_i\cdot\hat{R}_{ij})(\bar{\mu}_j\cdot\hat{R}_{ij})]/R^3_{ij}$. The eigenvalues E (lower left) were obtained by diagonalization; their values are given in units of $\mu^2_{01}\langle R^{-3}\rangle$, as are the matrix elements. Here, μ_{01} corresponds to the transition matrix elements for the ν_3 mode (0.39 D). The corresponding transition strengths are displayed in units of the monomer transition strength. The indication for an unperturbed degenerate state (e.g. 7z) is a shorthand (meaning that of all 3n possible ν_3 excitations the 7th molecule is excited and vibrates along its z-axis).

	1x	1y	1z	2x	2y	2z	3x	3y	3z	4x	4y	4z	5x	5v	5z	6x	6y	6z	7x	7y	7z	8x	8y	8z
1x		E		$\frac{-5}{4}$	$\frac{3\sqrt{4}}{3}$	0	$\frac{-5}{4}$	$\frac{3\sqrt{4}}{3}$	0	0	0	$-\sqrt{2}$	0	0	$\sqrt{2}$	$\frac{-5\sqrt{32}}{6}$	0	$\frac{-1\sqrt{8}}{3}$	$\frac{35}{36}$	$\frac{-5\sqrt{3}}{36}$	$\frac{-2\sqrt{2}}{18}$	$\frac{35}{36}$	$\frac{5\sqrt{3}}{36}$	$\frac{-\sqrt{2}}{9}$
1y	0 0 0			$\frac{-3\sqrt{4}}{3}$	$\frac{1}{4}$	0	$\frac{3\sqrt{4}}{3}$	$\frac{1}{4}$	0	0	1	0	0	1	0	0	$\frac{3\sqrt{32}}{6}$	0	$\frac{-5\sqrt{3}}{36}$	$\frac{13}{12}$	$\frac{-5\sqrt{6}}{9}$	$\frac{5\sqrt{3}}{36}$	$\frac{13}{12}$	$\frac{5\sqrt{6}}{9}$
1z	1 1 1 strength			0	0	1	0	0	1	$-\sqrt{2}$	0	-1	$\sqrt{2}$	0	-1	$\frac{-1\sqrt{8}}{3}$	0	$\frac{1\sqrt{16}}{6}$	$\frac{-2\sqrt{2}}{18}$	$\frac{-5\sqrt{6}}{9}$	$\frac{1}{9}$	$\frac{-\sqrt{2}}{9}$	$\frac{5\sqrt{3}}{9}$	$\frac{1}{9}$
2x			E				1	0	0	$\frac{3}{4}$	$\frac{-1\sqrt{4}}{3}$	$\frac{1\sqrt{2}}{2}$	$\frac{3}{4}$	$\frac{-1\sqrt{4}}{3}$	$\frac{-1\sqrt{2}}{2}$	$\frac{-13}{36}$	$\frac{7\sqrt{12}}{3}$	$\frac{-7\sqrt{9}}{2}$	$\frac{-7}{9}$	$\frac{4\sqrt{3}}{9}$	$\frac{\sqrt{28}}{9}$	$\frac{\sqrt{3}}{8\sqrt{8}}$	$\frac{-3}{4\sqrt{8}}$	$\frac{\sqrt{3}}{16}$
2y	-2 -1 -1 1 1 2						0	-2	0	$\frac{-1\sqrt{4}}{3}$	$\frac{1}{4}$	$\frac{1\sqrt{2}}{6}$	$\frac{-1\sqrt{4}}{3}$	$\frac{1}{4}$	$\frac{-1\sqrt{2}}{6}$	$\frac{7\sqrt{12}}{3}$	$\frac{1}{4}$	$\frac{1\sqrt{3}}{6}$	$\frac{4\sqrt{3}}{9}$	$\frac{2}{9}$	$\frac{-2\sqrt{6}}{9}$	$\frac{-3}{4\sqrt{8}}$	$\frac{-3\sqrt{3}}{8\sqrt{8}}$	$\frac{1\sqrt{2}}{8\sqrt{8}}$
2z	2 0 0 2 2 0 strength						0	0	1	$\frac{1\sqrt{2}}{2}$	$\frac{1\sqrt{2}}{6}$	-1	$\frac{-1\sqrt{2}}{2}$	$\frac{1\sqrt{2}}{6}$	-1	$\frac{-7\sqrt{9}}{2}$	$\frac{1\sqrt{3}}{6}$	$\frac{1}{9}$	$\frac{\sqrt{28}}{9}$	$\frac{-2\sqrt{6}}{9}$	$\frac{1}{9}$	$\frac{\sqrt{3}}{16}$	$\frac{3\sqrt{2}}{8\sqrt{8}}$	$\frac{2\sqrt{3}}{8\sqrt{8}}$
3x								E		$\frac{3}{4}$	$\frac{1\sqrt{4}}{3}$	$\frac{1\sqrt{2}}{2}$	$\frac{3}{4}$	$\frac{1\sqrt{4}}{3}$	$\frac{1\sqrt{2}}{2}$	$\frac{-13}{36}$	$\frac{-7\sqrt{3}}{12}$	$\frac{-7\sqrt{9}}{2}$	$\frac{\sqrt{3}}{8\sqrt{8}}$	$\frac{3}{4\sqrt{8}}$	$\frac{\sqrt{3}}{16}$	$\frac{7}{9}$	$\frac{-4\sqrt{3}}{9}$	$\frac{8\sqrt{2}}{9}$
3y	-2.50 -1.93 -1.93 -1.00 -1.00 1.43 1.43 2.00 3.50									$\frac{1\sqrt{4}}{3}$	$\frac{1}{4}$	$\frac{1\sqrt{2}}{6}$	$\frac{1\sqrt{4}}{3}$	$\frac{1}{4}$	$\frac{-1\sqrt{2}}{6}$	$\frac{-7\sqrt{12}}{3}$	$\frac{1}{4}$	$\frac{-1\sqrt{3}}{6}$	$\frac{3}{4\sqrt{8}}$	$\frac{-3\sqrt{3}}{8\sqrt{8}}$	$\frac{-3}{16}$	$\frac{-4\sqrt{3}}{9}$	$\frac{2}{3}$	$\frac{2\sqrt{6}}{9}$
3z	0 2.17 2.17 0 0 0.83 0.83 3.00 0 strength									$\frac{1\sqrt{2}}{2}$	$\frac{-1\sqrt{2}}{6}$	-1	$\frac{-1\sqrt{2}}{2}$	$\frac{1\sqrt{2}}{6}$	-1	$\frac{-7\sqrt{9}}{2}$	$\frac{-1\sqrt{3}}{6}$	$\frac{1}{9}$	$\frac{\sqrt{3}}{16}$	$\frac{-3}{16}$	$\frac{2\sqrt{3}}{8\sqrt{8}}$	$\frac{8\sqrt{2}}{9}$	$\frac{2\sqrt{6}}{9}$	$\frac{1}{9}$
	1x	1y	1z	2x	2y	2z	3x	3y	3z	4x	4y	4z	5x	5v	5z	6x	6y	6z	7x	7y	7z	8x	8y	8z

	1x	1y	1z	2x	2y	2z	3x	3y	3z	4x	4y	4z	5x	5y	5z	6x	6y	6z	7x	7y	7z	8x	8y	8z
4x													$\frac{3\sqrt{32}}{6}$	0	0	$\frac{-16}{9}$	0	$\frac{5\sqrt{9}}{2}$	$\frac{11}{36}$	$\frac{25\sqrt{3}}{36}$	$\frac{-5\sqrt{2}}{18}$	$\frac{11}{36}$	$\frac{-25\sqrt{3}}{36}$	$\frac{-5\sqrt{2}}{18}$
4y	-2.50	-2.50	-2.50	-1.85	-1.85	-1.85	0.50	0.50	2.39	2.39	2.39	5.00	0	$\frac{3\sqrt{32}}{6}$	0	0	1	0	$\frac{25\sqrt{3}}{36}$	$\frac{-13}{12}$	$\frac{5\sqrt{6}}{18}$	$\frac{-25\sqrt{3}}{36}$	$\frac{-13}{12}$	$\frac{-5\sqrt{6}}{18}$
	0	0	0	2.23	2.23	2.23	0	0	1.77	1.77	1.77	0	0	0	$\frac{-6\sqrt{32}}{6}$	$\frac{5\sqrt{9}}{2}$	0	$\frac{7}{9}$	$\frac{-5\sqrt{2}}{18}$	$\frac{5\sqrt{6}}{18}$	$\frac{7}{9}$	$\frac{-5\sqrt{2}}{18}$	$\frac{5\sqrt{6}}{18}$	$\frac{7}{9}$
4z																								
5x																0	0	$\frac{-27\sqrt{125}}{2}$	$\frac{81}{500}$	$\frac{27\sqrt{3}}{500}$	$\frac{27\sqrt{2}}{250}$	$\frac{81}{500}$	$\frac{-27\sqrt{3}}{500}$	$\frac{27\sqrt{2}}{250}$
5y	-3.09	-3.09	-2.50	-2.04	-2.04	-1.97	-1.80	-0.86	-0.86	1.86	1.86	2.63	2.63	3.51	5.76	0	$\frac{27}{125}$	0	$\frac{27\sqrt{2}}{500}$	$\frac{27}{500}$	$\frac{-27\sqrt{6}}{250}$	$\frac{-27\sqrt{3}}{500}$	$\frac{27}{500}$	$\frac{27\sqrt{6}}{25}$
	0	0	0	1.33	1.33	4.46	0	1.00	1.00	0	0	2.66	2.66	0.54	0	$\frac{-27\sqrt{125}}{2}$	0	$\frac{-27}{125}$	$\frac{27\sqrt{2}}{250}$	$\frac{-27\sqrt{6}}{250}$	$\frac{-27}{125}$	$\frac{27\sqrt{2}}{250}$	$\frac{27\sqrt{6}}{250}$	$\frac{-27}{125}$
5z																								
6x																			$\frac{-27}{100}$	$\frac{81\sqrt{3}}{500}$	0	$\frac{27}{100}$	$\frac{-81\sqrt{3}}{100}$	0
6y	-3.34	-3.32	-2.88	-2.56	-2.21	-2.12	-1.90	-1.57	-1.47	-1.36	0.54	0.59	2.54	2.61	2.63	3.36	4.24	6.25	$\frac{81\sqrt{3}}{500}$	$\frac{27}{500}$	0	$\frac{-81\sqrt{3}}{100}$	$\frac{27}{500}$	0
	0	0	0.01	0.38	4.13	1.07	0.44	0.94	0	2.70	1.06	1.60	0.10	0	3.31	1.87	0.38	0	0	0	$\frac{27}{125}$	0	0	$\frac{27}{12}$
6z																								
7x																						$\frac{27}{125}$	0	0
7y	-3.51	-3.35	3.35	-2.65	-2.65	-2.39	2.14	-2.14	-1.79	1.79	-1.27	0.47	0.62	0.62	0.69	3.01	3.14	3.14	4.33	4.33	6.65	0	$\frac{2.27}{125}$	0
	0	0	0	0.73	0.73	0.78	2.48	2.48	0.87	0.87	0.49	0	2.10	2.10	2.81	2.91	0.16	0.16	0.66	0.66	0	0	0	$\frac{27}{125}$
7z																								
8x																								
8y	-3.51	-3.51	-3.51	-2.97	-2.97	-2.49	-2.49	-2.49	-2.07	-2.07	-2.07	-0.94	0.47	0.47	0.47	0.79	0.79	0.79	3.58	3.58	4.38	4.38	4.38	7.02
	0	0	0	0	0	2.19	2.19	2.19	0.79	0.79	0.79	0	0	0	0	4.15	4.15	4.15	0	0	0.87	0.87	0.87	0
8z																								

E

strength

E

strength

E

strength

E

strength

$$r_2 t = \tfrac{1}{3} \frac{F}{c} \frac{\mu_{01}^2}{\hbar^2 \varepsilon_0} \frac{g_{2\,m} S_{2\,m} (\Gamma_{2\,m}/2)}{(\omega - \omega_{2\,m})^2 + (\Gamma_{2\,m}/2)^2} \qquad (1)\,*$$

The fluency is indicated by F, $\Gamma_{2\,m}$, $g_{2\,m}$ and $S_{2\,m}$ describe the line-width, the degeneracy and the line-strength of the mth transition of the dimer, $\omega_{2\,m}$ being the corresponding transition frequency at the centre of the assumed Lorentz line profile

In the following, we wish to take into account the possibility of orientational hole-burning effects, which in eqn (1) are neglected, introducing the factor 1/3 on the right-hand side, *i e* by taking the usual spatial average over all orientations of the dimer axis As long as saturation effects are weak, this is a permissible procedure, however, as soon as the fluency exceeds a few tenths of 1 J m^{-2} these orientational effects show up clearly for $(SF_6)_2$ predissociation, as already indicated in ref (4), fig 3, where the asymptotic beam attenuation for large laser power was shown to no longer follow an exponential law

The blue dimer peak around the P(8) CO_2 laser line corresponds to an excitation of the two oscillating dipole moments parallel to each other and perpendicular to the dimer axis If the end-over-end rotation of the dimer is characterized by the quantum numbers L and M_L, M_L being defined along the direction $\hat{\boldsymbol{e}}$ of the polarization of the CO_2 laser, one finds that the blue peak corresponds to a transition with $|\Delta L| = 0,1$ In this case, the factor $\frac{1}{3}$ in $r_2 t$ has to be replaced by $\frac{1}{4}(1 - \cos^2\theta)$ and to be spatially averaged over all directions, in the exponent of $[1 - \exp(-r_2 t)]$ Here, θ stands for the angle between $\boldsymbol{L}$ and $\hat{\boldsymbol{e}}$

The red peak around the P(30)CO_2 laser line corresponds to an excitation of the two oscillating dipole moments parallel to each other and parallel to the dimer axis Thus one has $L \to L \pm 1$ transitions with the factor $\frac{1}{3}$ replaced by $\frac{1}{2} \sin^2\theta$ Again one has to average over all directions with equal weight, $\sin^2\theta$ occurring in the exponent of $[1 \quad \exp(-r_2 t)]$

It is evident that for weak fluency with $[1 - \exp(-r_2 t)] \approx r_2 t$ this spatial averaging yields the factor 1/3, in all cases In general, however, $1 - \exp(-r_2 t)$ becomes, for the red line

$$1 - \exp(-r_2 t) \xrightarrow{\text{spatial average}} 1 - \frac{1}{\sqrt{(3r_2 t/2)}} \exp[-(3/2)r_2 t] \int_0^{\sqrt{(3r_2 t/2)}} \mathrm{d}\mathscr{H} \exp(\mathscr{H}^2)$$

$$\text{(for strong fluency)} \qquad = 1 \quad \frac{1}{3r_2 t} + \qquad (2)$$

For the blue line one finds

$$1 - \exp(-r_2 t) \xrightarrow{\text{spatial averaging}} 1 - \frac{1}{\sqrt{(3r_2 t/4)}} \exp(\quad 3r_2 t/4) \int_o^{\sqrt{(3r_2 t/4)}} \exp(-\mathscr{H}^2) \mathrm{d}\mathscr{H}$$

$$\text{(for strong fluency)} \longrightarrow 1 - \frac{\sqrt{\pi}}{2\sqrt{(3r_2 t/4)}} \exp(-3r_2 t/4) \qquad (3)$$

Here, $r_2 t$ is defined as in eqn (1) The asymptotic formulae show that the blue line reaches its saturation value significantly faster than the red one, in disagreement with fig 3 of ref (4)

The line-shape, too, is affected by this spatial averaging, for high fluencies Whereas the far wings of the Lorentzian remain unchanged the line-width may appear wider than corresponds to a power-broadened pure Lorentzian However, whereas

* To be consistent with the use of c g s units in the rest of the paper, put $\varepsilon_0 = 1/4\pi$

one observes pronounced effects for the above-discussed power dependence, the changes of the line-shape amount to at most 2% for the red line and 10% for the blue line; this can be seen from table 3. In fig. 3 experimental results are compared with a fit with and without proper spatial averaging, for fluencies differing by about a factor 10.

TABLE 3.—CHANGE OF ABSORPTION FOR PROPER SPATIAL AVERAGING

The first column displays different values for the transition probability, $r_2 t$. For the red transition of $(SF_6)_2$

$$\nu_{red} = [1 - b^{-1} \exp(-b^2) \int_0^b \mathrm{d}\mathscr{H} \exp(\mathscr{H}^2)]/[1 - \exp(-r_2 t)]$$

is shown; here, b stands for $(3r_2 t/2)^{\frac{1}{2}}$ The equivalent ratio for the blue line is given in the last column.

$r_2 t$	red line, ν_{red}	blue line, ν_{blue}
0.1	1.00	1.00
0.5	0.96	0.99
1.0	0.93	0.99
1.5	0.92	0.98
2.0	0.91	0.99
10.0	0 97	1.00

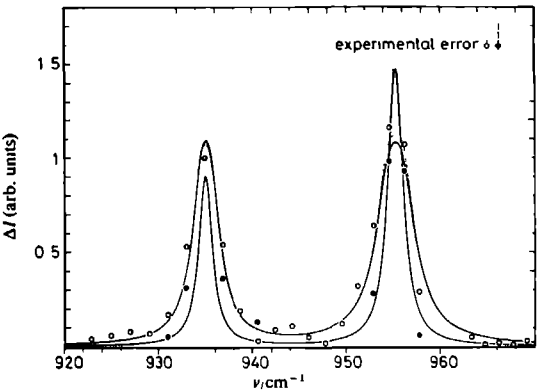

FIG. 3 —Beam attenuation plotted against laser frequency. The full circles and curves with narrow peaks correspond to 1 W laser power, *i e.* 1.3 J m^{-2} fluency. The open circles and wider curves correspond to 10 W, *i.e.* 13 J m^{-2} fluency. The calculated curves are fit with the same parameters (Γ = 1.6 cm^{-1}, $\mu_{01}^2 \langle R^{-3} \rangle$ = 6.75 cm^{-1}, unshifted frequency 948.5 cm^{-1}), applying eqn (3) and (4); broken lines are calculated using eqn (1), *i e.* without proper spatial averaging. The two strong-fluency peak heights correspond to a beam attenuation of 0 8%.

2.4. PURE AND MIXED DIMERS

The ν_3 vibration frequency of SF_6 is especially sensitive to isotopic substitution. For $^{34}SF_6$ (4% natural abundance) the excitation occurs 16 cm^{-1} red-shifted with

respect to the $^{32}SF_6$ molecule (*ca* 948 cm^{-1}) Dimer spectra are obtained by diagonalizing 2 × 2 sub-matrices (see the general scheme in table 2) The results of this diagonalization are given in table 4, including the corresponding eigenfunctions For pure dimers all diagonal elements are identical, for the mixed ones the difference of 16 cm^{-1} leads to the significantly altered eigenfunctions and eigenvalues of the lower part of table 4 The symmetry breaking renders all four eigenvalues observable, in

TABLE 4.—EIGENVALUES, TRANSITION STRENGTHS AND EIGENSTATES OF $(^{32}SF_6)_2$ AND $^{32}SF_6$ $^{34}SF_6$, CALCULATED WITH $\mu_{01}^2 \langle R^{-3} \rangle = 6\,8\ cm^{-1}$

eigenvalues/ cm^{-1}	g	strength	eigenfunction
−13 6	1	2	$2^{-\frac{1}{2}}[\|z_1^+\rangle + \|z_2^+\rangle]$
−6 8	2	0	$2^{-\frac{1}{2}}[\|x_1^+\rangle - \|x_2^+\rangle]$ or $x \rightleftarrows y$
+6 8	2	2	$2^{-\frac{1}{2}}[\|x_1^+\rangle + \|x_2^+\rangle]$ or $x \rightleftarrows y$
+13 6	1	0	$2^{-\frac{1}{2}}[\|z_1^+\rangle - \|z_2^+\rangle]$
24 7	1	1 85	$0\,49\|z_1^+\rangle + 0\,87\|z_2^+\rangle$
19 6	2	0 36	$-0\,94\|x_1^+\rangle + 0\,34\|x_2^+\rangle$ or $x \rightleftarrows y$
+2 4	2	1 64	$0.34\|x_1^+\rangle + 0\,94\|x_2^+\rangle$ or $x \rightleftarrows y$
+7 5	1	0 14	$-0\,87\|z_1^+\rangle + 0\,49\|z_2^+\rangle$

principle, up to now we have searched and found only the line shifted to 921 5 cm^{-1}, slightly different from the theoretical prediction but this difference still being within the experimental uncertainty [3]

3 THE HYPERFINE STRUCTURE OF MAGNETIC TRANSITIONS OF H_2–H_2, H_2–Ne, H_2–Ar AND H_2–Kr

3 1 THE EXPERIMENT

The experimental apparatus for m b r measurements has been described in detail in ref (6) and (7) It consists of a beam machine with two deflection fields each 40 cm long, a field-free transition region where transitions are induced by means of Ramsey's double-coil technique,[8] a sensitive detection system which permits the measurement of the dimer intensities on the masses H_3^+ for $(H_2)_2$, HNe^+ for H_2Ne, HAr^+ for H_2Ar and HKr^+ for H_2Kr, and a nozzle-skimmer system to produce dimers by supersonic expansion, in sufficient concentrations

It is a convenient feature of the systems studied here that their transitions can be well predicted so that lengthy scanning of wide spectral ranges can be avoided before finding the first inkling of the presence of dimers In any event, to resolve lines from a large noisy background many hours of signal averaging were required utilizing a completely automated set-up

The quantum numbers I and M_L describe the end-over-end rotation of the complexes, the $L = 0$ states being predominantly occupied as we achieved rather low internal temperatures ($T = 3 \perp 2$ K) during the expansion States with $L = 0,1,2$ were investigated.

3 2 OUTLINE OF THEORY

The theoretical analysis is facilitated by a number of facts First, the angle-dependent forces within a H_2–X dimer are rather weak Although we adhered to

exact methods of diagonalizing the complete Hamiltonian [ref (6) and (7)] perturbative approaches have served to guide us and to give a good insight into the physics involved Secondly, as the rotational constant of the H_2 molecule is large (60 cm^{-1}) the admixture of higher j states becomes negligible, *i e* the H_2 molecule rotates freely inside the complex Thirdly, H_2 being homonuclear there only occur even Legendre polynomials in the expansion of the intermolecular potential V

$$V = V_0(R) + V_2(R)P_2(\hat{r}\ \hat{R}) + V_4(R)P_4(\hat{r}\ \hat{R}) +$$

Furthermore, the $V_4(R)$ terms even can be omitted in our case, as we have seen that we can restrict ourselves to the $j = 1$ state of *ortho*-hydrogen, which does not couple with the fourth-order Legendre polynomial

Roses hardly bloom without thorns, a number of complicating factors must, therefore, be mentioned As we are considering hyperfine states we have to cope with the nuclear spin I of H_2 For the coupling scheme we have chosen $[(jL)JI]F$ with $j = I = 1$ Further, the continuum influences the h f s transitions once we have made our choice for this coupling scheme, *e g* $L = 2$ states are predissociating for *ortho*-hydrogen *para* hydrogen dimers, $(H_2)_2$, but they are still the main terms yielding off-diagonal elements in the diagonalization procedure Consequently, one has to incorporate the continuum states in the analysis

In the following we restrict ourselves to h f s states which, apart from some admixture, belong to $L = 0$, the general analysis is extensively treated in ref (7) The chosen coupling scheme (without off diagonal elements) leads to a transition $[(j = 1, L = 0)\ J = 1, I = 1]F = 0 \rightarrow F = 1$ with a frequency at 546 437 kHz, unshifted with respect to the corresponding H_2 h f s transition [9] and independent of the dimer partner X In table 5 the line positions are given for the various clusters as calculated

TABLE 5 –RESULTS OF H_2 DIMER H F S MEASUREMENTS

For four systems, results from theoretical or empirical potentials [ref (9) (12)] are compared with experimental ones [ref (7)] In the last column, the transition frequencies are given (to be compared with the unshifted value of 546 437 kHz) In the next to last column, corresponding values of the dimensionless experimental parameter (see text) are given

system	ref	$\lvert V_{20}'(E_2 \quad E_0)\rvert$	transition/kHz $L = 0, J = 1, F = 0 \rightarrow F' = 1$
H_2–Ne	10	0 0419(29)	546 36
	11	0 1663(8)	545 12
	12	0 1696(8)	545 07
(expt)	7	0 1892(78)	544 74(15)
H_2–Ar	10	0 9779(4)	497 12
	11	0 9491(4)	499 84
(expt)	7	1 0537	489 94(15)
H_2–Kr	10	1 7318(7)	421 86
	11	1 3472(7)	460 24
(expt)	7	1 622(15)	432 42

system	ref	$[\Sigma_\nu \lvert V_{20}'(E_2 - E_0)\rvert_\nu^2]^{\frac{1}{2}}$	transition/kHz $L = 0, J = 0, F = 0 \rightarrow F' = 1$
H_2–H_2	9	0 174(2)	545 07
(expt)	7	0 23(1)	544 05(10)

using recent potentials for $(H_2)_2$,[9] for H_2–Ne [10-12] and for H_2 Ar, H_2–Kr [10 11] The shift varies from *ca* 1 5 kHz for $(H_2)_2$ to *ca* 115 kHz for H_2–Kr In all cases, the $V_2(R)$ term of the intermolecular potential is mainly responsible for this shift having chosen to analyse here only *o*-H_2–*p*-H_2, even the normally dominant quadrupole-quadrupole interaction between hydrogen molecules is eliminated

The shift in the h f s transition frequency reflects the value of the parameter $|V_{20}/(E_2 - E_0)|$ (see table 5) It turns out that $(E_2 \quad E_0)$ is astonishingly system-independent, corresponding to *ca* 96 – 4 GHz for H_2–Ne, H_2–Ar and H_2–Kr Here, E_L designates the energy of bound dimer states with L 0 and 2, calculated from the isotropic potential $V_0(R)$ and corresponding to zero Van der Waals stretching excitation Consequently, the large variation of this shift is predominantly due to the different values assumed by $|V_{20}|$ It does not mean, however, that the isotropic potential has no influence, as V_{20} corresponds to the matrix element of $V_2(R)$ sandwiched between the Van der Waals stretching vibration functions $\langle R|L,v\rangle$ with $v = 0$ and $L = 0$ and 2 Classically the V_2 term is probed between the turning points of the vibrational eigenfunctions, the precise position of the turning points being determined by the isotropic term $V_0(R)$ [In reality the probing region extends well beyond these turning points, as is discussed in ref (7)]

In the case of $(H_2)_2$, the $L - 2$ state is not bound, and therefore one has to deal with continuum states Nevertheless, the determining parameter

$$[\sum_{v} |V_{20}/(E_2 - E_0)|^2]^{\frac{1}{2}}$$

still permits one to recognize its counterpart for bound $L - 2$ states, only that here a number of states (obtained with box-normalization) [7] contribute additively This parameter is nearly independent of where precisely the properly chosen box-normalization is introduced, we used $R_{max} = 32$ Å

3 3 RESULTS

In table 5 experimental results are displayed yielding the corresponding molecular parameter of the first column

For H_2–Ne, excellent agreement was found with the empirical potential obtained by the Gottingen group of Buck and coworkers [13] from elastic and inelastic differential scattering measurements, simultaneously taking into account total cross-section measurements with oriented H_2 molecule [14] For evidence of a small blister term in $V_2(R)$ in the neighbourhood of the potential well see ref (7)

For H_2–Ar and H_2 Kr, the agreement with existing empirical and semi-empirical potentials [10 11] in general is less satisfying, however, it is not disquieting, in view of one's still rather crude knowledge of these systems

The *piece de resistance* seems to be the system $(H_2)_2$, where very precise experimental and empirical potentials exist,[15 16] as well as an excellent and highly sophisticated *ab initio* calculation by Meyer [9] The discrepancy arises near the zero crossing of $V_0(R)$, where experimental data point to a 0 1 Å shift to shorter distances with respect to the *ab initio* results (see fig 4) [15 16] Based upon the dimer spectroscopic results we had to add a sizeable blister term to $V_2(R)$ [admittedly in an entirely *ad hoc* manner, see ref (7)] to find agreement with the experimental molecular parameter of table 3 without impairing the agreement with other experimental findings In particular, the inelastic differential cross-section measurements are expected to go along with the potential of fig 4, as care was taken to conserve $V_2(R)/V_0(R)$ in the repulsive region, a requirement dictated by recent results of Buck [16]

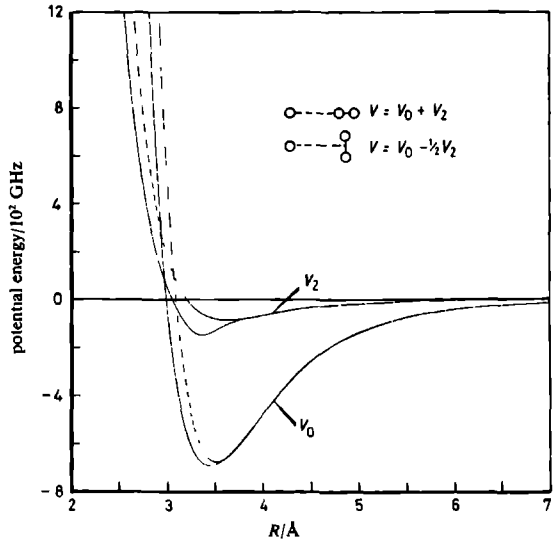

FIG 4 —Intermolecular potential for *ortho*-H_2–*para* H_2, *i.e.* the isotropic $V_0(R)$ term and the $V_2(R)$ term. The broken lines correspond to *ab initio* calculations, the full curves represent empirical adjustments of these *ab initio* results

This work is part of the research program of the " Stichting voor Fundamenteel Onderzoek der Materie (F.O.M.) " and has been made possible by financial support from the " Nederlandse Stichting voor Zuiver-Wetenschappelijk Onderzoek (Z.W.O.)."

[1] Leonardo da Vinci, in *De divina proportione* by L. Pacioli (Milan, 1496).
[2] A. Bonissent and B Mutaftschiev, *J. Chem. Phys.*, 1973, **58**, 3727.
[3] J. Geraedts, S. Stolte and J. Reuss, *Z. Phys.*, in press.
[4] J. Geraedts, S. Setiadi, S Stolte and J Reuss, *Chem Phys. Lett* , 1981, **78**, 277.
[5] D P Craig, in *Physics and Chemistry of the Organic Solid State*, ed D. Fox, M. M. Labes and A. Weissberger (J. Wiley, New York, 1963), vol. 1.
[6] J. Verberne and J Reuss, *Chem Phys.*, 1980, **50**, 137; 1981, **57**, 189.
[7] M. Waayer, M Jacobs and J. Reuss, *Chem Phys.*, 1981, **63**, 247; 257; 263.
[8] N. F Ramsey, *Molecular Beams* (Oxford University Press, 1956).
[9] W. Meyer and J. Schafer, personal communication.
[10] J. S. Carley, *Thesis* (University of Waterloo, Waterloo, Ontario, 1978); R. J. Le Roy and J. S. Carley, *Adv. Chem. Phys* , 1980, **42**, 353.
[11] K. T. Tang and J. P Toennies, *J. Chem. Phys.*, 1978, **68**, 5501, 1981, **74**, 1148.
[12] J Andres, U. Buck, F. Huisken, J. Schleusener and F Torello, *J. Chem. Phys* , 1980, **73**, 5620.
[13] L. Zandee and J. Reuss, *Chem. Phys.*, 1977, **26**, 327, 1977, **26**, 345.
[14] U. Buck, F. Huiskens, J. Scheusener and J. Schafer, *J Chem. Phys.*, 1981, **74**, 535.
[15] I. F. Silvera and V. V. Goldmann, *J. Chem Phys.*, 1978, **69**, 4205.
[16] U. Buck, personal communication.

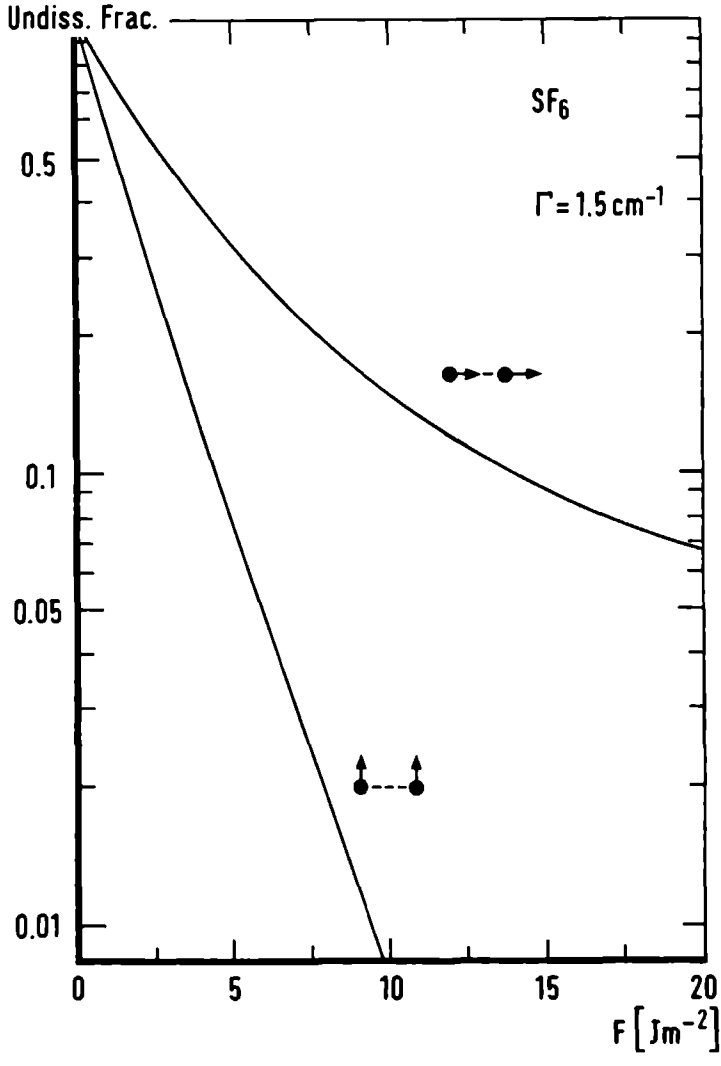

Fig. 1: The undissociated dimer fraction at resonance as a function of the fluence F. The curves are calculated with $\Gamma = 1.5\ cm^{-1}$ *and* $\mu_{01} = 0.387$ *D. The curve indicated with* [→ - →] *corresponds to the parallel transition (red peak) and the curve indicated with* [↑ - ↑] *corresponds to the perpendicular transition (blue peak).*

IV.4. Line shape and saturation behaviour

In section IV.3. the theoretical framework has been presented for orientational hole burning effects in dimer-dissociation measurements. As a function of the fluence the attenuation of the $(SF_6)_2$ parallel transition (red peak) does not equal the attenuation of the $(SF_6)_2$ perpendicular transition (blue peak). In figure 1 the dependence of the undissociated dimer fractions on the fluence F is shown. We performed these calculations using equations (2) and (3) of section IV.3. with $\Gamma_2 = 1.5\ cm^{-1}$ and $\mu_{01} = 0.387$ D. The most striking result of this saturation study is the fact that for increasing fluence the red dimer peak $[\rightarrow - \rightarrow]$ reaches the saturation value significantly slower than the blue dimer peak $[\uparrow - \uparrow]$.

The dependence of the attenuation ratio of the two dimer peaks $\Delta I_R/\Delta I_B$, on the fluence F is shown in the upper part of figure 2. The width γ of the measured attenuation profiles depends also strongly on the used fluence F. This is shown in the lower part of figure 2.

To investigate the saturation behaviour on the red and blue dimer peak a 5% SF_6 - 95% He has been used at a source pressure $P_o = 900$ torr. At this source pressure we expect only SF_6 dimers to be present in the molecular beam. The laser beam was focused between nozzle and skimmer with a fluence of about 50 Jm^{-2}. Further experimental conditions are summarized in table 1.

Theoretically we expect the ratio $\Delta I_R/\Delta I_B = 0.97$ at this fluence; the measured value equals 0.89 ± 0.03. This difference of 8 ($\pm$ 3)% is probably an indication that $\Gamma_{2,1} > \Gamma_{2,3}$. There are experimental indications that the linewidth of the red peak ($\Gamma_{2,1}$) is greater than the linewidth of the blue peak ($\Gamma_{2,3}$), see figure 4 (section IV.2) and figure 3 (section IV.3).

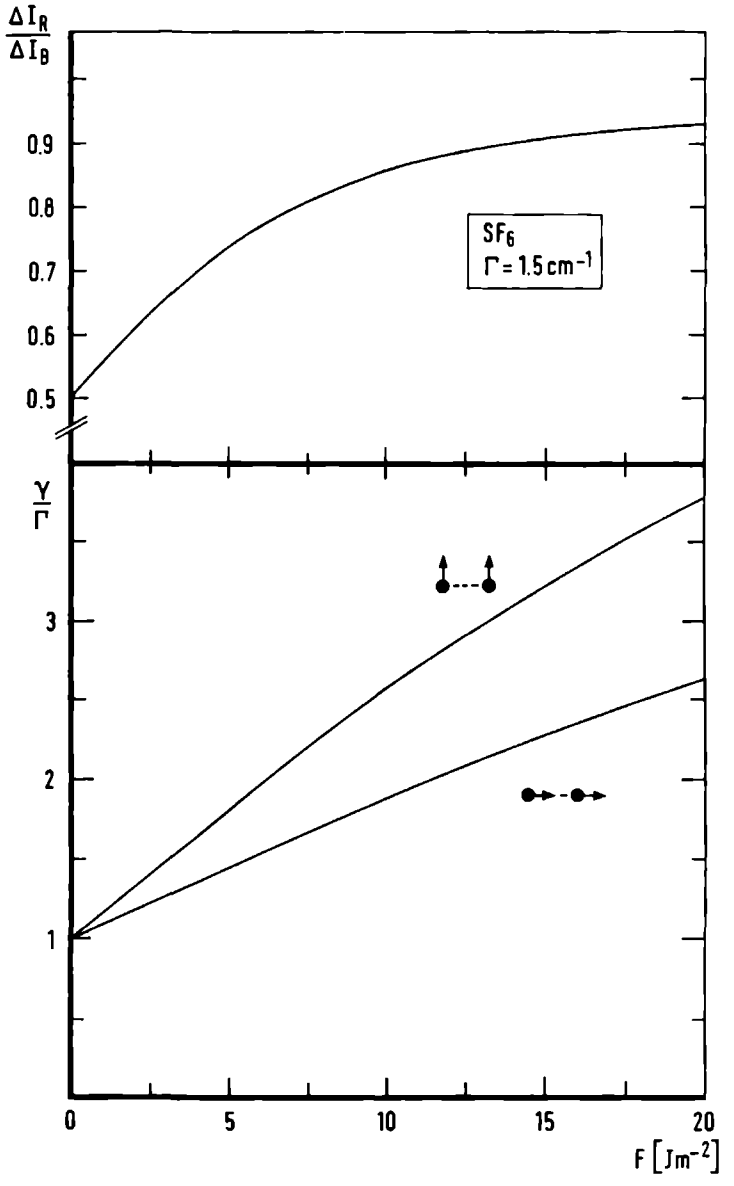

Fig. 2: Upper part: the attenuation ratio of the red dimer peak (ΔI_R) and the blue dimer peak (ΔI_B) as a function of the fluence F. Lower part: the normalized full width half maximum γ/Γ as a function of the fluence F. Further details in the caption of fig. 1.

At a reservoir pressure P_o = 1850 torr the ratio $\Delta I_R/\Delta I_B = 0.94 \pm 0.06$ was found for F = 50 Jm^{-2}; the attenuation of the beam was 16% for the red peak. From an earlier measurement (table 4, section IV.2) fitted with dimers and trimers, we have extrapolated about 7% attenuation. In the mean time, however, the skimmer opening was reduced from 1.1 mm Ø to 0.5 mm Ø. The difference in attenuation indicates that larger clusters of SF_6 have a lower recoil velocity than small clusters.

Table 1 *Compilation of beam modulations at different cluster conditions. The molecular beam consists of a 5% SF_6-95% He mixture. The reservoir conditions are T_o = 233 K, d_o = 30 µm and P_o is displayed in the first column. The mass-spectrometer is tuned to $^{32}SF_5^+$. The modulation laser m is focused between nozzle and skimmer. The fluence is about 50 Jm^{-2}, the frequency ν_m and the modulation of the ion-signal $\Sigma_n \Delta I_n^*$ are given in column two and three. The cw probe laser p, set on frequency ν_p and with fluence F_p, attenuates the modulated signal by $\Sigma_n \Delta_p I_n^*$ (column 4, 5 and 6). The last column refers to the figures, taken at the conditions mentioned.*

source	modulation laser m		probe laser p			figure
P_o [torr]	ν_m [cm^{-1}]	$\Sigma_n I_n^*$ %	ν_p [cm^{-1}]	F_p [Jm^{-2}]	$\Sigma_n \Delta_p I_n^*$ %	
900	934.9	4.0 ± 0.1	-	-	-	-
900	954.6	4.5 ± 0.1	954.6	0.40±0.04	10 ± 1	3 (•)
1850	934.9	16.0 ± 1.0	-	-	-	-
1850	954.6	17.0 ± 1.0	954.6	2.1 ± 0.2	47 ± 3	4 (•)
1850	963.3	3.0 ± 0.2	963.3	2.1 ± 0.2	32 ± 3	4 (○)
1500	920.6	0.4 ± 0.1	934.9	2.0 ± 0.2	42 ± 4	5 (•)
2250	920.6	1.1 ± 0.2	934.9	2.0 ± 0.2	26 ± 3	5 (○)

It is possible to create a molecular beam containing only monomers and dimers. When the reservoir pressure P_o increases or the temperature T_o decreases trimers, tetramers, etc. are formed in the beam expansion. The predissociation spectra will contain a contribution of several clusters. It is very difficult to fit the experimental cluster spectrum unambiguously if this spectrum contains contributions from more than two different clusters. The most important reason for this restriction is the line tunability of the CO_2 laser with a spacing of about 2 cm^{-1}. The maximum number of measurement points in a SF_6 cluster spectrum therefore is about 25.

To isolate one specific cluster we applied a two-laser modulation technique. In practice the modulation of one single cluster is difficult as each cluster line possesses a certain linewidth. For larger clusters the density of lines is so high that the cluster lines overlap (see section IV.2).

For modulation we use a second laser, cl 2, which modulates the cluster beam with a given frequency ν_m. The other laser, cl 1, probes the cluster beam as a function of the frequency ν_p. The positions of intersection with the molecular beam are given in chapter II, figure 1. For one specific cluster n the dissociated fraction ΔI_n produced by the probe laser is

$$\Delta I_n = N_n\left[1 - f(r_n \cdot t)\right] \tag{4.1}$$

and by the modulation laser

$$\Delta I_n^* = N_n\left[1 - f(r_n^* \cdot t^*)\right] \tag{4.2}$$

where N_n is the total number of the n-cluster per second in the molecular

beam, $r_n(r_n^*)$ the rate of excitation to a predissociative state, $t(t^*)$ the laser interaction time and the asterisk (*) refers to the modulation laser. The function $f(r_n \cdot t)$ is defined in equation 4.3 (section IV.2).

The attenuation of the modulated signal ΔI_n^* by the continuous probe laser equals

$$\Delta_p I_n^* = \Delta I_n^* \, f(r_n \cdot t) \tag{4.3}$$

The spectrum of the n-cluster is given by

$$\begin{aligned} \Delta_m I_n &= 1 - \Delta_p I_n^* / \Delta I_n^* \\ &= 1 - f(r_n \cdot t) = \Delta I_n / N_n \end{aligned} \tag{4.4}$$

For low fluence $f(r_n \cdot t) = \exp(-r_n \cdot t)$.

In the case of imperfect selection several clusters are modulated simultaneously

$$\sum_n \Delta_m I_n = 1 - \sum_n I_n \left[1 - f(r_n^* \cdot t^*)\right] \cdot f(r_n \cdot t) / \sum_n I_n \left[1 - f(r_n^* \cdot t^*)\right] \tag{4.5}$$

Operating the modulation laser at high and the probe laser at low fluences leads to

$$\sum_n \Delta_m I_n = \sum_n I_n \left[1 - \exp(-r_n \cdot t)\right] / \sum_n I_n \tag{4.6}$$

In the figures 3 and 4 we show two cluster spectra obtained by the two-laser modulation technique. Again 5% SF_6 seeded in He has been used to produce the SF_6 cluster beam. The experimental conditions are listed in table I. The pure dimer spectrum (fig. 3) is measured with the modulation laser tuned to $\nu_m = 954.6\ cm^{-1}$. The improved resolution of the blue peak is due to the use of the N_2O laser. The cluster spectrum at $P_o = 1850$ torr (fig. 4, lower part) is measured with the modulation laser tuned to $\nu_m = 954.6\ cm^{-1}$ (•) to observe dimers and trimers and to $\nu_m = 963.3\ cm^{-1}$ (○) to observe contri-

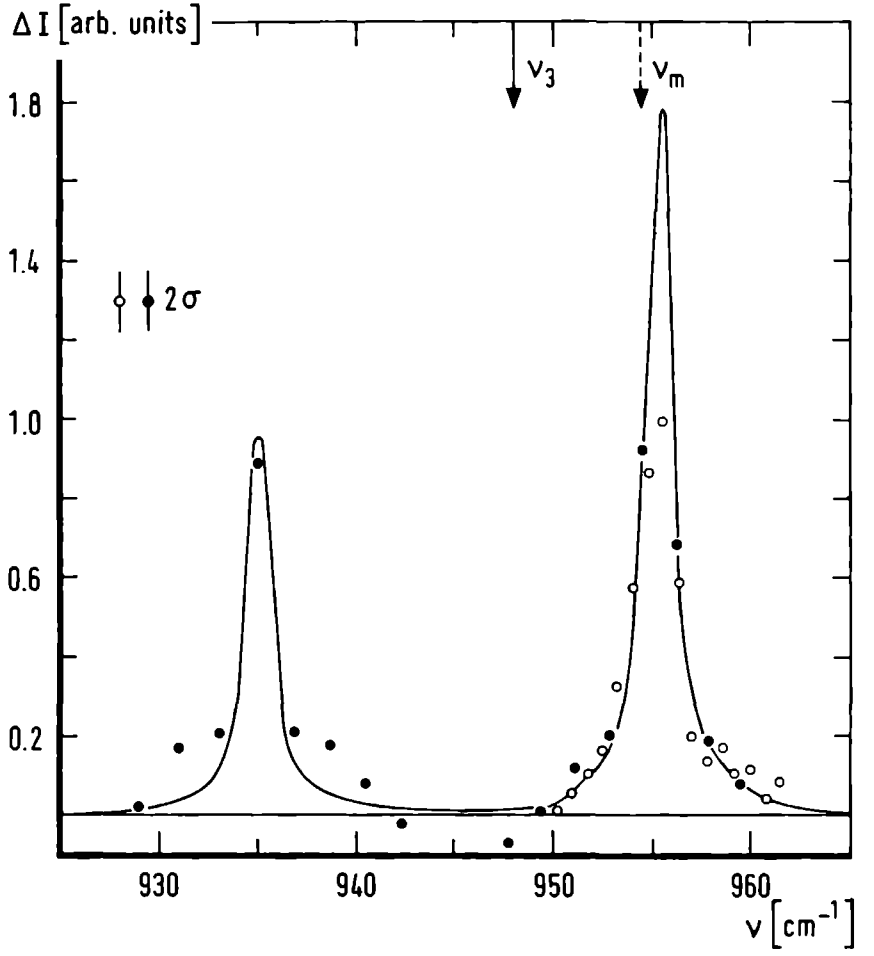

Fig. 3: Predissociation spectrum of SF_6 dimers derived with the two-laser modulation technique. The experimental conditions are summarized in table 1. The frequency of the ν_3 mode is indicated by an arrow as measured for the SF_6 monomer. The second arrow ν_m indicates the modulation frequency. Full points (•) are measured with the CO_2 laser; open points (○) with the N_2O laser. The solid line is the fit of the spectrum (see table 2).

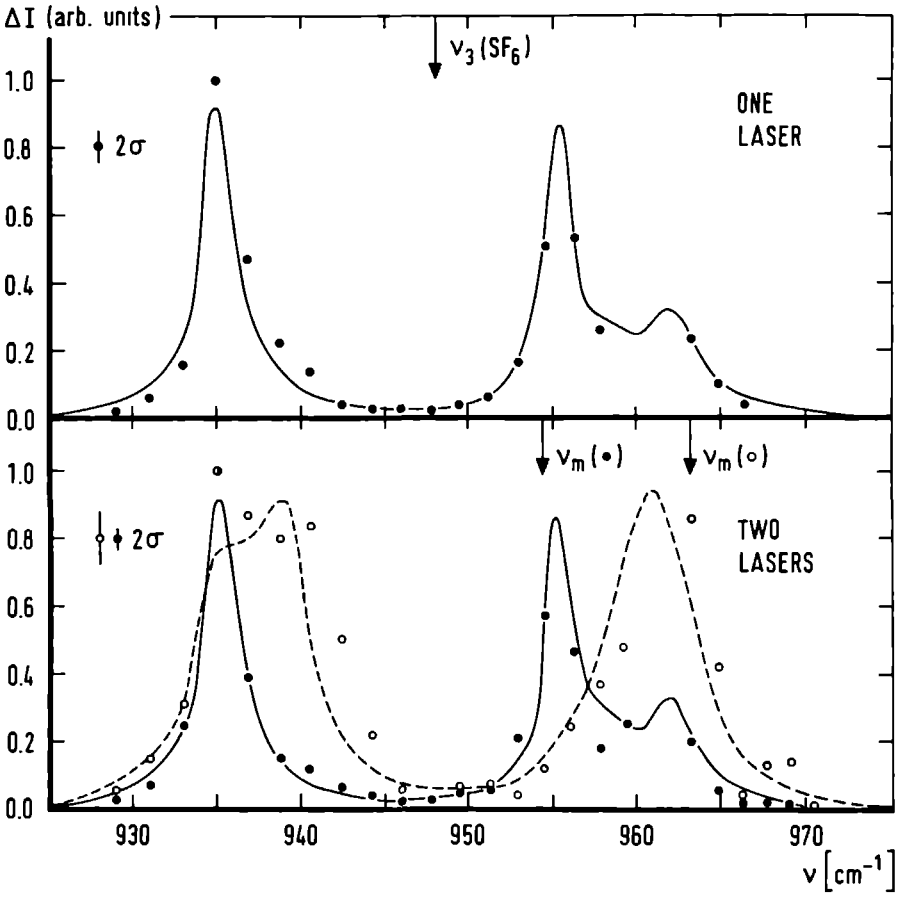

Fig. 4: Upper part: predissociation spectrum of SF_6 clusters derived with one laser. The beam conditions are summarized in table 1. This figure is equal to figure 7 (section IV.2). As the fit suggests there are only dimers and trimers in the beam.

Lower part: spectra obtained with the two-laser modulation technique. The experimental conditions are summarized in table 1. The arrow ν_m indicates the modulation frequencies. The solid and the dashed curves are fits of the spectra (see table 2). The dashed curve shows there are also tetramers in the beam.

butions of larger clusters to the spectrum. For comparison we show the normal spectrum in the upper part of figure 4, obtained with one laser and at the same source conditions.

The pure dimer spectrum (fig. 3) proves that the modulation technique is useful to isolate one specific cluster. By modulating any transition frequency of the dimer it is possible to scan the entire dimer spectrum with the probe laser. Moreover, this spectrum gives a strong indication that the dimer is homogeneously broadened. A least square fit is made of the spectrum to obtain the parameters for the dimer, i.e. the linewidth Γ and the normalization factor $(4\pi\varepsilon_o)^{-1}\cdot\mu_{01}^2\cdot\langle R^{-3}\rangle$ (table 2). In figure 4 (lower part) the modulation technique is used to separate clusters of different size by modulating at $\nu_m = 954.6\ cm^{-1}$ and $\nu_m = 963.3\ cm^{-1}$. The former modulation yields almost the same spectrum (•) as shown in the upper part of the figure, which is ascribed to dimers and trimers (fig. 7, IV.2). The latter gives an entirely different predissociation spectrum (o); the shoulder at 960 cm^{-1} is clearly favoured and at 940 cm^{-1} a new structure is coming in. The first

Table 2 *Results of the least square fits used with the linewidth Γ and the normalization factor $(4\pi\varepsilon_o)^{-1}\cdot\mu_{01}^2\cdot\langle R^{-3}\rangle$ as free parameter and with the theoretical spectrum and dissociation probabilities as given in section 2 and 3. The quantity $\langle R^{-3}\rangle^{-1/3}$ is also displayed for the transition moment $\mu_{01}(SF_6) = 0.387$ D. The unshifted frequency was taken to be 948.5 cm^{-1}.*

	Γ [cm^{-1}]	$(4\pi\varepsilon_o)\cdot\mu_{01}^2\cdot\langle R^{-3}\rangle$ [cm^{-1}]	$\langle R^{-3}\rangle^{-\frac{1}{3}}$ [nm]	figure
dimer	1.5 ± 0.2	6.8 ± 0.1	0.482	3 (•)
trimer	2.8 ± 0.6	6.8 ± 0.1	0.482	4 (•)
tetramer	3.0 ± 1.6	5.2 ± 0.3	0.529	4 (o)

spectrum (•) is fitted to obtain the trimer parameters and the last spectrum (○) to obtain the tetramer parameters. More information from this spectrum should be obtainable by modulating the cluster beam at 940 cm^{-1}; an experiment not yet carried out.

The results of the fits (table 2) show that $\langle R^{-3} \rangle^{-\frac{1}{3}} \simeq 0.48$ nm for the dimer and trimer and $\langle R^{-3} \rangle^{-\frac{1}{3}} \simeq 0.52$ for the tetramer. High energy electron diffraction has been used to determine the SF_6 cluster structure in a molecular beam [4]. It was found that the SF_6 cluster pattern is body-centred-cubic (bcc) with a unit-cell dimension of 0.58 nm and a nearest neighbour distance of 0.49 nm. The intermolecular distances are thus in agreement for both experiments. For very large cluster sizes the structure displayed in table 1 (section IV.2), used for the calculation of the stick spectrum (fig. 2, section IV.3), must change to the bcc structure.

Finding a linewidth two times larger for trimers and tetramers than for the dimer linewidth ($\Gamma_2 = 1.5$ cm^{-1}) may point to a shorter lifetime. Another reason for inhomogeneous extra-broadening can be a larger state density of the trimers (tetramers).

Table 3 *Transition frequencies, transition strengths and abundances of* $(^{32}SF_6)_n$, $1 \leq n \leq 4$ *and* $(^{32}SF_6)_n{}^{-34}SF_6$, $0 \leq n \leq 3$. *The index m describes a transition from the ground state to an individual excited level m. The column* $\hbar\omega$ *describes the transition frequency and g.S the total transition strength. The calculations are performed with* $(4\pi\varepsilon_o)^{-1} \cdot \mu_{01}^2 \cdot \langle R^{-3} \rangle = 6.8\ cm^{-1}$.

	$(^{32}SF_6)_n$			$(^{32}SF_6)_n{}^{-34}SF_6$		
m	$\hbar\omega_{n,m}$ [cm^{-1}]	$(g.S)_{n,m}$	abundance %	$\hbar\omega_{n,m}$ [cm^{-1}]	$(g.S)_{n,m}$	abundance %
monomer n=1			95.0	n=0		4.2
1	948.0	3.00		930.8	3.00	
dimer n=2			90.3	n=1		8.0
1	934.4	2.00		923.3	1.85	
2				928.4	0.72	
3	954.8	4.00		950.4	3.28	
4				955.5	0.15	
trimer n=3			85.7	n=2		11.9
1				922.0	0.35	
2	935.4	4.34		922.3	1.88	
3				927.4	0.22	
4	958.2	1.66		934.5	2.18	
5	962.1	3.00		949.7	0.47	
6				957.2	1.10	
7				958.2	2.78	
8				967.8	0.02	
tetramer n=4			81.4	n=3		15.0
1				921.5	0.47	
2	935.6	6.70		921.7	1.91	
3				934.9	4.51	
4	964.8	5.30		947.4	0.10	
5				960.7	2.92	
6				963.8	2.09	

IV.6. Isotopic clusters

The natural abundance of SF_6 amounts to 95.0% of the sulphur isotope 32 and to 4.2% of the sulphur isotope 34. The dimer of SF_6 will therefore include 8% of the isotopomer $^{34}SF_6$-$^{32}SF_6$. The ν_3 mode for $^{34}SF_6$ is 17.2 cm^{-1} red shifted with respect to the ν_3 mode of $^{32}SF_6$ (Appendix A1).
In section IV.2., figure 9, a measured transition is shown at $921 \pm 2\ cm^{-1}$ compatible with the theoretical value 923.3 cm^{-1} for $(4\pi\varepsilon_o)^{-1} \cdot \mu_{01}^2 \cdot \langle R^{-3} \rangle = 6.8\ cm^{-1}$. In section IV.3, table 4, the eigenvalues, transition strengths and eigenfunctions of the isotopomer are displayed.

Spectra of isotopically mixed clusters are calculated by diagonalizing the energy matrix (section IV.2., table 2). Before diagonalization the ν_3 frequencies of $^{34}SF_6$ and $^{32}SF_6$ vibrations are divided by the normalization factor $(4\pi\varepsilon_o)^{-1} \cdot \mu_{01}^2 \cdot \langle R^{-3} \rangle$. In order to obtain the real transition frequencies the eigenvalues have to be multiplied with the normalization factor. In table 3 the transition frequencies and transition strengths are shown for the pure and isotopic dimers, trimers and tetramers.

In the upper part of figure 5 the stick spectra for the isotopically mixed clusters are shown. In the lower part the measurements with the modulation laser tuned to the frequency $\nu_m = 920.6\ cm^{-1}$ are displayed.
The experimental conditions are listed in table 1. At P_o = 1500 torr laser m modulates the SF_5^+ signal by about 0.4%, at 2250 torr by about 1.1%. A modulation depth of 1.1% of the partial beam signal (SF_6) indicates that the molecular beam contains 2.2% isotopically mixed clusters. Given the setting of laser m at $\nu_m = 920.6\ cm^{-1}$ it is clear that the measured spectra correspond to the trimers and tetramers present in the beam. We find

$$\frac{\langle R^{-3}(^{32}S\text{-}^{34}S)\rangle}{\langle R^{-3}(^{32}S\text{-}^{32}S)\rangle} \simeq \frac{\mu_{01}(^{32}SF_6)}{\mu_{01}(^{34}SF_6)}$$

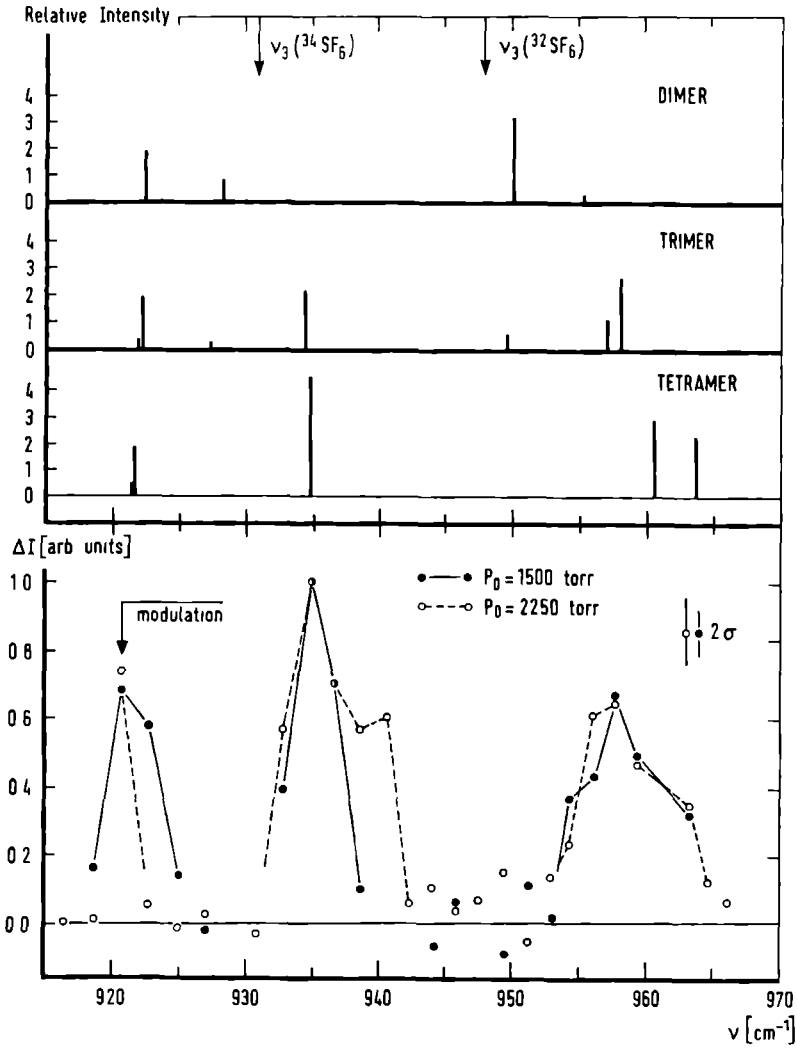

Fig. 5: Upper part: the stick spectrum for isotopically mixed clusters of SF_6. The relative intensity corresponds to g.S, see table 3. The two arrows indicate the ν_3 mode frequencies of $^{32}SF_6$ and $^{34}SF_6$.

Lower part: predissociation spectra obtained with the two-laser modulation technique. The beam and laser conditions are summarized in table 1. The arrow indicates the modulation frequency.

This result leads to speculations about the suitability of the laser-cluster fragmentation process as a method for isotope separation. This method has the advantage that only one infrared photon is necessary for dissociation instead of about 35 (SF_6) or 60 (UF_6) needed for multiphoton dissociation. We have performed the calculations of the transition frequencies and strengths for the isotopomers of UF_6, a much discussed molecule.

The natural abundance of $^{235}UF_6$ is 0.711% and of $^{238}UF_6$ 99.283%. For $^{238}UF_6$ the fundamental frequency of the ν_3 mode is 626($\pm$1) cm^{-1} [5] and the transition moment μ_{01} = 0.342 D [6]; we assume $\langle R^{-3}(UF_6)\rangle \approx \langle R^{-3}(SF_6)\rangle$. The isotope shift for $^{235}UF_6$ relative to $^{238}UF_6$ is 0.65 ($\pm$ 0.09) cm^{-1} [5].
In table 4 we show the result of the calculation. Around 621 cm^{-1} there is no transition frequency for isotopically pure dimers. The transition strength for the isotopomers at this frequency is very low. Therefore a reasonable dissociation probability at 621 cm^{-1} can only be obtained with a large fluence. In this case the pure dimer line at 615 cm^{-1} would overlap the isotopomer line.

Table 4 *Transition frequencies, transition strengths and abundances of $(^{238}UF_6)_2$ and $^{238}UF_6$-$^{235}UF_6$. The calculations are performed with μ_{01} = 0.342 D [6] and $(4\pi\varepsilon_0)^{-1}\cdot\mu_{01}^2\cdot\langle R^{-3}\rangle$ = 5.3 cm^{-1}.*

frequency [cm^{-1}]	strength	abundance %	frequency [cm^{-1}]	strength	abundance %
$^{238}UF_6$		99.3	$^{235}UF_6$		0.7
626.0	3.0000		626.7	3.0000	
$^{238}UF_6$-$^{238}UF_6$		98.6	$^{238}UF_6$-$^{235}UF_6$		1.4
615.4	2.0000		615.6	1.9995	
620.7	0		621.0	0.0037	
631.3	4.0000		631.7	3.9963	
636.6	0		637.0	0.0005	

IV.7. SF_6 in Argon clusters

In chapter III, fig. 2, we have displayed one of our first measurements of SF_6 clusters. The molecular beam consisted of 5% SF_6 in an argon carrier gas. The spectrum, taken with the mass spectrometer, shows three clearly resolved peaks, near 935, 944 and 955 cm^{-1} respectively. With the SF_6 cluster model the first and the third frequency can be understood. For the remaining peak there are two possible explanations; either the peak belongs to higher clusters or to a Ar_n-SF_6, $n \geq 1$, complex. We will show that the last of these two possibilities is the most probable one.

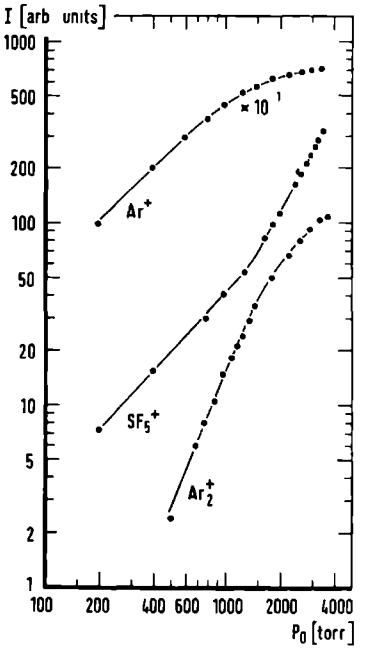

Fig. 6: Ion intensities of Ar^+, SF_5^+ and Ar_2^+ versus reservoir pressure P_o. A 1% SF_6-99% He mixture was employed. Measurements obtained at T_o = 294 K and d_o = 30 μm.

The seeding ratio was changed to favour Ar_n-SF_6 complexes in the beam. The measurements displayed in figure 6 and 7 are obtained with a 1% SF_6 in Ar beam.

Figure 6 shows the ion current I of the mass spectrometer as a function of the P_o for T_o = 294 K. Also on the ion-mass Ar-SF_5^+ a signal was found; at P_o = 3000 torr we measured $I(Ar\text{-}SF_5^+) \simeq 2\times10^{-3}\ I(SF_5^+)$. Figure 7 shows the spectrum obtained on ion-mass SF_5^+ at P_o = 3000 torr. Again the peak near 944 cm^{-1} appears. The attenuation of the SF_5^+ signal amounts to about 8% under the experimental conditions for $\nu \simeq 945\ cm^{-1}$. To be sure that the peaks near 935 and 955 cm^{-1} partly originate from $(Ar)_n$-$(SF_6)_m$ $n \geq 1$, $m \geq 1$ the attenuation of the $(Ar)_2^+$ ion signal was measured at ν = 933.0, 944.2 and 954.6 cm^{-1}; we found 0.65%, 0.20% and 0.60% respectively.

In figure 6 the SF_5^+ ion signal exhibits a kink in the slope at about P_o = 1000 torr. This sudden increase in the slope is taken as an indication that SF_6 molecules embedded in Ar atoms are formed. The ionization cross section for $(Ar)_n$-$SF_6 \rightarrow SF_5^+$ is apparently larger than for $SF_6 \rightarrow SF_5^+$. The $(Ar)_n$-SF_6 clusters explode upon ionization, yielding $(Ar)_n$ and SF_5^+.

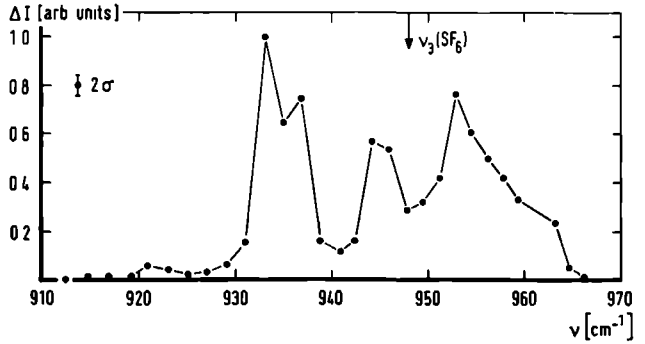

Fig. 7: The attenuation spectrum for $(SF_6)_m$ embedded in $(Ar)_n$ ($m \geq 1$, $n \geq 1$). The reservoir conditions were T_o = 293 K, P_o = 3000 torr and d_o = 30 μm. The attenuation is measured on ion mass SF_5^+ with a laser fluence $F = 6\ Jm^{-2}$.

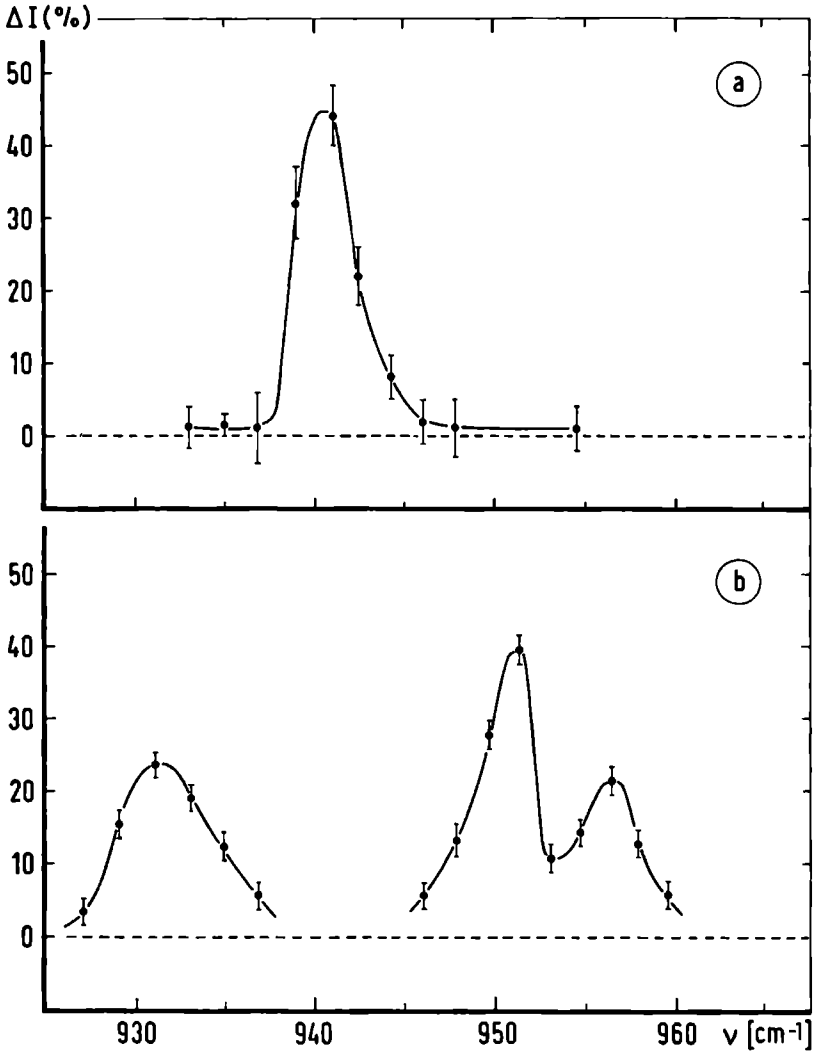

Fig. 8: The attenuation spectra for $(SF_6)_m$ embedded in $(Ar)_n$ ($m \geq 1$, $n \geq 1$). Figure (a) shows the monomer attenuation spectrum; figure (b) the $(SF_6)_m$ ($m \geq 2$) spectrum. A 0.5% SF_6-99.5% He mixture was employed. The reservoir conditions were T_o = 233 K, P_o = 2250 torr and d_o = 30 μm. The attenuation spectrum (a) is measured on ion mass Ar-SF_5^+ with a laser fluence F = 16 Jm^{-2}; spectrum (b) on SF_6-SF_5^+ with F = 6 Jm^{-2}.

In figure 8 the attenuation spectra are shown for a 0.5% SF_6 in Ar beam. The reservoir conditions are chosen in order to get maximum $(Ar)_n$-$(SF_6)_m$ complex formation. In figure 8a the attenuation spectrum is shown obtained on ion mass Ar-SF_5^+. The "monomer peak" appears to be shifted to 940 cm^{-1}, as consequence of the presence of the Ar atoms in the neutral parent cluster $(Ar)_n$-SF_6. Under essentially the same conditions the spectrum has been recorded on mass SF_6-SF_5^+ (fig. 8b). The SF_6 dimer spectrum appears to be shifted by about 4 cm^{-1} to the red and is only slightly changed. The blue peak at 956 cm^{-1} is attributed to trimers embedded in Ar. The high fluence used in the experiment increases the observed linewidths.

Recently T. Gough et al [7] have measured the predissociation spectra of SF_6 embedded in Ar, too. The investigations have been performed using a steady state molecular beam, a cw CO_2 laser and an optothermal (bolometric) detector. They have measured the spectral shift of $(Ar)_n$-SF_6 as a function of increasing reservoir pressure P_o. At the highest pressures the spectral position of the $(Ar)_n$-SF_6 stabilizes near 939 cm^{-1} and the linewidth becomes about 2 cm^{-1}. High resolution spectra by Swanson and Jones [8] have shown that SF_6 in an Ar matrix at a temperature T = 10 K has a considerable amount of fine structure in the 938 cm^{-1} region.

From the present study of SF_6 embedded in Ar atoms we confirm that it is possible to obtain low resolution matrix spectra not only of one SF_6 molecule but also of SF_6 clusters in a rare gas solid, using the molecular beam technique.

For the sake of completeness we have searched for the existence of $(He)_n$-$(SF_6)_m$, $n \geq 1$, $m \geq 1$. The molecular beam consisted of 5% SF_6 in a He carrier gas. The reservoir conditions were P_o = 2250 torr, T_o = 233 K and d_o = 30 μm. The attenuation of the He^+ ion signal was measured with a laser fluence of 13 Jm^{-2} at ν = 934.9 cm^{-1}, 947.8 cm^{-1} and 956.2 cm^{-1}. The attenuations were

0.30(± 0.06)%, 0.15(± 0.05)% and 0.15(± 0.05)%, respectively. At a laser fluence of 35 Jm^{-2} (saturation) the attenuation measured at ν = 934.9 cm^{-1} was 0.5(±0.1)%. From the occurrence of the attenuation at 947.8 cm^{-1} we conclude that $(He)_n$-SF_6 exist in the molecular beam; from the attenuation at 934.9 cm^{-1} and 956.2 cm^{-1} that at least $(He)_n$-$(SF_6)_2$ exist.

Under the same source conditions we have not found a significant attenuation at ν = 947.8 cm^{-1} on mass SF_5^+. The main reason is supposed to come from the small repulsion that a SF_5 molecule undergoes upon dissociation of a $(He)_n$-SF_6 complex.

References

1. J. Geraedts, S. Stolte and J. Reuss
   Z. Phys. A 304 (1982) 167
2. J. Geraedts, M. Waayer, S. Stolte and J. Reuss
   Faraday Disc. Chem. Soc. 73 (1982) 375
3. J. Geraedts
   Faraday Disc. Chem. Soc. 73 (1982) 416
4. G. Stein
   J. Appl. Phys. 51 (1980) 6419
5. R.S. McDowell, L.B. Asprey and R.T. Paine
   J. Chem. Phys. 61 (1974) 3571
6. W. Person and J. Overend
   J. Chem. Phys. 66 (1977) 1447
7. T.E. Gough, D.G. Knight and G. Scoles
   Chem. Phys. Lett. 97 (1983) 155
8. B.I. Swanson and L.H. Jones
   J. Chem. Phys. 47 (1981) 3209

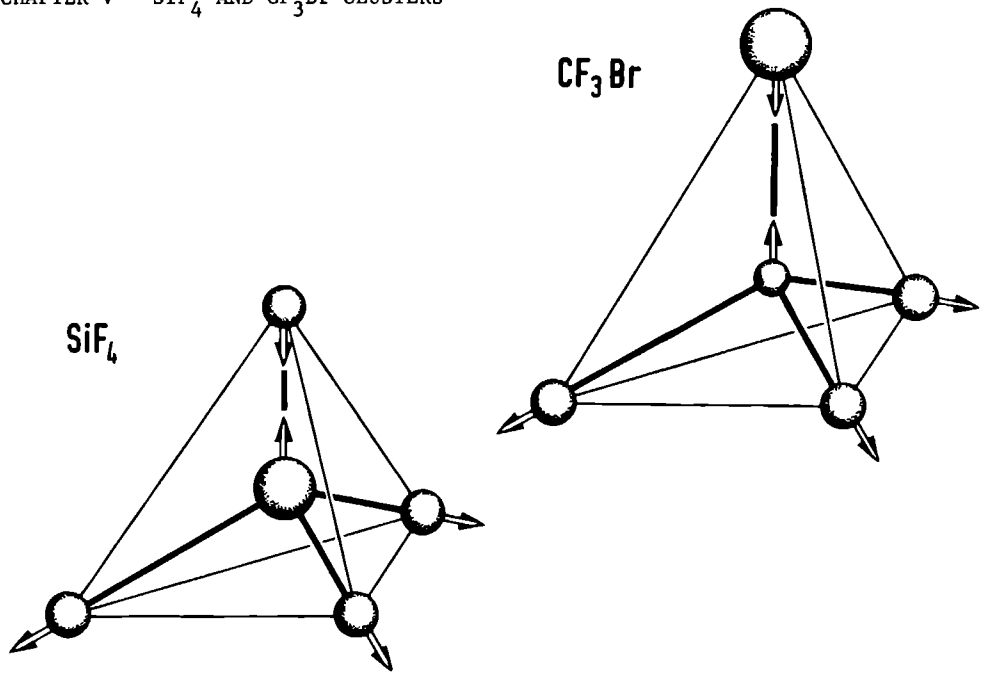

V.1. Introduction

This chapter deals with clusters of the molecules, SF_6, SiF_4 and CF_3Br. We will compare SF_6 with SiF_4 and SiF_4 with CF_3Br to demonstrate what the similarities and differences are of these three molecules.

Both the molecules SF_6 and SiF_4 possess a high symmetry. By excitation of the threefold degenerate vibrational ν_3 mode the transition dipole moment has no preferential direction within the molecule. The behaviour of the infrared excited dimers SF_6-SF_6 and SiF_4-SiF_4 must therefore be similar. We have to expect strong effects due to resonant dipole-dipole forces between two infrared active in-phase vibrations, one along the intermolecular axis and the other perpendicular to it. Consequently SiF_4-SiF_4 must show a predissociation spectrum with two peaks, one with a negative energy shift (-2Δ) and the other one with a positive energy shift (Δ).

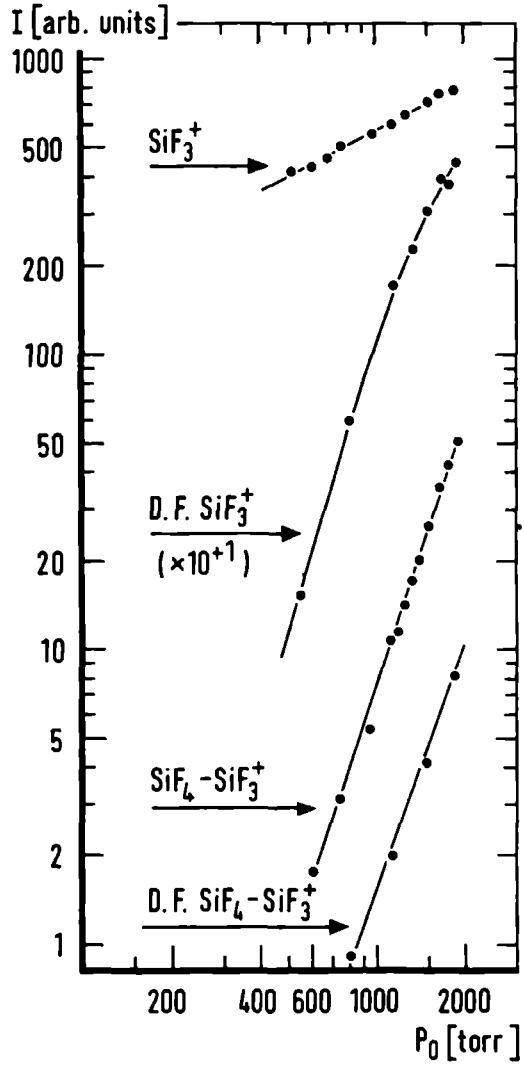

Fig. 1 *The intensities of SiF_3^+ and SiF_4-SiF_3^+ versus P_o. A 5% SiF_4-95% He mixture was employed. Measurements obtained at T_o = 199 K and d_o = 30 μm. The dissociated fractions (D.F.) measured on SiF_3^+ and SiF_4-SiF_3^+ are obtained with the CO_2 laser tuned to ν = 1037.4 cm^{-1} and with a fluence F = 2 Jm^{-2}.*

The molecules SiF_4 and CF_3Br show nearly the same molecular structure (see Appendix A3 and A4). In the case of CF_3Br the ν_1 mode does not show the three-fold degeneracy, as the ν_3 mode of SiF_4, which leads to decoupling of the transition dipole moment from the molecular frame. Consequently CF_3Br-CF_3Br will show a very different predissociation spectrum with respect to the SiF_4-SiF_4 spectrum.

V.2. Comparison between $(SF_6)_2$ and $(SiF_4)_2$

We have investigated the SiF_4 cluster spectra using a beam of 5% SiF_4 in He. In figure 1 the various ion signals are displayed as a function of P_o. The reservoir conditions are T_o = 199 K and d_o = 30 μm; the electron energy of the ionizer is 50 eV. The ions shown are the result of a fragmentation process where one F atom leaves the parent ion. The signal on SiF_4^+ is about 20 times smaller than that on SiF_3^+, under pure monomer conditions. Even at high pressure it was not possible to detect any signal on $(SiF_4)_2$-SiF_3^+.

Also displayed are the dissociated fractions (D.F.) of both ion masses SiF_3^+ and SiF_4-SiF_3^+. These fractions have about the same slope as the full SiF_4-SiF_3^+ signal. From the ratio of these two signals and from their saturation behaviour for high laser fluences - not shown - we deduce that the dimer, $(SiF_4)_2$, shows up after ionization on mass SiF_3^+ about seven times more likely than on mass SiF_4-SiF_3^+.

In figure 2 the predissociation spectra are shown, measured as an attenuation on mass SiF_3. The reservoir conditions are P_o = 1500 torr, d_o = 30 μm and T_o = 233 K and T_o = 199 K, respectively. The laser fluence and the attenuation on top of the predissociation spectrum are summarized in table 1.

With respect to the unshifted ν_3 frequency the blue peak is shifted by about

Table 3 *Compilation of results for SiF_4 and CF_3Br mixtures. The pressure P_o, the temperature T_o and the diameter d_o are the stagnation conditions of the source. The beam is detected at the mass-spectrometer setting given in the column "mass". The stream velocity v_s and the beam temperature T// are derived from the velocity distribution. The fluence F is given at the point of beam intersection and the "peak height" is the beam attenuation taken at the maximum of the absorption profile. The last column refers to the figures, taken at the conditions mentioned*

gas composition	P_o [torr]	T_o [K]	d_o [10^{-6}m]	mass	v_s [ms^{-1}]	T// [K]	F [Jm^{-2}]	peakheight %	figure
5% SiF_4 in He	1500	233	30	SiF_3^+	-	-	1.3	0.3	2 (o)
	1500	199	30	SiF_3^+	-	-	1.1	1.5	2 (•)
	1500	233	30	SiF_4-SiF_3^+	-	-	2.2	25	3 (o)
	1500	199	30	SiF_4-SiF_3^+	-	-	1.1	11	3 (•)
5% CF_3Br in He	1000	243	30	CF_3^+	907	13	1.6	0.9	5 (•)
	1000	243	60	CF_3^+	-	-	2.0	1.3	5 (o)
	1500	243	60	CF_3^+	-	-	2.0	3.0	6

$\Delta_2 = 6.2 \pm 0.2$ cm^{-1}. The width is $\Gamma_2 = 4.7 \pm 0.4$ cm^{-1}. The red peak, expected from our experience with $(SF_6)_2$, could not be measured completely. Below 1019 cm^{-1} no $^{12}CO_2$ laser lines were available when we measured this spectrum. The spectrum shows a clear indication of the presence of the red peak. The broken line shows a dimer fit analogous to the $(SF_6)_2$ procedure (chapter IV.2.4), with Δ and Γ given above. (The measured point at 1019 cm^{-1} has an uncertainty twice that indicated.)

In figure 3 similar attenuation spectra are shown as in figure 2. The attenuation is measured on mass SiF_4-SiF_3^+. The higher temperature spectrum (o) is well reproduced by the dimer fit curve (full line). The lower temperature spectrum (•) appears to be contaminated by trimer fragments; the broken line reflects an admixture of about 30% trimers. The dimer peak position remains unchanged with respect to figure 2. The fitted trimer parameter is the linewidth $\Gamma_3 = 6.4 \pm 3.4$ cm^{-1} for a fixed $\Delta_3 = 6.2$ cm^{-1}.

Table 2 *Survey of the measurements on $(SiF_4)_2$ and $(SF_6)_2$. The transition dipole moment μ_{01} of the monomer, the normalization factor Δ, the linewidth Γ and the dimer distance $\langle R^{-3}\rangle^{-1/3}$ are displayed.*

		$(SiF_4)_2$	$(SF_6)_2$
μ_{01}	[D] a)	0.267 ± 0.013	0.387 ± 0.006
Δ_2	[cm^{-1}] b)	6.2 ± 0.2	6.8 ± 0.1
Γ_2	[cm^{-1}]	4.7 ± 0.4	1.5 ± 0.2
$\langle R^{-3}\rangle^{-\frac{1}{3}}$	[nm]	0.39 ± 0.02	0.48 ± 0.01

a) references in Appendix A1 and A3

b) Δ_2 equals $\Delta_{2,3}$ from table 2, section IV.2

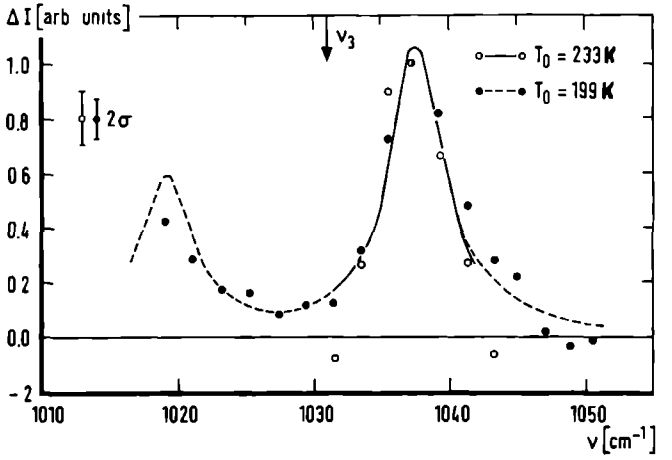

Fig. 2 *The attenuation spectra of the SiF_4 dimer measured on the SiF_3^+ mass at two different T_o. The experimental conditions are summarized in table 1. The arrow indicates the i.r. active ν_3 mode of the SiF_4 monomer. The curves are calculated with $\Gamma_2 = 4.7$ cm^{-1} and $\Delta_2 = 6.2$ cm^{-1}.*

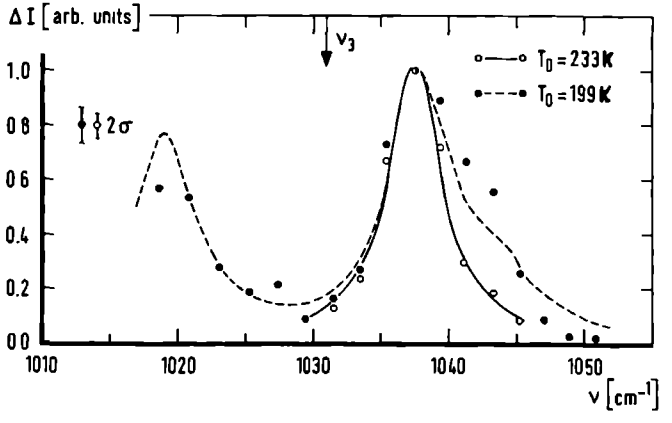

Fig. 3 *The attenuation spectra of SiF_4 clusters measured on the mass SiF_4-SiF_3^+ at two different T_o. The experimental conditions are summarized in table 1. The arrow indicates the i.r. active ν_3 mode of the SiF_4 monomer. The fit (solid curve) yields $\Gamma_2 = 4.7 \pm 0.4$ cm^{-1} and $\Delta_2 = 6.2 \pm 0.2$ cm^{-1}. The fit (dashed curve) with fixed $\Gamma_2 = 4.7$ cm^{-1} and $\Delta_2 = \Delta_3 = 6.2$ cm^{-1} yields $\Gamma_3 = 6.4 \pm 3.4$ cm^{-1}.*

In table 2 the fit parameters of $(SiF_4)_2$ are compared with those of $(SF_6)_2$. The value of Δ_2 depends on the transition dipole moment and the expectation value $\langle R^{-3} \rangle$, where R is the dimer distance. For $(SiF_4)_2$ the dimer distance is smaller than for $(SF_6)_2$. The lifetime of the excited dimer is expected to be shorter for smaller dimer distances yielding an increased value for Γ_2 (see table 2).

V.3. Comparison between $(SiF_4)_2$ and $(CF_3Br)_2$

The CF_3Br cluster spectra are investigated using a beam of 5% CF_3Br in He. In figure 4 the mass spectrometer signals are shown as function of P_o, for different masses. The reservoir conditions are T_o = 243 K and d_o = 60 μm; the electron energy of the ionizer is 50 eV. It is evident that the slopes for the

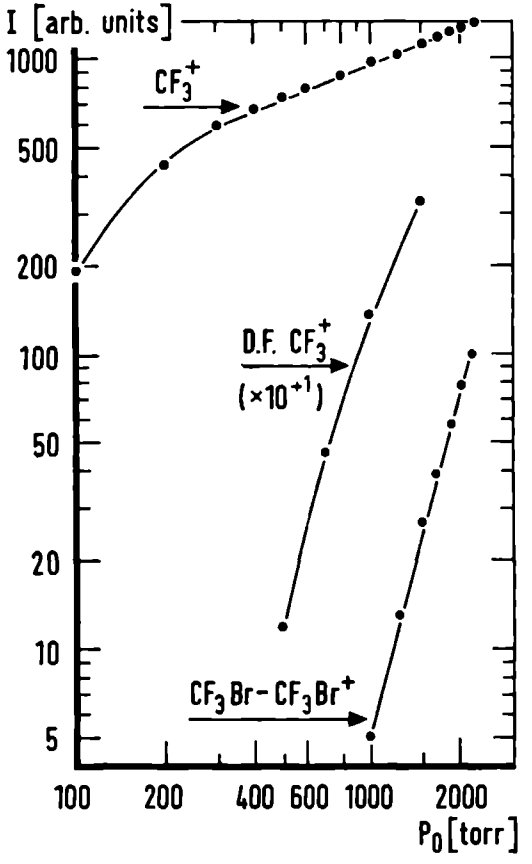

Fig. 4 The intensities of CF_3^+ and CF_3Br-CF_3^+ versus P_o. A 5% CF_3Br-95% He mixture was employed. Measurements obtained at T_o = 243 K and d_o = 60 μm. The dissociated fraction (D.F.) measured on CF_3^+ is obtained with the CO_2 laser tuned to ν = 1084.6 cm^{-1} and with a fluence F ≃ 2 Jm^{-2}.

predissociated fraction of CF_3^+ and the full CF_3Br-CF_3^+ signal are nearly equal. At P_o = 1500 torr an attenuation of 13% of the CF_3^+ signal has been observed for a high laser fluence at ν = 1084.6 cm^{-1}. Therefore this reservoir pressure leads to heavy clustering.

In figure 5 the predissociation spectrum measured as an attenuation on mass of CF_3^+ is shown. The experimental conditions are summarized in table 1.

In the CF_3Br monomer the ν_1 mode (1084.8 cm^{-1}) shows a weak Fermi resonance with the overtone $2\nu_5$ at 1095.5 cm^{-1} [1]. The latter borrows its total intensity from the ν_1 vibration. A transition strength of about one tenth of that at 1084.8 cm^{-1} is observed in the gas phase [2].

The $2\nu_5$ peak is evident in figure 5. Its strength seems to be enhanced with respect to the monomer case. In accordance, the $2\nu_5$ peak should be slightly blue shifted. Unfortunately the $^{12}CO_2$ laser possesses no lines above 1095 cm^{-1}. A measurement of the entire $2\nu_5$ peak was not possible.

The peak around 1085 cm^{-1} is asymmetric and shows a small shoulder at 1080 cm^{-1}. Tentatively, we have decomposed this peak in two, one centred at 1086 cm^{-1} and the second at 1080 cm^{-1}. Their relative integrated strength shows the approximate ratio of 13:10.

Each CF_3Br has a non-degenerate vibration at 1084.8 cm^{-1}. What does one expect for $(CF_3Br)_2$, a dimer with a double degenerate ν_1 excitation, if the interaction between its constituents is neglected? When there is some interaction between the two constituents the degeneracy is lifted. A possible interaction is the dipole-dipole interaction. The single transition splits symmetrically in two; generally both transitions have different strengths. This is what one finds in figure 5. There is one exception, the centre frequency at 1083 cm^{-1} of the two peaks appears to be shifted slightly to the red with respect to

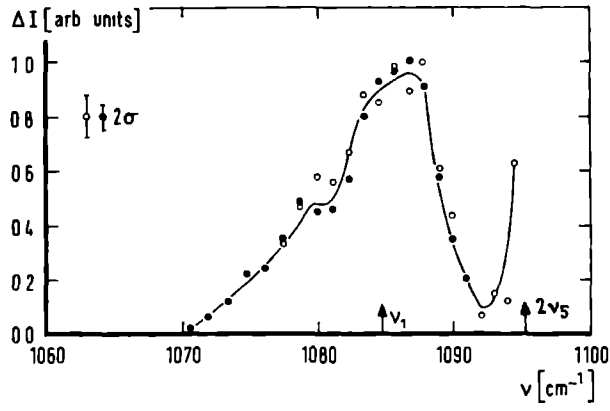

Fig. 5 *The attenuation spectra of CF_3Br clusters measured on CF_3^+ at P_o = 1000 torr. The solid points (●) are measured with d_o = 30 μm and the open points (o) with d_o = 60 μm. The experimental conditions are summarized in table 1. The arrow indicates the i.r. active ν_1 mode of the CF_3Br monomer.*

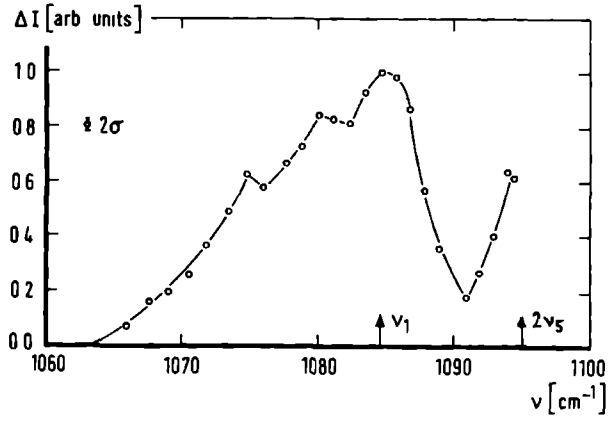

Fig. 6 *The attenuation spectrum of CF_3Br clusters measured on CF_3^+ at P_o = 1500 torr. The experimental conditions are summarized in table 1. The arrow indicates the i.r. active ν_1 mode of the CF_3Br monomer.*

the monomer frequency at 1084.4 cm^{-1}. This shift fits in with a slight increase of the Fermi resonance between the ν_1 and $2\nu_5$ modi observed for the dimer.

In figure 6 the predissociation spectrum is displayed for higher P_o. The most striking feature is the second shoulder at 1075 cm^{-1}. A reasonable explanation for this peak can be found in the contribution of larger clusters. More information about this spectrum should be obtainable by using the two-laser modulation technique (chapter IV.5). The $2\nu_5$ peak is significantly broadened as a result of the increased pressure P_o.

From the present study of CF_3Br clusters we conclude that the predissociation spectrum is very different from the SiF_4 spectrum. The measured two peak spectrum for $(CF_3Br)_2$ looks like OCS [3] and N_2O cluster spectra [4].

References

1. K. Burczyk, H. Bürger, A. Ruoff amd P. Pinson
   J. Mol. Spectr. 77 (1979) 109
2. H. Bürger
   private communication
3. M.A. Hoffbauer, K. Liu, C.F. Giese and W.R. Gentry
   preprint
4. T.E. Gough, R.E. Miller and G. Scoles
   J. Chem. Phys. 69 (1978) 1588

CHAPTER VI INFRARED EXCITATION OF CLUSTERS CONTAINING ETHYLENE

J. Geraedts, M. Snels, S. Stolte and J. Reuss

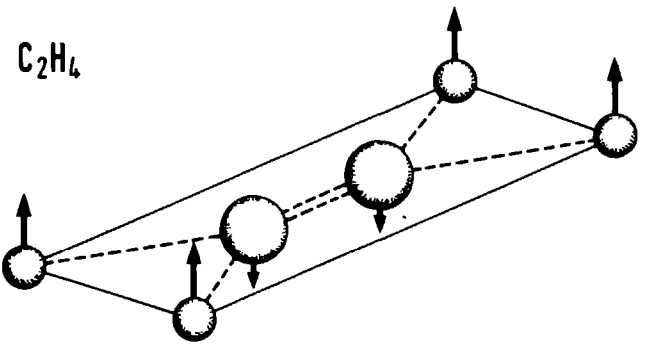

Abstract

IR photodissociation spectra of clusters containing ethylene have been studied. A molecular beam containing the clusters has been attenuated by crossing it with one (or two) line-tunable cw CO_2 laser(s) of moderate power. Attention is given to the line shape and saturation behaviour as influenced by orientational averaging effects. Effects of inhomogeneous line broadening have been observed. The dipole moments, shifts and line widths measured in recent studies are reviewed and discussed together with our own measurements in the light of the sum rule and Fermi resonances.

1. Introduction

In recent years C_2H_4 cluster spectra have often been studied by combining the supersonic molecular beam technique with infrared laser spectroscopy [1,2]. In the expansion of the molecular beam the thermal energy of the gas decreases rapidly; i.e. a beam temperature of a few degrees Kelvin can be achieved and supersaturation of the gas occurs. By collisions dimers, trimers, etc. are generated; these are referred to as clusters. All sorts of clusters are formed upstream and stabilized by evaporation processes. After a distance of about 10 times the nozzle diameter d_0 the density of the expanding gas has decreased far enough to render formation and destruction of clusters by collision negligible; the cluster process appears to be frozen [3,4]. The total amount of clusters in the beam can be adequately regulated by a careful choice of the source conditions.

The constituents of a cluster are bound by the Van der Waals interaction. After vibrational excitation of an i.r. active mode of one constituent a predissociation process is started. The energy of the excited mode is often higher than the Van der Waals binding energy and the constituents decay into a continuum. The cluster fragments leave the collimated beam owing to the recoil upon dissociation; consequently the molecular beam signal is attenuated. The frequency dependence of this attenuation produces a cluster predissociation spectrum.

It is the purpose of this paper to analyze recent C_2H_4 cluster experiments [1,2] together with our own measurements. The experimental results will also be confronted with ab initio calculations e.g. of Van der Avoird *et al* [5].

The investigations reported by Casassa et al [1] have been performed using a steady state molecular beam and a cw CO_2 laser; the laser molecular beam geometry in this experiment is collinear and the laser fluence used is about 40 Jm^{-2}. This fluence is merely an estimate deduced from the measured laser intensity, the approximate interaction length of molecular and laser beam and the calculated molecular beam velocity. Investigated are C_2H_4 bound to Ne, Ar, Kr, C_2H_4, C_2F_4 and larger ethylene clusters.

Hoffbauer et al [2] have employed a pulsed molecular beam and one or two simultaneously pulsed CO_2 lasers; the laser molecular beam geometry is nearly collinear (inclination $3\text{-}5.10^{-2}$ rad) and the laser fluence used is about 400 Jm^{-2}. This fluence is determined by the laser pulse energy and its intensity distribution. Moreover, the predissociation spectra, the recoil velocity and the angle distribution of the fragments were determined too. The investigated clusters are C_2H_4-C_2H_4, C_2D_4-C_2H_4 and C_2D_4-C_2D_4.

Our experiment utilizes a steady state molecular beam and one or two cw CO_2 lasers; the laser molecular beam geometry is perpendicular and the laser fluence used is about 4 Jm^{-2}. The determination of this fluence will be discussed in the next section. The use of a mechanical velocity selector and of a beam source with an adjustable temperature (100 - 300 K) belongs to our experimental possibilities. We have investigated C_2H_4 bound to Xe, Xe-Xe, C_2H_4 and SF_6.

Casassa et al arrive at the following conclusions:

- the C_2H_4 dimer transition frequency is 952.3 ± 0.5 cm^{-1};
- for clusters containing C_2H_4 the observed lineshapes are homogeneous;

- the observed transitions strengths are proportional to the number of ethylene constituents for clusters containing three or less ethylene constituents.

Hoffbauer et al conclude:

- the C_2H_4 dimer transition frequency is 952.8 ± 0.2 cm^{-1};
- in a dimer the vibrational excitation of the ground state shows a homogeneously broadened absorption;
- the observed transitions are not proportional to the number of ethylene constituents in the cluster;
- the dissociation products are scattered isotropically in the center of mass system. The average translation energy of the cluster fragments corresponds only to a small fraction (10 - 15%) of the available energy for dissociation.

There are three ab initio studies of the ethylene dimer in the ground state. By minimizing the binding energy as a function of the dimer structure the most stable geometry can be obtained. Van der Avoird et al [5] have deduced the most stable orientation of the ethylene ground state dimer by fitting an analytical atom-atom potential energy curve to the ab initio results. They found the staggered parallel structure to be the most stable one. Padma Malar et al [6] have used the perturbation theory for the exchange-Hamiltonian to calculate the dimer interaction energies. Their conclusion is that the equilibrium geometry of the ethylene ground-state dimer has a planar T-shaped structure. Suzuki et al [7] have computed the intermolecular potential of the ethylene dimer for nine orientations using the exchange perturbation theory, too. Their conclusion is that a slightly shifted parallel structure in one plane is the most stable one.

The relaxation channels of vibrationally excited Van der Waals molecules can also be studied. Ewing [8] has examined the results of Van der Avoird [5] and suggests a new approach to the calculation of vibrational predissociation of excited Van der Waals molecules. In this approach the curve crossing of the intermolecular potential is important for Van der Waals molecules bound by strongly anisotropic interactions. His conclusion is that the overall relaxation lifetime may fall in the picosecond time scale.

2. The experimental results

2.1. Experimental set-up

To measure the predissociation of clusters after vibrational excitation a molecular beam apparatus and two cw line-tunable CO_2 lasers of moderate power are used. The cluster concentration in the beam is varied by choice of the source conditions, i.e. the source pressure P_o, the source temperature T_o and the source nozzle diameter d_o. The molecular beam is detected by means of an efficient electron-bombardment ionizer, followed by a magnetic mass spectrometer. Each laser beam crosses the molecular beam at right angles. The first laser m is focused between nozzle and skimmer by a lens with a focal length of 100 mm. Its diameter in the interaction region has been roughly estimated to be 0.5 ± 0.2 mm. The second laser p is focused downstream a skimmer by a lens with a focal length of 3000 mm. At the point of intersection the molecular beam has a diameter of 3.2 ± 0.1 mm and the laserbeam p has a diameter of 7.2 ± 0.2 mm. The principal features of the apparatus and the CO_2 lasers have been outlined previously [9a].

2.2. Theoretical background

As nearly all the experiments deal with dimer absorption spectra, we shall confine ourselves to dimers in this chapter. After excitation the dimer fragments leave the collimated beam, due to the recoil upon dissociation. If there are no other fragmentation processes upon ionization in the mass spectrometer the dimer beam attenuation can be measured on the dimer ion-mass $C_3H_5^+$ [1b] and can be described by (see [9a], eq. 4.2)

$$\Delta I = I_o \left[1 - \exp(-r.t)\right] \tag{2.1}$$

where ΔI is the difference of the mass spectrometer signal with and without laser action, I_o the total number of dimers per second in the molecular beam, r the rate of excitation to a predissociative state and t the laser interaction time. Measuring ΔI as a function of the laser frequency ν reflects the absorption spectrum. In general the excitation probability r.t can be written as

$$r.t = \frac{2}{3} \frac{\mu_{01}^2}{h^2 \varepsilon_o} \frac{F}{c} \frac{\Gamma/2}{(\nu-\nu_o)^2 + (\Gamma/2)^2} \tag{2.2}$$

where μ_{01} is the transition moment of the C_2H_4 monomer; the factor 1/3 is due to the spatial averaging over all orientations of the dimer, h the Planck constant, ε_o the permittivity of vacuum, F the laser fluence, c the speed of light in vacuum, ν the laser frequency and Γ and ν_o the line width and the transition frequency at the centre of the presupposed homogeneous Lorentz line profile. The frequency dependent absorption cross section of the dimer is related to the excitation probability by the expression

$$\sigma(\nu) = (r.t).(h.\nu)/F \tag{2.3}$$

At resonance we find for the excitation probability

$$r_o t = r.t\Big|_{\nu=\nu_o} = \frac{2}{3} \frac{\mu_{01}^2}{h^2 \varepsilon_o} \frac{F}{c} \frac{2}{\Gamma}$$

The full width half maximum (fwhm) of the measured absorption profile γ follows from equation 2.1 and is given by

$$\gamma = \Gamma \left[\frac{r_o t}{\ln 2 - \ln\left[1+\exp(-r_o t)\right]} - 1\right]^{\frac{1}{2}} \tag{2.4}$$

For $r_o t << 1$ the attenuation ΔI is proportional to the fluence and the exponential in equation 2.1 can be replaced by the expansion up to the linear term, thus $\gamma \approx \Gamma$. For high fluences, $r_o t >> 1$, one has to take into account the possibility of "orientational hole burning" [9b]. We can distinguish two limiting cases, the first corresponds to an excitation of two oscillating dipole moments parallel to each other and to the dimer axis and the second to an excitation of two parallel oscillating dipole moments perpendicular to the dimer axis.

For the parallel case $[\rightarrow - \rightarrow]$ the orientational average $1-\exp(-r.t)$ in equation 2.1 becomes

$$1 - \frac{1}{\sqrt{2b}} \cdot \exp(-2b) \cdot \int_0^{\sqrt{2b}} \exp(u^2)du \qquad (2.5)$$

and for the perpendicular case $[\uparrow - \uparrow]$

$$1 - \frac{1}{\sqrt{b}} \cdot \exp(-b) \cdot \int_0^{\sqrt{b}} \exp(-u^2)du \qquad (2.6)$$

where $b = \frac{3}{4} r \cdot t$. For the parallel and the perpendicular case as well as for the general treatment (eqs. 2.1 and 2.2) the dependence of the undissociated dimer fraction on top of the absorption profile is shown in fig. 1a as a function of the fluence F. The connection between the measured line width γ and the undissociated dimer fraction on top of the absorption profile is shown in fig. 1b. For these calculations we used $\Gamma = 11\ cm^{-1}$ for the fwhm of the Lorentzian dimer absorption profile and $\mu_{01} = 0.188$ D for the transition moment [10].

Clearly visible is that in the parallel case $[\rightarrow - \rightarrow]$ the beam attenuation will reach its saturation value significantly slower than in the perpendicular $[\uparrow - \uparrow]$ or the general average case [0A] for increasing fluence.

For interpretation of the two laser experiment we must modify eq. 2.1. The first laser m modulates the dimer beam at a given frequency ν_m; the second laser p probes the dimer beam continuously as a function of the frequency ν_p. The modulation produced by laser m yields

$$\Delta I_m \sim I_o \left[1 - \exp(-r_m \cdot t_m)\right]$$

The attenuation of ΔI_m by the probe laser p yields

$$\Delta I_p \sim \Delta I_m \cdot \exp(-r_p \cdot t_p)$$

The quantity

$$(\Delta I_m - \Delta I_p)/\Delta I_m = 1 - \exp(-r_p \cdot t_p) \qquad (2.7)$$

leads to an expression (independent of I_o) which for small $r_p t_p$ - i.e. small F_p - is proportional to the excitation probability $r_p t_p$ of the cluster fraction selected by ν_m. In this case orientational hole burning can be neglected.

A velocity selector permits us to determine the parallel beam temperature $T_{//}$ and the average stream velocity <v> under experimental conditions. For the determination of the fluence we use

$$F = \frac{P}{2a \cdot \langle v \rangle} \cdot \mathrm{erf}(\sqrt{2} \cdot \frac{a}{w}) \qquad (2.8)$$

where P is the laser power at the point of beam intersection, a the diameter of the molecular beam and w the diameter of the gaussian laser beam (e^{-1} points). The energy balance gives an indication of the internal energy ΔE_{int} of the ethylene dimers after expansion for the pure C_2H_4 beam. The energy balance can be written as ([11], p. 39)

$$4kT_o + \int_0^{T_o} C_v(\mathrm{vib}) \cdot dT = \frac{3}{2}kT_{//} + kT_{\perp} + \frac{1}{2}m \cdot v_s^2 + \Delta E_{int} \qquad (2.9)$$

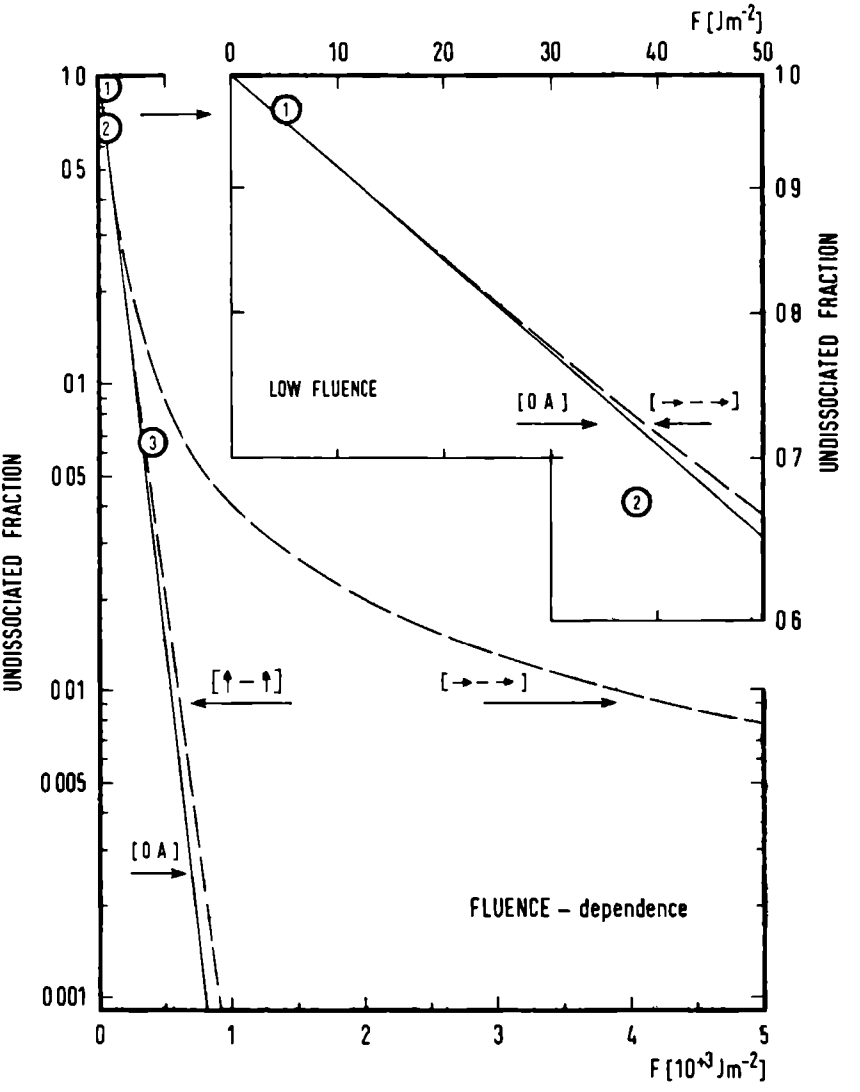

Fig. 1a: The undissociated dimer fraction at resonance as a function of the fluence F. The inset shows the low fluence behaviour. The experimental results (●) are compared to the theoretical curves calculated with $\Gamma = 11\ cm^{-1}$ *and* $\mu_{01} = 0.188\ D$. *The solid curve corresponds to the general treatment (OA) and the dashed curves to the parallel* $[\rightarrow - \rightarrow]$ *and perpendicular* $[\uparrow - \uparrow]$ *case. The numbers of the experimental results (●) are: 1 = this work, 2 = ref. 1b and 3 = ref. 2b.*

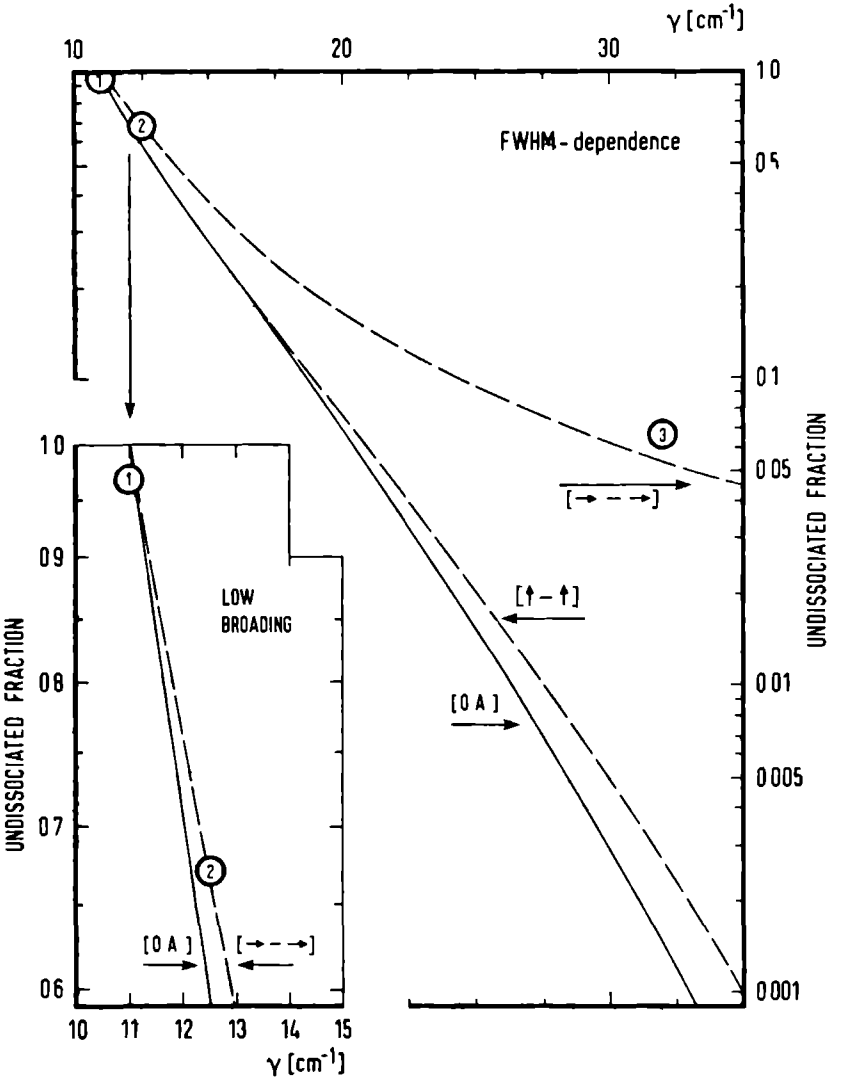

Fig. 1b: The undissociated dimer fraction at resonance as a function of the measured linewidth γ. Further details in the caption of fig. 1a.

Table 1

gas composition	P_o [torr]	T_o [K]	d_o [10^{-6}m]	mass	v_s [ms^{-1}]	$T_{//}$ [K]	<v> [ms^{-1}]	F [Jm^{-2}]	peak height %	figure
100% C_2H_4	1300	233	30	$C_2H_4^+$	716	24	730			
	1300	233	30	$C_3H_5^+$	707		714	5.0	3.2	2a
	1300	233	30	$C_3H_5^+$	707		714	2.9		2b
1% C_2H_4-	3000	169	30	$C_2H_4^+$	660	2.8	662			
9% Xe - He	3000	169	30	Xe^+	666	8.2	668			
	3000	169	30	C_2H_4-Xe^+	654		655	2.1	3.5	3a
	3000	169	30	$C_3H_5^+$	655		656			
	750	178	200	C_2H_4-$(Xe)_2^+$					9.5	3b
9.5% C_2H_4 - 0.5% SF_6 - He	1480	187	30	SF_5^+					3.8	4
2% C_2H_4- He	3000	169	30	$C_2H_4^+$	1213	5.3	1214			
	3000	169	30	$C_3H_5^+$	1202		1204	1.0	4.5	5

Compilation of results for pure C_2H_4 and C_2H_2-He, C_2H_4-Xe-He and C_2H_4-SF_6-He mixtures. The pressure P_o, the temperature T_o and the diameter d_o are the stagnation conditions of the source. The beam is detected at the mass-spectrometer setting given in the column "mass". The stream velocity v_s, the beam temperature $T_{//}$ and the average stream velocity <v> are derived from the velocity distribution. The fluence F is given at the point of beam intersection and the "peak height" is the attenuation taken at the maximum of the absorption profile. The last column refers to the figures, taken at the conditions mentioned.

where T_o is the source temperature, $C_v(vib)$ the vibrational specific heat, $T_{//}$ and $T_{\perp}$ the beam temperature parallel and perpendicular to the flow and m the molecular weight. Downstream the nozzle ($x/d_0 \simeq 10^4$) this formula can be simplified assuming that $T_{\perp} \simeq 0$ and $T_{rot} = T_{//}$

$$\Delta E_{int} = \frac{3}{2} kT_{//} + \int_0^{T_{vib}} C_v(vib)dT$$

and

$$\int_0^{T_{vib}} C_v(vib)dT = k\left[4T_0 - 3T_{//}\right] + \int_0^{T_o} C_v(vib)dT - \frac{1}{2} m v_s^2 \qquad (2.10)$$

2.3. The experimental spectra

The experimental conditions of our measurements - the stagnation pressure P_o, the source temperature T_o, the source diameter d_o, the setting of the mass spectrometer, the beam temperature $T_{//}$, the stream velocity v_s, the laser fluence F and the attenuation on top of the predissociation spectrum (peak height) - are summarized in table 1. Dimer spectra are measured on ion mass $C_3H_5^+$, the most intense daughter ion of $(C_2H_4)_2$ [1b].

We have investigated the dimer spectrum in a pure C_2H_4 expansion at $P_o = 1300$ torr and $T_o = 233$ K. First the spectrum is measured with the probe laser p, adjusted to 10 W; secondly we have scanned the same spectrum with laser m, also adjusted to 10 W. These spectra are shown in figure 2a. In both cases the spectra have been fitted with a Lorentzian line shape; this results in a maximum of the spectra at $\nu = 952.4 \pm 0.2$ cm^{-1} and a linewidth $\gamma_p = 10.9 \pm 0.8$ cm^{-1} and $\gamma_m = 13.6 \pm 0.4$ cm^{-1} for the spectrum measured with laser p and laser m, respectively.

In figure 2b the dissociation spectrum is displayed, obtained under the

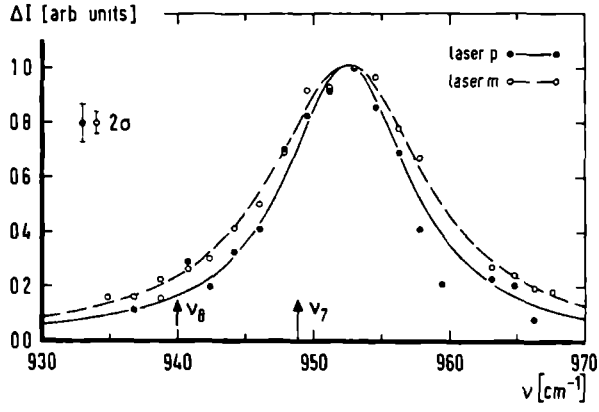

Fig. 2a: The predissociation spectrum of the ethylene dimer. The experimental conditions are summarized in table 1. The solid points (•) are measured at a low fluence with laser p and the open points (o) at high fluence with the modulation laser m. The i.r.-active ν_7 mode and the Raman active ν_8 mode are indicated by arrows as measured for the monomer. The solid and dashed curves are fits of the spectra with two Lorentzians centred at $\nu_p = \nu_m = 952.4$ cm^{-1} and with $\gamma_p = 10.9$ cm^{-1} and $\gamma_m = 13.1$ cm^{-1}.

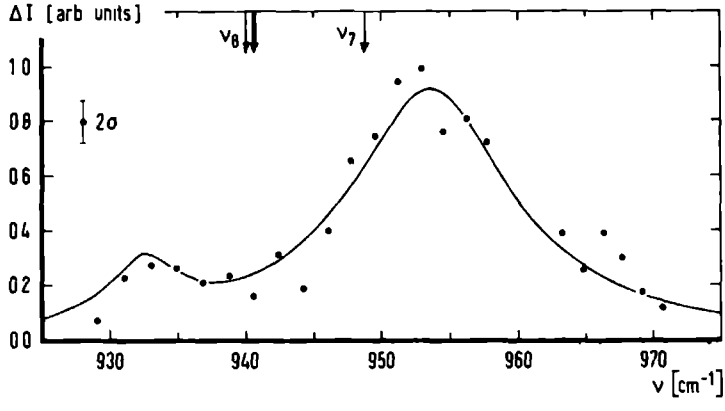

Fig. 2b: The predissociation spectrum of the ethylene dimer, obtained by two-laser-modulation technique. The experimental conditions are summarized in table 1. The heavy arrow indicates the frequency at which laser m modulates the $C_3H_5^+$ ion signal (10% modulation depth). Laser p scans in an on-off mode the full spectrum and produces a decrease in modulation depth which is displayed as ΔI. The dimer interaction incites the ν_8 mode to a partially i.r. active behaviour (Fermi resonance). Shown as a solid line is a fit of the spectrum invoking two Lorentzians centred at $\nu_{8'} = 932.5$ cm^{-1} and $\nu_{7'} = 953.5$ cm^{-1} with fwhm $\gamma_{8'} = 6$ cm^{-1} and $\gamma_{7'} = 15$ cm^{-1}.

same source conditions using laser m and laser p simultaneously. The dissociation spectrum changes from a Lorentzian shape into a structured one. The modulation laser m is fixed at 940.5 cm^{-1} and modulates the $C_3H_5^+$-ion signal about 10%. The probe laser is again adjusted at 10 Watt. The absorption spectrum has been fitted with two Lorentzian line shapes, one with a maximum at ν_r = 932.5 cm^{-1} and γ_r = 6 cm^{-1} and the second one at ν_b = 953.5 cm^{-1} with γ_b = 15 cm^{-1} (for the discussion see the next section).

In figure 3a and 3b the dissociation spectra of complexes consisting of ethylene and one or two Xe atoms are shown. The measurements are performed with a 1% C_2H_4 - 9% Xe - 90% He mixture. The spectra are measured with laser p. The source conditions for the dimer (C_2H_4-Xe) spectrum are different as compared to the conditions for the trimer (C_2H_4-Xe_2) spectrum (it was not possible to get a sufficient signal to noise ratio with the 30 μm nozzle, see table 1). In spite of the totally different source condition we get - in accordance with our expectation - the same Lorentzian line shape fits for the two spectra within one standard deviation. The average value for the maximum of the Lorentzian is ν = 948.3 ± 0.5 cm^{-1}.

In figure 4 the dissociation of the complex C_2H_4-SF_6 is shown. In this experiment the molecular beam is formed by expansion of an 0.5% SF_6-9.5% C_2H_4 - 90% He mixture at P_o = 1480 torr and T_o = 187 K. The measurement is performed with laser p; the mass spectrometer signal is taken on the ion mass SF_5^+. We would not observe a specific daughter ion of the C_2H_4-SF_6 dimers, e.g. SF_6-$C_2H_4^+$ or C_2H_4-SF_5^+. Due to fragmentation detection of C_2H_4-SF_6 is possible on ion mass SF_5^+ or $C_2H_4^+$. We have chosen the ion mass SF_5^+ because the signal to noise ratio was better; also, there are no $(SF_6)_n$ absorption lines near 943.7 cm^{-1}, where the maximum attenuation for C_2H_4-SF_6 occurs. The features on each side of this

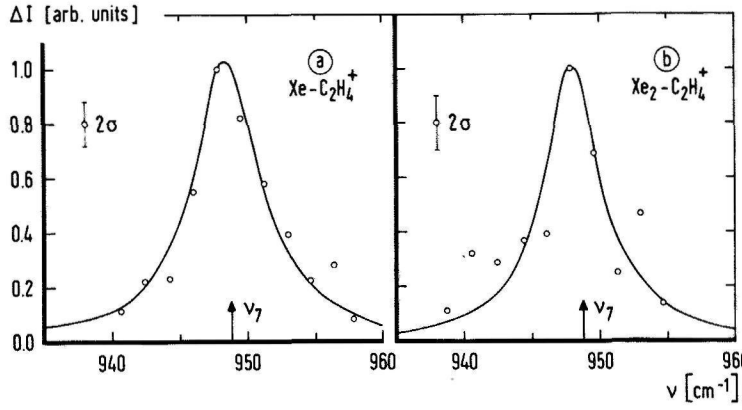

Fig. 3: The C_2H_4-$(Xe)_n$, $n \geq 1$ predissociation spectra measured at the ion masses $Xe\text{-}C_2H_4^+$ and $(Xe)_2\text{-}C_2H_4^+$. The experimental conditions are summarized in table 1. The arrow indicates the i.r. active ν_7 mode of the ethylene monomer. The solid lines are fits of the spectra with two Lorentzians. In case a the line centre is at $\nu_0 = 948.4\ cm^{-1}$ and $\gamma = 5.8\ cm^{-1}$; in case b $\nu = 948\ cm^{-1}$ and $\gamma = 5\ cm^{-1}$ (see table 2).

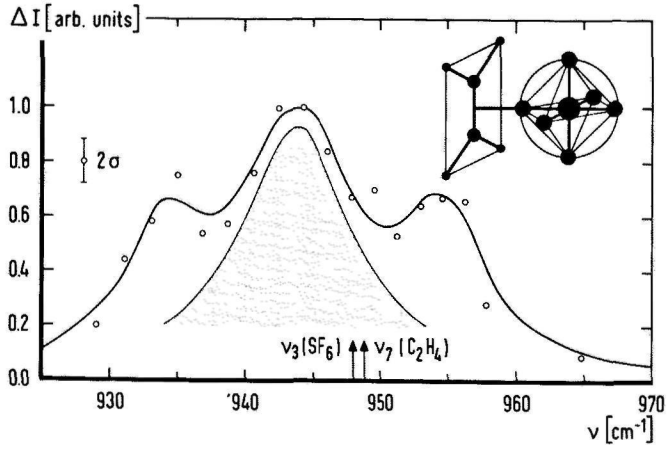

Fig. 4: The C_2H_4-SF_6 predissociation spectrum measured at the ion mass SF_5^+. The experimental consitions are summarized in table 1. The arrows indicate the i.r. active ν_7 mode of C_2H_4 and the i.r. active ν_3 mode of SF_6. The solid line is a fit of the spectra with three Lorentzians. The shaded area shows the Lorentzian with $\nu = 943.7\ cm^{-1}$ and $\Gamma = 10\ cm^{-1}$ (see table 2). The inset shows the configurations of the two molecules in the mixed dimer as suggested by the spectral data.

peak are attributed to SF_6-clusters, mainly due to $(SF_6)_2$. A fit shows that the shift of the SF_6-C_2H_4 complex is -4.3 ± 0.3 cm^{-1} with respect to the SF_6 monomer band origin; the linewidth amounts to $\gamma = 10.0 \pm 1.5$ cm^{-1}.

In figure 5 our narrowest infrared $(C_2H_4)_n$-dissociation spectrum (γ = 10.1 cm^{-1}) is shown. In this case the molecular beam is formed by expansion of a 2% C_2H_4 - 98% He mixture at P_o = 3000 torr and T_o = 169 K, conditions presumably leading to heavy clustering in the beam. The measurement is performed with laser p adjusted to only 6 Watt, corresponding to a fluence of 1 Jm^{-2}. At 953 cm^{-1} (near the maximum of the dissociation spectrum) the power dependence of the attenuation signal has been checked. In the range 0-8 Watt all the data points fall on a straight line; from its slope a transition strength is deduced, $|\mu_{01}|^2 = 0.345$ D^2, i.e. 10 times the monomer value. The dissociation spectrum is described with a Lorentzian line shape with the maximum at $\nu = 953.2$ cm^{-1} and a linewidth $\gamma = 10.1$ cm^{-1}.

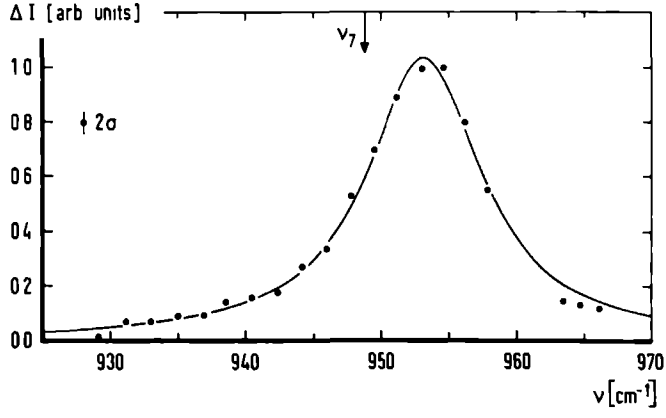

Fig. 5: The predissociation spectrum of ethylene clusters. The experimental conditions are summarized in table 1. The arrow indicates the i.r. active ν_7 mode of the ethylene monomer. The solid line is a fit of the spectrum with a Lorentzian with the line centre at $\nu = 953.1$ cm^{-1} and $\gamma = 10.1$ cm^{-1} (see table 2).

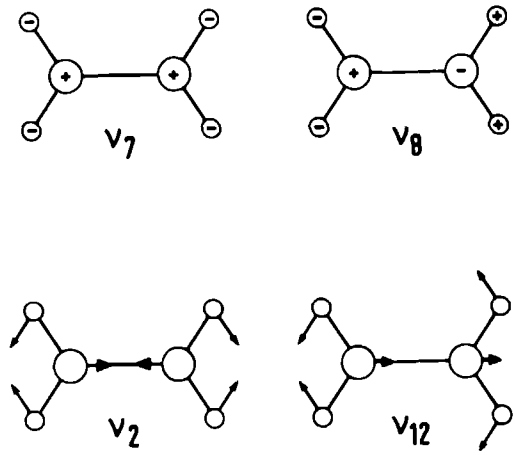

Fig. 6: Normal vibrations of a C_2X_4 molecule of point group V_h [21]. It is assumed that the mass X is smaller than of C. The ν_7 and ν_{12} modi are i.r. active; the ν_8 and ν_2 modi are Raman active. Note the correspondence between the ν_7-ν_8 modi and the ν_2-ν_{12} modi as concerns the left side of the molecules.

3. Discussion

The observed spectra of clusters containing C_2H_4 possess three important features; the shift, the linewidth and the transition moment. From these parameters we deduce properties of the ethylene dimers. We will restrict this discussion to geometrical properties of the C_2H_4 (C_2D_4) dimers and to Fermi resonances between the ν_7 and ν_8 out of plane (wagging) modi of C_2H_4 and the ν_2 and ν_{12} in plane (scissor) modi of C_2D_4 (figure 6 and table 2).

The absorption spectra of atoms and molecules fulfill the conditions of the Thomas-Reiche-Kuhn sum rule [12]; the contribution of all electric dipole transitions to the integrated absorption spectrum is proportional to the number of participating electrons and independent of other molecular parameters. In the case of clusters the vibrational transition strengths of the constituents in the cluster influence each other in a very limited absorption band [12]. Therefore, the integrated transition strength for such an absorption band should be the same, before and after dimer formation, i.e. the linear transition probability of a cluster is equal to the sum of the absorption transition probabilities of each constituent in the cluster. We will refer to this statement as to the sum rule.

Based upon this sum rule we conclude that the results for the transition moment of the ethylene dimer of each laboratory are afflicted with errors. Casassa *et al* [1b] have omitted directional effects altogether; as a result correction of the experimental transition moments is necessary. Their squared transition dipole moments have to be multiplied by a factor 3 in the approximation of equation 2.2, valid for low fluences. The adjusted transition strengths are shown in the fifth column of table 2.

Table 2

complex	ν_o [cm^{-1}]	γ [cm^{-1}]	$\langle\mu_{01}^2\rangle$ [$10^{-3}.D^2$]	$\langle\mu_{01}\rangle_c^2$ [$10^{-3}.D^2$]	reference/ figure
$(C_2H_4)_2$	952.4 ± 0.2	10.9 ± 0.8	53 ± 10		fig.2a
$(C_2H_4)_n$	953.1 ± 0.2	10.1 ± 0.4	345 + 25		fig.6
$(C_2H_4)_2$	952.8 ± 0.2	17.5	87.6 ± 10.9	55 ± 7	ref.2b
C_2H_4-C_2D_4	953.8 ± 0.3	13.8	44.1 ± 7.3	29 ± 5	ref.2b
C_2H_4-C_2D_4	1076.6 ± 0.1	3.5	3.7 ± 0.8	3.2±0.7	ref.2b
$(C_2D_4)_2$	1075.1 ± 0.1	5.0	2.4 ± 0.3	2.3±0.3	ref.2b
$(C_2H_4)_2$	952.3 ± 0.5	12.1 ± 1.5	32.0 ± 3.0	87 ± 8	ref.1b
$(C_2H_4)_3$	952.3 ± 0.5	10.6 ± 1.7	47.1 ± 3.6	128 ±10	ref.1b
$(C_2H_4)_5$	953.2 + 0.9	16.1 ± 2.8	33.4 ± 2.1	91 ± 8	ref.1b
$(C_2H_4)_7$	953.2 + 0.9	16.1 ± 2.8	33.4 ± 2.1	91 ± 8	ref.1b
C_2H_4-Ar	950.0 ± 0.5	9.0 ± 2.5	14.3 ± 1.8	39 ± 5	ref.1b
C_2H_4-Kr	949.1 ± 0.7	9.7 ± 3.2	13.1 ± 1.7	36 ± 5	ref.1b
C_2H_4-Xe	948.4 ± 0.2	5.8 ± 0.6	72 ± 5		fig.3
C_2H_4-$(Xe)_2$	948.0 ± 0.4	5.1 ± 1.0			fig.3
C_2H_4-C_2F_4	954.7 ± 0.2	6.0 ± 0.7	15.4 ± 2.1	42 ± 6	ref.1b
C_2H_4-SF_6	943.7 ± 0.3	10.0 ± 1.5			ref.4
C_2H_4 (ν_7)	948.8		35.3 ± 1.5		ref.10
C_2H_4 (ν_8)	940		0		ref.13,17
C_2D_4 (ν_{12})	1077.9		1.9 ± 0.2		ref.10
C_2D_4 (ν_2)	1514		0		ref.13
C_2F_4 (ν_{11})	1186.0		?		ref.18
SF_6 (ν_3)	948.0		150 ± 5		ref.19

Survey of the measurements on C_2H_4 clusters. The constituents of the cluster, the line centre ν_0, the linewidth γ and the transition moment $\langle\mu_{01}^2\rangle$ are obtained from the measured predissociation spectra. The corrected $\langle\mu_{01}^2\rangle_c$ is derived after analysis of the measurements (see text). The last column refers to the figures or references where the measurements can be found. In the lower part one finds the fundamental frequencies and transition moments of the constituents.

Our measurement of Γ yields the value of 10.9 ± 0.8 cm^{-1}; the value of Casassa et al is 12 ± 1.4 cm^{-1}. The average linewidth Γ is in consequence 11 ± 1 cm^{-1}. In figure 1a the dependence of the undissociated dimer fraction is shown as a function of the fluence F. In figure 1b the measured linewidth γ is shown as a function of the undissociated dimer fraction. In both figures the measurements of each laboratory are marked. Within the experimental errors the measurements [1b] are in agreement with the calculated curves, for $\Gamma = 11$ cm^{-1} and $\mu_{01}(C_2H_4\text{-}C_2H_4) = \sqrt{2} \cdot \mu_{01}(C_2H_4)$, according to the sum rule.

Hoffbauer et al [2b] have reported too large a value for the linewidth, $\Gamma = 17.5$ cm^{-1}. The squared transition dipole moment is proportional to the linewidth Γ and we therefore conclude that their value for the transition moment of $(C_2H_4)_2$ is too high. We have multiplied their value of Γ by a factor 0.63 to be consistent with the proper linewidth of 11 cm^{-1}. The adjusted transition strength is shown in the fifth column of table 2.

In figure 1a and 1b, the experimental findings of Hoffbauer et al are confronted with a calculation based on the sum rule value for the transition moment and on $\Gamma = 11$ cm^{-1}. Moreover, the orientational averaging effects have been taken into account producing large effects for the high fluence used. The near coincidence of the experimental value 3 with the upper curve [→ - →] in figure 1b suggests that the two molecular planes of each C_2H_4 constituent are nearly perpendicular to the dimer axis. In this way one is able to understand finally the very large linewidth (17.5 cm^{-1}) reported.

Our measurement of the transition strength of $(C_2H_4)_2$ is not very accurate; we have not checked the fluence dependence of the dissociated dimer fraction over an extended range. From figure 1a it is clear, however, that these

measurements are in agreement with theoretical expectation.
For the seeded beam we have measured the dissociation spectrum under heavy clustering conditions (see figure 5). The transition strength derived from this measurement is 0.345 D^2. From the sum rule we conclude that the average number of constituents is about 10 in this case.

The observed ethylene cluster transitions are slightly shifted with respect to the band origin of the ν_7 mode of the monomer. A qualitative explanation of this feature can be derived from a Fermi resonance. If one of the molecules in an ethylene dimer is excited in the ν_7 mode - symmetrical out of plane wagging mode, i.r. active, 948.8 cm^{-1} - a coupling occurs with the ν_8 mode - asymmetrical out of plane wagging mode, Raman active, 940 cm^{-1} - due to the presence of the other dimer constituents (see figure 6 and table 2). The resonance will lead to a blue shift (4 cm^{-1} observed). Mixing the ν_8 and ν_7 modes leads to preferential hindrance of the wagging motion of one CH_2-end of the ethylene molecule. Possibly, the inactive ν_{10} mode (ν_{10} = 825.9 cm^{-1} [13]) can also play a role in this Fermi resonance shift.

Neglecting effects of Fermi resonances the absorption frequencies of the dimer are determined by two causes; the vibration mode of each oscillator and the intermolecular Van der Waals coupling. In order to separate these factors, we introduce a hypothetical model of a dimer with two separate oscillators where coupling is absent. In the first instance the ground state wave function of a dimer is a product of the wave functions of the two separate oscillators ψ_1, repsectively ψ_2.
The i.r. excited wave functions of the actual dimer ($\psi_+^\dagger$ and $\psi_-^\dagger$) and of the uncoupled dimer ($\psi_1^\dagger$ and $\psi_2^\dagger$) are connected by

$$\psi_+^\dagger = a\psi_1^\dagger\psi_2 + b\psi_1\psi_2^\dagger \tag{3.2a}$$

$$\psi_-^\dagger = b\psi_1^\dagger\psi_2 - a\psi_1\psi_2^\dagger \tag{3.2b}$$

The frequencies of the actual dimer ω^+ and ω^- can be obtained from the uncoupled frequencies ω_1 and ω_2 by

$$\omega^\pm = \frac{1}{2}\left[\omega_1 + \omega_2 \pm \kappa\right] \tag{3.3}$$

with

$$a = \frac{1}{\sqrt{2}}\left(1 + \frac{\Delta}{\kappa}\right)^{\frac{1}{2}},\quad b = \frac{1}{\sqrt{2}}\left(1 - \frac{\Delta}{\kappa}\right)^{\frac{1}{2}}$$

$$\kappa = (\Delta^2 + 4V^2)^{\frac{1}{2}} \text{ and } \Delta = \omega_1 - \omega_2$$

Here $V = -\langle\psi_1\cdot\psi_2^\dagger|H|\psi_1^\dagger\cdot\psi_2\rangle$ is a matrix element of interaction which determines the coupling of the two molecules in the dimer.

The transition strength of the dimer can be expressed by the parameters mentioned above

$$S_+ = |\langle\psi_1\psi_2|\vec{\mu}|\psi_\pm^\dagger\rangle|^2 \tag{3.4}$$

where $\vec{\mu}$ is the vector operator of the transition dipole moment of the dimer, $\vec{\mu} = \vec{\mu}_1 + \vec{\mu}_2$.

In the case of S_+ we can write

$$S_+ = a^2|\mu_1|^2 + b^2|\mu_2|^2 + 2ab|\mu_1|\cdot|\mu_2|\cos\alpha$$

where $|\mu_1|^2$ and $|\mu_2|^2$ are the transition strengths and α ($\leq 90^\circ$) the angle between the directions of the transitions dipole moments of the separate molecules in the dimer. In particular for the resonant case ($\omega_1 = \omega_2$, $|\mu_1|^2 = |\mu_2|^2$)

$$a = b = \frac{1}{\sqrt{2}} \quad \text{and} \quad S_\pm = |\mu_1|^2(1 \pm \cos\alpha)$$

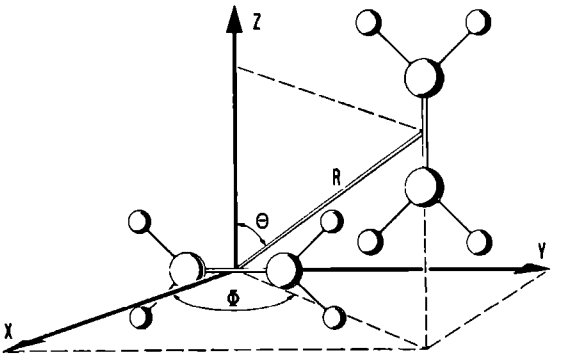

Fig. 7: Configuration of the ethylene dimer proceeding from analysis of different investigations. We proposed parallel C_2H_4 planes ($\alpha = 0$) and perpendicular C=C axis ($\alpha' = 90^o$). The remaining degrees of freedom are indicated by the polar coordinates R, Θ and Φ. The possible values for these coordinates are displayed in table 3. The most compatible with all evidence are $R = 4.2$ Å and $\Theta = \Phi \approx 45^o$. The angle β (see text) is defined as $\beta = \sphericalangle(\hat{X},\hat{R})$

For $(C_2H_4)_2$ only one dissociation peak is observed; we propose $S_- = 0$ and $S_+ \approx 2|\mu_1|^2$ (table 2). This assumption leads to $\alpha \approx 0$; the transition moments for the ν_7 mode in the C_2H_4 dimer are nearly parallel to each other and to the dimer axis $[\rightarrow - \rightarrow]$. Our geometry proposal rests upon three arguments. First, one line is observed. Second, the line intensity agrees with the sum rule. The third argument rules out the possibility of $\cos\alpha = 0$, i.e. two coinciding transitions of equal strength; the third argument is that the line broadening parameter γ for high fluences agrees only with $\alpha = 0$, see fig. 1b.

For this geometry, $[\rightarrow - \rightarrow]$, $\alpha = 0$, resonant dipole-dipole interaction would yield a red shift of about 4.8 cm^{-1} assuming a fixed intermolecular distance of 4.2 Å [16]. This shift depends strongly on the angle β between the dimer axis and the normal to the molecular planes of the C_2H_4 molecules (see fig. 7). For $\beta = 55^\circ$, this shift changes sign, for β about 50° it becomes 1.0 cm^{-1}. In our opinion the actual geometry of $(C_2H_4)_2$ does not lead to a strong effect from dipole-dipole interaction, because the mixed dimers like C_2H_4-Ar [16] yield an absorption peak at about the same frequency of 952 cm^{-1}. Moreover, the ν_7-ν_8Fermi resonance requires an angle $\beta \neq 0$ for symmetry reasons. The internal energy content of dimers in the molecular beam and the floppiness of the Van der Waals bond (see below) yield extra arguments to attenuate the influence of the dipole-dipole interaction.

For $(C_2D_4)_2$ a single dissociation peak is measured too [2b]. In table 2 the experimental value of the transition strength can be found, $S_+ \approx |\mu_1|^2$; it indicates that the transition moments for the ν_{12} mode in the C_2D_4 dimer must be nearly perpendicular with respect to each other, i.e. $\alpha' \approx 90^\circ$.

According to the sum rule there should be another absorption peak not measured so far. It could be, though it seems improbable, that this missing peak

lies outside the spectral range accessible to the CO_2 laser; it could also be that the missing peak is too narrow and falls between the probing grid of the CO_2 laser lines; finally it could be that this peak is too broad and therefore escapes observation.

The red shift of the ν_{12} dimer absorption peak (2.8 cm^{-1}, see table 2) may be due to a Fermi resonance in the C_2D_4 molecule switched on by the presence of the other constituent. There are two nearby vibrational frequencies, ν_2 = 1514 cm^{-1} and ν_3 = 984.6 cm^{-1}, both of A_g symmetry, which should be considered for such a mixing process with ν_{12} = 1077.9 cm^{-1}, B_{3u} symmetry. From a purely energetic point of view, the ν_3 mode would seem to be of dominating influence, yielding a blue shift. From the geometry of atomic motion, on the other hand, if the symmetric scissor-motion of the two CD_2 groups for the ν_{12} mode is mixed with the asymmetric scissor motion of the ν_2 mode (see fig. 6), the scissor motion of one end of the C_2D_4 molecule will preferentially be impeded by the other dimer constituent. This seems to occur in $(C_2D_4)_2$ causing the measured red shift. Dipole-dipole resonance forces are not expected to play an important role for C_2D_4 due to the small transition moment for the ν_{12} mode μ_{01} = 0.045 D.

For the sake of completeness and following the preceding procedure the measured transition moments for C_2H_4-C_2D_4 [2b] yield a = 0.18 ± 0.05 and b = 0.98 ± 0.01; i.e. the eigenfunctions of the two molecules C_2H_4 and C_2D_4 are slightly mixed. With these coefficients, however, the observed shifts for C_2H_4-C_2D_4 cannot be explained quantitatively.

The predissociation measurement for C_2H_4-C_2H_4 with two lasers (fig. 2b) shows two absorption peaks, ν_r = 932.5 cm^{-1} and ν_b = 953.5 cm^{-1}. The blue peak (ν_b) almost coincides with the one observed in a single laser experiment. The absorption spectrum demonstrates that the Lorentzian line shape, normally

found with one laser, conceals inhomogeneous structure. This feature can be brought into evidence by a suitable selection of molecules which preferentially contribute to the absorption in the wings of the absorption spectrum.

For the interpretation of the smaller peak at 932.5 cm^{-1} one is tempted to resort to the ν_8 mode (Raman active), which, as discussed above, is red shifted and becomes slightly infrared active by the ν_7-ν_8 Fermi resonance (effected by the presence of the other dimer constituent). The nearly symmetric shifts for the ν_7 mode (948.8 cm^{-1} → 953.5 cm^{-1}) and the ν_8 mode (~ 940 cm^{-1} → 932.5 cm^{-1}) are very suggestive. However, one runs into difficulties considering intensities. The expected intensity ratio $I(\nu_b):I(\nu_r)$ = 4:1 is observed only for the fraction selected by laser m (fig. 2b) and not for the total of dimers present (fig. 2a). The calculated ratios follow from the amplitudes a and b describing shifts and intensities. Whether admixture of the ν_{10} mode and/or the intermolecular interaction neglected so far are responsible for this discrepancy, is unclear at this moment.

The ground state intermolecular potential of the ethylene dimer has been studied theoretically [5,6 and 7]. From the potential surface of van der Avoird et al [5], with the dimer in a staggered geometry, but perpendicular C = C axis ($\alpha' = 90^o$) we calculate an interaction energy E = 4.03 $kJmol^{-1}$ at R = 4.3 Å (see table 3 and fig. 7). This value is about 100 K or 25 % above the minimum value of van der Avoird et al for a staggered geometry with parallel C=C axes ($\alpha' = 0$). In our opinion this difference corresponds to the uncertainty of the theoretical model which we consider to be of the same order as the differences between the various theoretical calculations [5,6,7].

With the experimental conditions of the dimer measurement of fig. 2a and 2b the energy balance yields (eq. 2.10)

Table 3 Stable C_2H_4 dimer structures

investigation	method	E [cm^{-1}] [a]	R [nm]	Θ [b]	Φ [b]	α' [c]	reference
theoretical	ab initio	-420	0.39	49°	27°	0	5
	ab initio	-147	0.42	0	0	90°	6
	ab initio	-323	0.40	45°	0	0	7
experimental	crystal [e]	-325	0.41	61°	13°	0	5
	viscosity	-135	0.42	-	-	-	20
	viscosity	-133	0.42	-	-	-	16
		-345	0.42	46°	45°	90°	this work [d]

a) 1 cm^{-1} = 1.2·10^{-2} kJmol^{-1} = 1.439 K

b) see figure 7

c) the angle between the directions of the C=C axes of the separate molecules in the dimer

d) the last row corresponds to our experimental analysis, α' = 90°. For this α'-value we have calculated those parameters R, Θ and Φ for which the energy assumes a minimum value E, within the model of ref. 5.

e) 1st neighbour pair

$$\int_0^{T_{vib}} C_v(vib)\, dT = 47 \pm 15 \text{ cm}^{-1}$$

The vibrational temperature of the dimer is thus 200 K $\leq T_{vib} \leq$ 233 K. The small differences for various geometries and this high vibrational temperature indicate that in the molecular beam dimers may be very floppy and not just frozen into a single geometry of minimum energy.

The predissociation spectra of Xe-C_2H_4 and C_2H_4-Xe_2 show one single peak at 948.2 ± 0.4 cm^{-1}. For Ar-C_2H_4 and Kr-C_2H_4 Casassa et al [1b] have observed a maximum at 950.0 cm^{-1} and 949.1 cm^{-1} respectively, just above the ν_7 mode frequency of C_2H_4. As a function of the mass of the rare gas atoms the frequencies of the predissociation spectra fall on a straight line. Spectra of matrices with a C_2H_4/Xe ratio of 1/24 at T = 15 K show a very strong absorption peak at 947 cm^{-1} [14]. The width γ of our C_2H_4-Xe spectrum is 5.8 ± 0.6 cm^{-1}, considerably smaller than for Ar-C_2H_4 (γ = 9 cm^{-1}) and Kr-C_2H_4 (γ = 10 cm^{-1}) [1b].

The predissociation spectrum of the C_2H_4-SF_6 complex (fig. 5) shows a red shift to ν = 943.7 cm^{-1}. The measured linewidth is about 10 cm^{-1}. The shift of the absorption peak can be understood by resonant dipole-dipole interactions [9a]. The interaction energy for two parallel oscillating dipoles is given by

$$V_{AB} = -\frac{1}{4\pi\varepsilon_o} \cdot \mu_{01}(A) \cdot \mu_{01}(B) \cdot \langle R_{AB}^{-3} \rangle \qquad (3.5)$$

Where A = SF_6, B = C_2H_4, $\mu_{01}(A)$ = 0.387 D, $\mu_{01}(B)$ = 0.188 D and R_{AB} the separation between the centre of mass of each molecule. With the combination rule for $R_m(A)$ = 5.13 Å [15] and $R_m(B)$ = 4.22 Å [16] one has $R_m(AB)$ = 4.7 Å. From $\langle R_{AB}^{-3} \rangle \approx [R_m(AB)]^{-3}$ the interaction energy becomes V_{AB} = -3.9 cm^{-1} and the perturbed energy of the C_2H_4-SF_6 complex becomes 943.5 cm^{-1} in good agreement with our result.

The C_2H_4-SF_6 dimer could also be excited with the oscillating dipole moment of the SF_6 constituent perpendicular to the dimer axis. There is no clear evidence for this oscillation in fig. 5; possibly the linewidth for this transition is too small or too large to observe it with the coarse probing CO_2 laser.

The numerical fit (fig. 5) produces also two lines, centered at 935 cm^{-1} and 956 cm^{-1} with a line width of about 6.7 cm^{-1}. These line centres coincide with our results for pure SF_6 dimers [9a]. Apparently and not unexpectedly $(SF_6)_2$ and $(SF_6)_2$-Ar_n are also present in the molecular beam.

Acknowledgement

This work is part of the research program of the "Stichting Fundamenteel Onderzoek der Materie" (F.O.M.) and has been made possible by financial support of the "Nederlandse Stichting voor Zuiver Wetenschappelijk Onderzoek" (Z.W.O.).

We wish to thank A. van der Avoird for his advice and for performing some calculations, and C. Sikkens and J. Holtkamp for their assistance. Our thanks are also due to H. Sigg for permitting us to use his CO_2 laser.

References

[1a] M. Casassa, D. Bomse, J. Beauchamp and K. Janda
J. Chem. Phys. 72 (1980) 6805

[1b] M. Casassa, D. Bomse and K. Janda
J. Chem. Phys. 74 (1981) 5044

[1c] M. Casassa, F. Celii and K. Janda
J. Chem. Phys. 76 (1982) 5295

[2a] M. Hoffbauer, W. Gentry, and C. Giese in 'Laser Induced Processes in Molecules', eds. K. Kompa and S. Smit, Springer Series in Chem. Phys. 6, Springer Verlag, Heidelberg, 1978.

[2b] M. Hoffbauer, K. Liu, C. Giese and W. Gentry
J. Chem. Phys. 78 (1983) 5567

[3] H. Godfried and I.F. Silvera
Phys. Rev. A27 (1983) 3008 and 3019

[4] P. Melion, J. Zellweger, R. Monot and H. van den Bergh
1983, in press

[5a] T. Wasiutyuski, A. van der Avoird and R. Berns
J. Chem. Phys. 69 (1978) 5288

[5b] A. van der Avoird, P. Wormer, F. Mulder and R. Berns
in 'Topics in Current Chemistry', 93 (1980) 1

[6] E. Padma Malar and A. Chandra
J. Phys. Chem. 85 (1981) 2190

[7] K. Suzuki and Iguchi
J. Chem. Phys. 77 (1982) 4594

[8a] G. Ewing
Chem. Phys. 63 (1981) 411

[8b] G. Ewing
Faraday Disc. Chem. Soc. 73 (1982) 325

[9a] J. Geraedts, S. Stolte and J. Reuss
Z. Phys. A 304 (1982) 167

[9b] J. Geraedts, M. Waayer, S. Stolte and J. Reuss
Faraday Disc. Chem. Soc. 73 (1982) 375

[9c] J. Geraedts, S. Stolte and J. Reuss
Chem. Phys. Lett. 97 (1983) 152

[10] T. Nakagena, S. Kondo and S. Saëki
J. Chem. Phys. 70 (1979) 2471

[11] J.B. Anderson, in 'Gas Dynamics' Vol. 4, ed. P. Wegner, Dekker, New York, 1974

[12] R. Loudon, in 'The Quantum Theory of Light', p. 69, Clarendon Press, Oxford, 1973
The here proposed modification of the Thomas-Reiche-Kuhn sum rule neglects small effects. The Van der Waals interaction causes one of these effects, by changing forbidden transitions into slightly allowed ones.

[13] J. Duncan and E. Hamilton
J. Mol. Struct. 76 (1981) 65

[14] E. Rytter and D. Gruen
Spectrochim. Acta 35A (1979) 199

[15] R.C. Reid and T.K. Sherwood, 'The properties of gases and liquids', McGraw-Hill, New York, 1966

[16] T. Spurling and E. Mason
J. Chem. Phys. 46 (1967) 322

[17] W. Knippers and G. Luijks
private communication

[18] D. Mann, N. Acquista and E. Plyer
J. Res. Natl. Bur. Stand. 51 (1953) 69

[19] D. Dunn, K. Scanlon and J. Overend
Spectroschim. Acta 38A (1982) 841

[20] R. Orcutt
J. Chem. Phys. 39 (1963) 605

[21] G. Herzberg, 'Infrared and Raman Spectra of Polyatomic Molecules', Van Nostrand, Princeton, 1945

CHEMICAL PHYSICS LETTERS

Volume 97, number 2

13 May 1983

IR DIMER SPECTROSCOPY AND FERMI RESONANCE

J GERAEDTS, S STOLTE and J REUSS

Fysisch Laboratorium Katholieke Universiteit Toernooiveld 6525 ED Nijmegen The Netherlands

Received 3 March 1983

A careful discussion of Fermi resonances is shown to explain qualitatively the many observed line shifts from molecular beam infrared predissociation experiments

1 Introduction

IR dimer spectroscopy has shown a rapid development in recent years, due to the relative simplicity of detection of pre dissociation in molecular beam experiments [1–10] One of the easily obtainable parameters in these experiments is the observed line shift of the excited fundamental mode or overtone or combination band, with respect to the line position of monomers in the gas phase Except for the linewidth, this parameter often is the only one extracted from pre dissociation measurements, namely if the dimer spectra show no clear structure at all, as occurs in the majority of cases A notable exception to this is formed by $(SF_6)_2$ [5–7], where resonant dipole–dipole forces produce two narrow lines $\approx 20\ cm^{-1}$ apart But here again, SF_6–rare-gas clusters show a structureless single line, which however is clearly red shifted [7,8]

So far the observed line shifts are as often to the red as to the blue An understanding has to start with at least a qualitative explanation of these features It is our aim to relate the observed line shifts to Fermi resonances These resonances can be perturbed and their effects diminished by the presence of the other dimer constituent, in case they are already present in the free molecule, e g in N_2O–N_2O (N_2O ν_3 = 2223 5 cm $^{-1}$ and $2\nu_2 + \nu_1 = 2461\ 5\ cm^{-1}$, both with the same symmetry), see ref [1] On the other hand such near coincidences between excited states of different symmetry can also become effective and cause Fermi resonance shifts as a consequence of a coupling (absent in the free molecule) due to the presence of the other dimer constituent

In all cases, this simple concept leads to agreement with observation, as will be shown in section 2

2 Discussion

In table 1 many dimer line shifts found so far by molecular beam pre dissociation measurements are collected, together with the frequency of the unshifted line position and its symmetry type One or more neighbouring lines are displayed too, with their symmetry type indicated

In the case of C_2H_4 the situation is badly defined, the neighbouring frequency $\nu_8(b_{2g})$ is known only very inaccurately [11] and the observed shifts appear to be very small except for $(C_2H_4)_2$, where a blue-shift of $+3\ cm^{-1}$ is found, probably enhanced by dipole–dipole interaction Our conclusion – with some caution – is that ν_8 lies below ν_7 causing a blue shift due to symmetry breaking by the presence of the other dimer constituent

C_2H_4–C_2F_4 dimers show a relatively strong blue-shift of $+5\ cm^{-1}$ [12] Here the Fermi resonance is active in a heteromolecular dimer, where in both constituents one has excited states of roughly the same energy In C_2F_4, at $914\ cm^{-1}$ there is the combination tone $\nu_7 + \nu_8$ (B_{3u}) of medium infrared activity [13] Infrared activity means the presence of a transition dipole moment guaranteeing an intermolecular Fermi resonance coupling through dipole–dipole

Table 1
Line shifts in dimers

System	Unshifted position (cm^{-1})	Shift (cm^{-1})	Neighbouring lines (cm^{-1})	Ref
$C_4H_4(\nu_7)-C_2H_4$	949 2 (b_{1u})	+3	ν_8 = 943–950 (b_{2g})	[2,3]
$C_2H_4(\nu_7)$- Ar	949 2	+1 2	ν_8	[3]
$C_2H_4(\nu_7)$-Kr, Xe	949 2	0	ν_8	[3,12]
$C_2H_4(\nu_7)-C_2F_4$	949 2	+5	ν_8 and $\nu_7 + \nu_8(C_2F_4)$ = 914 (B_{3u})	[3]
SI $_6(\nu_3)$–Ar	948 (f_{1u})	3	$\nu_5 + \nu_6$ = 885 (I_{1u}), $2\nu_5$ = 1048 (A_{1g}, E_g, Γ_{2g})	[5,8]
SI $_6(\nu_3)$ C_2H_4	948	5	$\nu_5 + \nu_6$ and $\nu_7(C_2H_4)$ = 949 2 (b_{1u})	[12]
$BCl_3(\nu_3)$–Ar	954 2 (e')	0	$2\nu_1$ = 942 (A_1'), $2\nu_4 + \nu_2$ = 941 ($A_2'' + E''$), $2\nu_4 + \nu_1$ = 957 ($E' + A_1'$)	[10]
$OCS(2\nu_2)$–OCS	1047 04 (Σ^+)	–2 3	ν_1 = 859 (Σ^+)	
$OCS(2\nu_2)$–Ar	1047 04	I	ν_1	[9]
$N_2O(\nu_3)-N_2O$	2223 5 (Σ^+)	+10	$2\nu_2 + \nu_1$ = 2461 (Σ^+)	[1]
$CO_2(\nu_1 + \nu_3)-CO_2$	3716 (Σ_g^+)	–1	$2\nu_2 + \nu_3$ = 3609 (Σ_g^+)	[4]

forces. Other C_2F_4 combination frequencies ($\nu_7 + \nu_{12}$ at 964 cm^{-1}, $\nu_2 + \nu_{10}$ at 996 cm^{-1}, $\nu_3 + \nu_{12}$ at 952 cm^{-1} or $\nu_2 + \nu_4$ at 968 cm^{-1}) are either infrared inactive or show too weak an activity to contribute significantly to the observed shift of +5 cm^{-1}

For SF_6, the ν_3 fundamental has F_{1u} symmetry, neighbouring excitations are $\nu_5 + \nu_6$ = 885 cm^{-1} (F_{1u}) and $2\nu_5$ at 1048 cm^{-1} ($A_{1g} + E_g + F_{2g}$). Again, due to symmetry breaking as a consequence of the presence of the other dimer constituent Ar, the coupling changes with these neighbouring states, both pushing the transition to the red

For SF_6 –C_2H_4 one has again a Fermi-resonance effect between two heteromolecular constituents with an energy difference for two neighbouring states of only ≈1 cm^{-1} Both excitations are strongly infrared active, with a total transition strength of $SF_6(\nu_3)$ about 10 times larger than the one of $C_2H_4(\nu_7)$. In this case one cannot only qualitatively explain the shift of –5 cm^{-1} The known transition dipole moments and intermolecular distance ($\mu_{01}(\nu_3)$ = 0.39 D, $\mu_{01}(\nu_7)$ = 0.19 D, R_{12} = 5 2 Å) allows one to calculate quantitatively the shift through dipole–dipole forces, assuming parallel oscillating dipole moments in both constituents

The system $BCl_3(\nu_3)$–Ar has been found to possess a strong blue-shift of +9 cm^{-1} [10]. Again the explanation is straightforward. The highest mode frequency occurring is ν_3 = 954 2 cm^{-1} (e'), two overtones and one combination tone of different symmetry are near and below that frequency, $2\nu_1$ = 942 cm^{-1} (A_1') and $2\nu_4 + \nu_2$ = 940 cm^{-1} ($A_2'' + E''$) The Ar atom breaks the D_{3h} symmetry and couples the different excited states, producing a blue-shift. In addition however, there is the combination tone $2\nu_4 + \nu_1$ = 957 cm^{-1} ($E' + A_1'$) which is very close and may produce a red-shift (A_1') or a blue-shift (E'). Apparently, all effects compensate each other

The next systems to be discussed are OCS–OCS, Ar with a red-shift of –2 3 and –1 cm^{-1} has been observed, respectively [9] for the $2\nu_2$ overtone at 1047.04, which for the free molecule shows strong Fermi-resonance effects due to the coupling to the fundamental ν_1 = 859 cm^{-1}, both having the same symmetry (Σ^+) By the presence of the dimer partner this symmetry is perturbed and the strong coupling is diminished (producing the red-shift).

For the ν_3 excitation of $(N_2O)_2$ a blue-shift of +10 cm^{-1} has been observed [1] The free molecules show strong interaction between the three Σ^+ states ν_3 = 2223.5 cm^{-1}, $\nu_1 + 2\nu_2$ = 2461.5 cm^{-1} and $2\nu_1$ = 2563.5 cm^{-1} Perturbation of the symmetry due to the other dimer constituent thus produces a strong blue-shift. The dimer transition at 2246 cm^{-1} with its smaller intensity seems to originate from a second non-equivalent molecular vibration, e.g. of a T-shaped

dimer (both molecules can vibrate and are subject to different symmetry breaking)

The last system in table 1, CO_2–CO_2, shows a red-shift of -1 cm^{-1}, for the combination tone $\nu_1 + \nu_3 =$ 3716 cm^{-1}, which for the free molecule is in (Fermi) resonance with the combination tone $2\nu_2 + \nu_3 =$ 3609 cm^{-1}, both having Σ_u^+ symmetry in the upper state Again this resonance effect is diminished by the presence of the dimer partner, leading to a red-shift

One may ask what happens if in the free molecules no (near) coincidences of energy levels are present to be perturbed by the presence of the other dimer constituent, i e what sign of the shift has to be expected, e g for an atom–diatom dimer The answer is a red-shift, as in this case both levels (before and after excitation) interact with nearby levels of the van der Waals stretch type, which are coupled to the molecular vibration of the diatom and produce, in general, a slight red-shift for those states with no van der Waals stretch excited However, the coupling is a little larger for the upper state where the molecular constituent is vibrationally excited, thus leading to an overall red-shift of the energy difference between both states, e g H_2–Ar [14]

References

[1] T E Gough, R F Miller and G Scoles, Chem Phys 69 (1978) 1588

[2] M A Hoffbauer, K Liu, C F Giese and R Gentry, J Chem Phys , to be published

[3] M P Casassa, D S Bomse, J L Beauchamp and K C Janda, J Chem Phys 72 (1980) 6805, M P Casassa, D S Bomse and K C Janda, J Chem Phys 74 (1981) 5044

[4] T E Gough, R F Miller and G Scoles, J Phys Chem 85 (1981) 4041

[5] J Geraedts, S Setiadi, S Stolte and J Reuss, Chem Phys Letters 78 (1981) 277

[6] J Geraedts, S Stolte and J Reuss, Z Physik A304 (1982) 167

[7] J Geraedts, M Waayer, S Stolte and J Reuss, Faraday Discussions Chem Soc 73 (1982) 375, J Geraedts, Faraday Discussions Chem Soc 73 (1982) 416

[8] T E Gough, D G Knight and G Scoles, Internal Report CP-208, University of Waterloo (Canada), to be published

[9] M A Hoffbauer, K Liu, C F Giese and W R Gentry, Preprint, University of Minnesota

[10] M P Casassa, D S Bomse and K C Janda J Phys Chem 85 (1981) 2623

[11] B P Stoicheff, J Chem Phys 21 (1953) 755

[12] J Geraedts, unpublished results

[13] G Herzberg, Infrared and Raman spectra of polyatomic molecules (Van Nostrand, Princeton, 1945)

[14] A R W McKellar, Faraday Discussions Chem Soc 73 (1982) 89

A1. The SF_6 molecule

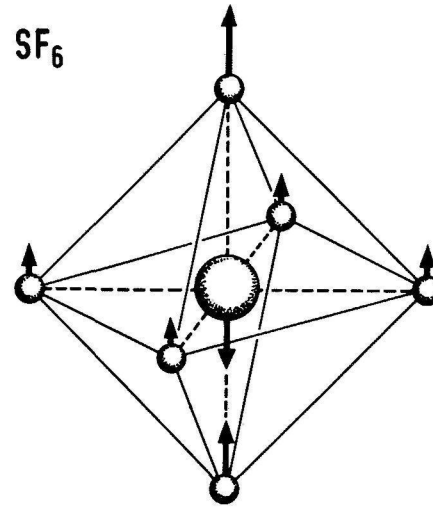

Fig. A1: ν_3 mode of vibration

-- Molecular bond lengths at 298 K [1] and the rotational constant [2]

$$r_e(S - F) = 0.1562 \quad (1) \text{ nm}$$

$$r_e(F - F)_c = 0.2209 \quad (1) \text{ nm}$$

$$r_e(F - F)_t = 0.3124 \quad (2) \text{ nm}$$

$$B_o = 0.091 \text{ cm}^{-1}$$

-- The vibrational modes [3] and transition moments μ_{01} [4]

mode	ν_1	ν_2	ν_3	ν_4	ν_5	ν_6
symmetry	A_{1g}	E_g	F_{1u}	F_{1u}	F_{2g}	F_{2g}
frequency [cm^{-1}]	774.5	643.4	948.0	615.0	523.5	347.0
degeneracy	1	2	3	3	3	3
μ_{01} [D]	0	0	0.387	0.134	0	0

-- Isotopic species

sulphur isotope	natural abundance	shift $\Delta\nu_3$ [cm^{-1}]
32	95.02 %	-
33	0.75 %	$-8^{a)}$ / $-8.8^{b)}$
34	4.21 %	$-17.2^{c)}$
36	0.017%	$-33^{a)}$

a) from ref. [5]
b) from ref. [6]
c) averaging of the values of refs. [5, 6, 7 and 8]

-- The ν_3 mode

The displacement coordinates [9] in the z-direction

sulphur atom $\Delta z = -7.64 \cdot 10^{-4}$ nm

fluor atoms in plane $\Delta z = +0.47 \cdot 10^{-4}$ nm

fluor atoms out of plane $\Delta z = +5.48 \cdot 10^{-4}$ nm

The derivate of the dipole moment μ [2]

$$\partial\mu/\partial z = 41.6 \pm 3.1 \quad Dnm^{-1}$$

The absorption cross section at $\nu = 947.7\ cm^{-1}$ (10P(16) line of the CO_2 laser) and at room temperature [10]

$$\sigma(\nu) = 4.10^{-22}\ m^{-2} \quad \text{at fluence} \quad F = 1\ Jm^{-2}$$
$$\sigma(\nu) = 2.10^{-22}\ m^{-2} \quad \text{at fluence} \quad F = 10\ Jm^{-2}$$

Average number of photons absorbed at $\nu = 947.7\ cm^{-1}$, roomtemperature and $F = 10\ Jm^{-2}$ [10]

$$\langle n \rangle = 0.1$$

Average number of photons absorbed at ν = 947.7 cm^{-1} in a 10% SF_6 - 90% He beam at more than four nozzle distances for our laser conditions [11]

$$\langle n \rangle_{max} = 0.6$$

A2. The C_2H_4 molecule

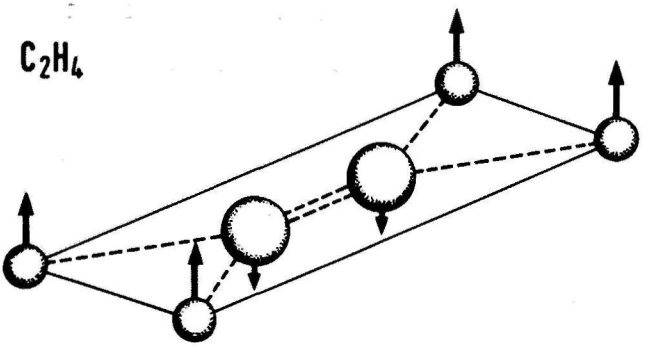

Fig. A2: ν_7 *mode of vibration*

-- Molecular bond lengths at 248 K [12] and the rotational constants for the ν_7 mode [13]

$r_e(CH)$ = 0.1081 nm

$r_e(CC)$ = 0.1334 nm

$\alpha_e(CHC)$ = 117.34°

A_o = 4.8715 cm^{-1}

B_o = 0.9951 cm^{-1}

C_o = 0.8295 cm^{-1}

-- The vibrational modes [15] and transition moments μ_{01} [14]

mode	ν_1	ν_2	ν_3	ν_4	ν_5	ν_6
symmetry	A_g	A_g	A_g	A_u	B_{1g}	B_{1g}
frequency [cm^{-1}]	3013.6	1630	1343.5[c]	1026.4[b]	3083.5[c]	1220
degeneracy	1	1	1	1	1	1
μ_{01} [D]	0	0	0	0	0	0

mode	ν_7	ν_8	ν_9	ν_{10}	ν_{11}	ν_{12}
symmetry	B_{1u}	B_{2g}	B_{2u}	B_{2u}	B_{3u}	B_{3u}
frequency [cm^{-1}]	948.8[b]	940	3104.9[a]	825.9[b]	3012.4[a]	1443.5
degeneracy	1	1	1	1	1	1
μ_{01} [D]	0.188	0	0.073	0.004[d]	0.066	0.054

a) from ref. [16]
b) from ref. [13]
c) from ref. [17]
d) this value has been calculated in ref. [14]

-- Isotopic Species

carbon isotope	natural abundance	shift $\Delta\nu_7$ [cm^{-1}]
12	98.89%	0
13	1.11%	?

-- The ν_7 mode

The derivate of the dipole moment with respect to the normal coordinate [14]

$$\partial\mu/\partial Q = 18.5 \pm 0.4 \text{ Dnm}^{-1}$$

A3. The SiF_4 molecule

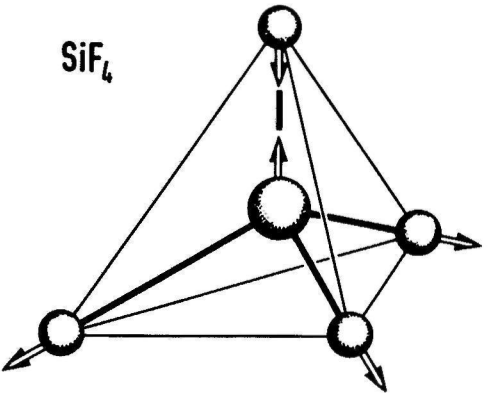

Fig. A3: ν_3 mode of vibration

-- Molecular bond lengths at 298 K [18] and the rotational constant [19]

$r_e(Si\text{-}F) = 0.1555\ (2)$ nm

$r_e(F - F) = 0.2534\ (3)$ nm

$B_o = 0.13676\ (3)\ cm^{-1}$

-- The vibrational modes [19] and transition moments [20]

mode	ν_1	ν_2	ν_3	ν_4
symmetry	A_1	E	F_2	F_2
frequency $[cm^{-1}]$	800.6	264.2	1031.4	388.4
degeneracy	1	2	3	3
μ_{01} [D]	0	0	0.276	0.197

-- Isotopic species [19]

silicon isotope	natural abundance	shift $\Delta\nu_3$ $[cm^{-1}]$
28	92.21%	-
29	4.70%	-8.98
30	3.09%	-17.40

A4. The CF_3Br molecule

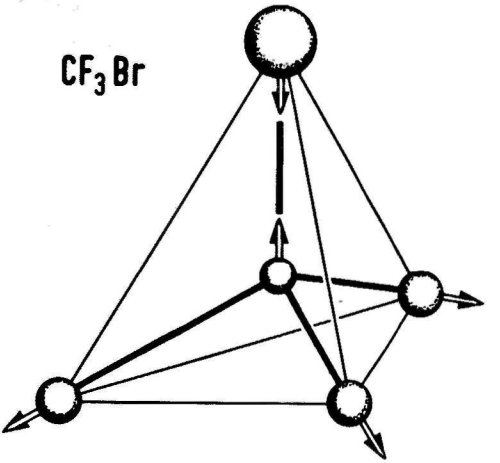

Fig. A4: ν_1 mode of vibration

-- Molecular bond lengths at 298 K [21] and the rotational constants [22] (isotopically averaged values)

r_e(C-F) = 0.1326 (3) nm

r_e(C-Br) = 0.1923 (4) nm

α_e(FCF) = 108.81°

A_o = 0.1906 cm^{-1}

B_o = 0.0696 cm^{-1}

-- The vibrational modes [22] and transition moments [23] for $CF_3{}^{79}Br$

mode	ν_1	ν_2	ν_3	ν_4	ν_5	ν_6
symmetry	A_1	A_1	A_1	E	E	E
frequency [cm^{-1}]	1084.8	762.1	351.1	1209.8	547.4	302.7
degeneracy	1	1	1	2	2	2
μ_{01} [D]	0.41	0.12	< 0.01	0.39	0.04	< 0.01

-- Isotopic species [22]

bromide	natural abundance	shift $\Delta\nu_1$ [cm^{-1}]
79	50.5%	-
81	49.5%	- 0.24

-- Dipole moment (isotopically weighted) [23]

μ = 0.64 (1) D

In this appendix the heat capacity γ is drawn for the used molecules, SF_6, SiF_4, CF_3Br and C_2H_4. The calculations are performed by using the theory of Herzberg [24] and the molecular data from appendix A.

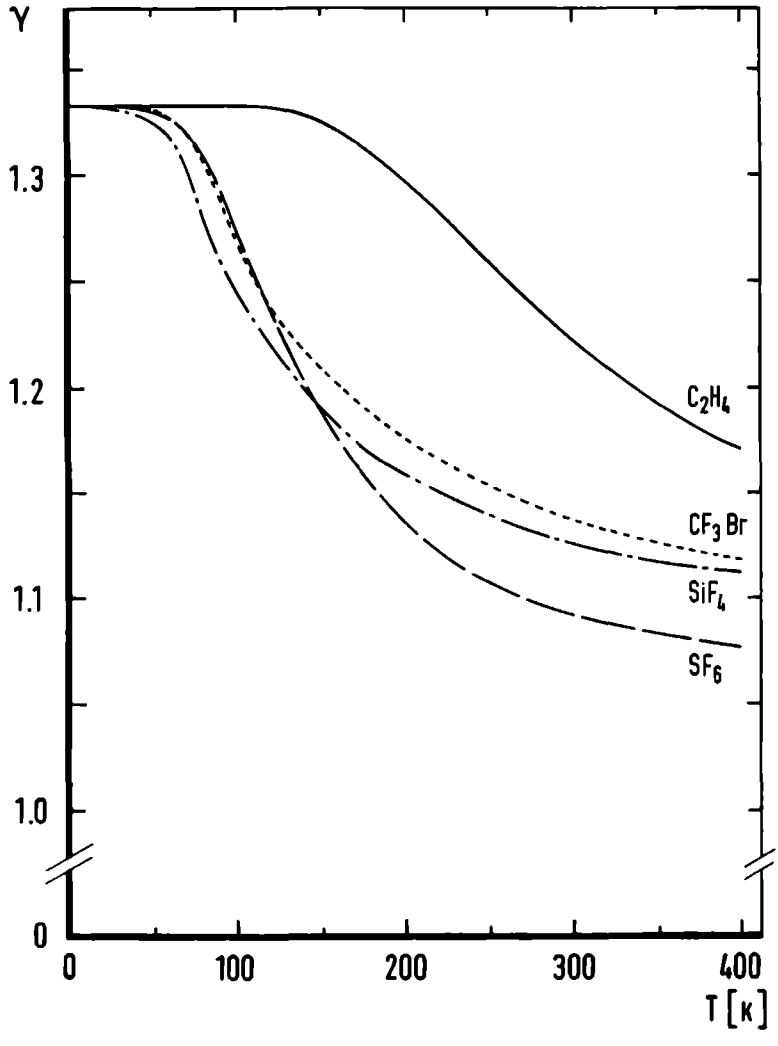

Fig. B1 The heat capacity γ versus the temperature T.

In this appendix the saturated-vapour lines of the gases used are drawn. The data for the picture are taken from [25].

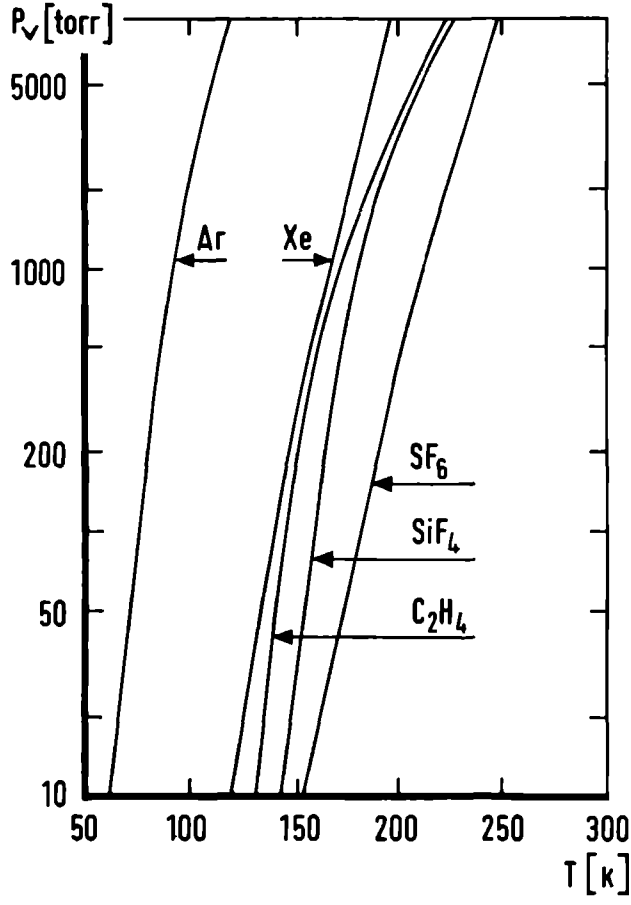

Fig. C1: The vapour pressure P_v versus the temperature T.

References

1. B.R. Miller and M. Fink
   J. Chem. Phys. 75 (1981) 5326
2. R.S. McDowell, J.P. Aldridge and R.F. Holland
   J. Phys. Chem. 80 (1976) 1203
3. D.S. Dunn, K. Scanlon and J. Overend
   Spectrochim. Acta 38A (1982) 841
4. C. Brodbeck, I. Rossi, H. Strapelias and J.-P. Bouanich
   Chem. Phys. 54 (1980) 1
5. V.D. Klimov and E.A. Lobicov
   Opt. Spectry. 30 (1971) 25
6. V.V. Bertsev, T.D. Kohomiitseva and N.M. Tsyganenko
   Opt. Spectry. 37 (1974) 263
7. M. Brunet and M. Perez
   J. Mol. Spectr. 29 (1969) 472
8. W. Fuss and J. Hartman
   J. Chem. Phys. 70 (1979) 5468
9. K. Scanlon, R.A. Eades and D.A. Dixon
   Spectrochim. Acta 38A (1982) 849
10. J.L. Lyman and K.M. Leary
    J. Chem. Phys. 69 (1978) 1858
11. G. Luijks, J. Timmerman, S. Stolte and J. Reuss
    Chem. Phys. 77 (1983) 169
12. J.L. Duncan
    Mol. Phys. 28 (1974) 1177
13. C. Lambeau, A. Fayt, J.L. Duncan and T. Nakagawa
    J. Mol. Spectr. 81 (1980) 227
14. T. Nakanaga, S. Kondo and S. Saëki
    J. Chem. Phys. 70 (1980) 2471
15. J.L. Duncan and E. Hamilton
    J. Mol. Struct. 76 (1981) 65
16. A. Fayt
    Can. J. Phys. 61 (1983) 514
17. R.B. Foster, G.W. Hills and W.J. Jones
    Mol. Phys. 33 (1977) 1589

18. B. Beagley, P. Brown and J.M. Freeman
J. Mol. Struct. 18 (1973) 337
19. R.S. McDowell, M.J. Reisfeld, C.W. Patterson, B.J. Krohn, M.C. Vasquez and G.A. Laguna, J. Chem. Phys. 77 (1982) 4337
20. K. Fox and W.B. Person
J. Chem. Phys. 64 (1976) 5218
21. A.P. Cox, G. Duxbury, J.A. Hardy and Y. Kawashima
J.C.S. Faraday II 76 (1980) 339
22. V.K. Burczyk, H. Bürger, P. Schultz and A. Ruoff
Z. Anorg. Allg. Chem. 474 (1981) 74
23. W.B. Person and S.R. Polo
Spectrochim. Acta 17 (1961) 101
24. G. Herzberg
"Infrared and Raman Spectra of Polyatomic Molecules"
Van Nostrand, Princeton, 1945, pp. 501-530
25. Landolt-Börnstein,
"Zahlenwerte und Funktionen aus Physik - Chemie - Astronomie - Geophysik - Technik", vol. 6, Springer Verlag, Berlin, 1960

Vibrationele aanslag van klusters door infrarood straling

Een kluster is een groep monomeren (atomen en/of molekulen) die gebonden zijn door Van der Waals krachten. Deze krachten zijn erg zwak met als gevolg dat de bindingsenergie van een kluster vele malen kleiner is dan de chemische bindingsenergie. De onderzochte klusters worden voornamelijk gevormd uit de monomeren SF_6, SiF_4, C_2H_4, CF_3Br, Ar en Xe. De grootte van een kluster kan varieren van twee (= dimeer) tot zeer veel atomen en/of molekulen.

In een molekulaire-bundelopstelling worden de klusters gevormd door de expansie van het monomeer gas in vakuum, waarbij de monomeren sterk worden afgekoeld. Bij goed gekozen kondities voor de expansie zullen er in de bundel klusters worden gevormd door botsingen. Deze klustervorming stopt als de dichtheid in de bundel zo ver is afgenomen dat er geen botsingen meer optreden. In de praktijk is het mogelijk bundels te maken waarin zich naast monomeren enkele procenten klusters bevinden.

De metingen werden verricht door een CO_2 laserbundel te kruisen met de molekulaire bundel. Als nu een van de molekulen in het kluster vibrationeel wordt aangeslagen door een laserfoton zal het kluster dissocieren. Dit komt omdat de energie van de aangeslagen vibratie groter is dan de bindingsenergie van het kluster. De klusterfragmenten verdwijnen na dissociatie uit de molekulaire bundel met als gevolg dat het bundelsignaal afneemt. Door de laser in frekwentie te verstemmen kan het dissociatiespektrum van een kluster gemeten worden.

Een verbeterde meetgevoeligheid is bereikt door twee CO_2 lasers te gebruiken. De eerste laser moduleert met een vaste frekwentie een specifiek kluster terwijl de tweede laser de verandering van het gemoduleerde bundelsignaal meet als funktie van de frekwentie. De metingen met twee lasers maakten het

mogelijk om een bepaalde kluster populatie in de molekulaire bundel te isoleren. Een tweede voordeel van deze modulatiemethode is de mogelijkheid om te bepalen of een kluster-dissociatiespektrum al dan niet homogeen verbreed is.

De gemeten dissociatiespektra van SF_6- en SiF_4-dimeren laten een dubbele piek struktuur zien. De monomeren SF_6 en SiF_4 bezitten een drievoudig ontaarde, infrarood aktieve ν_3 trilling. Deze ontaarding wordt in het dimeer opgeheven door een Fermi-resonantie: de resonante dipool-dipool interaktie. De naar lagere frekwentie verschoven piek korrespondeert met een trilling langs de verbindingsas in het dimeer; de naar hogere frekwentie verschoven piek met een trilling loodrecht op de verbindingsas. De resonante dipool-dipool interaktie is sterk hoekafhankelijk. Hierdoor kan voor kleine klusters een verband gelegd worden tussen hun geometrie en het te verwachten spektrum. Het is nu mogelijk uit een gemeten spektrum de bijdrage van ieder kluster apart te bepalen.

Het spektrum van C_2H_4-dimeren laat een brede piek zien. Het monomeer C_2H_4 bezit een niet ontaarde, infrarood aktieve ν_7 trilling en een niet ontaarde, infrarood inaktieve ν_8 trilling die praktisch dezelfde frekwentie bezitten. Het centrum van de C_2H_4 dimeer piek is naar hogere frekwentie verschoven ten opzichte van de ν_7 trilling. Deze verschuiving wordt ook door een Fermi-resonantie verklaard. Nu hebben we niet te maken met het opheffen van een ontaarding, zoals bij SF_6, maar met twee nabij gelegen frekwenties. In het dissociatiespektrum wordt een verschoven ν_7 frekwentie waargenomen omdat bij wisselwerking de energienivo's in het dimeer elkaar zullen afstoten. Uit de meting volgt verder dat de totale overgangsterkte van een kluster gelijk is aan de som van alle overgangsterktes van de losse monomeren, die samen het kluster vormen. Uit de gemeten overgangsterktes kan informatie verkregen worden over de geometrie van het dimeer.

Levensloop

15-06-1952	geboren te Swalmen
juni 1969	eindexamen HBS-B Roermond
augustus 1976	afgestudeerd aan de Technische Hogeschool Eindhoven, afdeling der Technische Natuurkunde in de groep Stromingsleer
1976-1978	student Wijsbegeerte, Katholieke Universiteit Nijmegen
1979-1983	promotie-onderzoek in dienst van "Stichting Fundamenteel Onderzoek der Materie" aan de Katholieke Universiteit Nijmegen, fakulteit der Wiskunde en Natuurwetenschappen in de groep Atoom- en Molekuulfysika
september 1983	research medewerker bij Océ-Nederland B.V. te Venlo

ERRATA IN REPRINTS

Chem. Phys. Lett. 78 (1981) 277

p. 45 column 1, line 6 from the bottom:
beam temperature $\tau//$ → beam temperature $T//$

p. 48 table 1, column 10:
0.8 ± 0.3 → 0.7 ± 0.3
0.9 ± 0.3 → 1.3 ± 0.3

Z. Phys. A. 304 (1982) 167

p. 57 column 1, line 5 from the top:
14 mm pole diameter → 140 mm pole diameter

p. 57 column 1, line 10 from the bottom:
a wast of → a waist of

p. 62 column 1, line 6 from the bottom:
±1 → ±0.1

p. 62 column 2, line 13 from the bottom:
[11] → [12]

p. 63 column 2, line 8 from the top:
well fuctioning → well functioning

Faraday Disc. Chem. Soc. 73 (1982) 375

p. 71 line 2 from the top:
at most 2% for the red and 10% for the blue → at most 10% for the red and 2% for the blue

Chem. Phys. Lett. 97 (1983) 152

p. 140 column 1, line 2 from the bottom:
a strong blue-shift of +9 cm^{-1} → no shift

STELLINGEN

1. Invoering van hoogwaardige technologie zal steeds gepaard gaan met een aanpassing van ons waardesysteem.

   N.R.C. Handelsblad, 9 augustus 1983.

2. De schatting van de rotatie-relaxatietijd van HF in de toestand ($v = 1$, $J \geq 8$) die Copeland *et al* maken is in tegenspraak met hun eigen metingen van de rotatie-relaxatietijd voor de toestand ($v = 2$, $J \leq 8$).

   R.A. Copeland, D.J. Pearson, J.M. Robinson and F.F. Crim, J. Chem. Phys. 77 (1982) 3974.

3. De geometrische structuren die J. Burdett voor een aantal Van der Waals complexen voorspelbaar acht met "extended-Hückel" berekeningen zijn reeds bepaald door de gekozen randvoorwaarde.

   J.K. Burdett, J. Chem. Phys. 73 (1980) 2825.

4. Bij de analyse van het chemiluminescente signaal als functie van de laserfluence bij de reactie Xe* plus gepolariseerd IBr verwaarlozen de Vries *et al* ten onrechte de invloed van de stand van de as van het IBr molekuul bij hogere laserfluences.

   M.S. de Vries, V.I. Srdanov, C.P. Hanaran and R.M. Martin, J. Chem. Phys. 78 (1983) 5582

5. Het is mogelijk een supersone bundel van O_2-dimeren in de singlet toestand te produceren.

6. In analogie met infrarood reflectie-absorptie metingen aan CO op Pt is het interessant na te gaan of bij SF_6 op Pt de invloed van de resonante dipool-dipool krachten meetbaar is als functie van de polarisatie van de gereflecteerde infrarood bundel.

   A. Crossley and D.A. King, Surface Sci. 95 (1980) 131.

7. Om de rendabiliteit van stadsverwarmingsbedrijven te verhogen dient men bij de dimensionering in de periferie rekening te houden met gelijktijdigheidsfactoren bij de afname door de gebruikers en met het thermisch-dynamisch gedrag van de wooneenheden.

Studie van de Commissie Optimalisatie Ruimteverwarming, 1982.

8. Bij de integratie van de absorptie spectra van SF_6 in krypton-matrices moeten Jones *et al* ook rekening houden met de aanwezigheid van SF_6-paren in de matrices.

L.H. Jones and B.I. Swanson, J. Chem. Phys. 79 (1983) 1516.

9. Het model van SF_6-dimeren leidt tot een eenvoudige en experimenteel te toetsen hoekverdeling van de fragmenten na predissociatie. Uit de verhouding van de intensiteiten van de fragmenten bij verschillende polarisaties van de excitatie laser is de levensduur van het aangeslagen dimeer te relateren aan zijn rotatieperiode.

Dit proefschrift.

10. De versterking van de $\nu_1-2\nu_5$ Fermi-resonantie in het CF_3Br-molekuul door de Van der Waals binding is het best meetbaar in een Van der Waals complex met een edelgas zoals bijvoorbeeld Ar-CF_3Br.

Dit proefschrift.

11. Bij woningen zonder onderlinge verbindingen via de achtertuin zal het bevestigen van deurbellen op aangepaste hoogte het sociale kontakt tussen kleuters bevorderen en de ontwikkeling van agressieve methodes om toch opgemerkt te worden afremmen.

23 september 1983

Jo Geraedts